NASA-CR-200687

HIGH-PERFORMANCE COMPUTING FOR THE ELECTROMAGNETIC MODELING AND SIMULATION OF INTERCONNECTS

Final Report

*IN 32--
0.-T
: 796 2*

NASA - FAR Grant NAG 2-823

Jose E. Schutt-Aine

Department of Electrical and Computer Engineering

University of Illinois , Urbana, IL

February 1996

*MAR 0 5 1996
CAST*

SUMMARY

The electromagnetic modeling of packages and interconnects plays a very important role in the design of high-speed digital circuits, and is most efficiently performed by using computer-aided design algorithms. In recent years, packaging has become a critical area in the design of high-speed communication systems and fast computers, and the importance of the software support for their development has increased accordingly. Throughout this project, our efforts have focused on the development of modeling and simulation techniques and algorithms that permit the fast computation of the electrical parameters of interconnects and the efficient simulation of their electrical performance.

PROJECT DESCRIPTION

The development of efficient and accurate computer-aided design tools is essential for the implementation of high-speed digital circuits used in computer systems and communication networks. With current trends in which network complexity and signal speed keep increasing, problems associated with signal integrity such as crosstalk, distortion, losses can compromise the overall electrical performance of computers and communication systems.

Presently, industrial needs for computer support in network design is increasing rapidly; however the availability of design and analysis tools capable of handling the complexity and volume of manufactured systems lags seriously. Future winners in the competitive world of high-speed communications will have to possess sophisticated packaging analysis and design tools and system performance will be more and more determined by the adequacy of these tools.

Because of their important role in the design process, CAD tools must offer certain essential features such as speed, accuracy, availability of extensive library and good user interface. CAD tools will insure minimum manufacturing cost, faster turnaround time and more reliable hardware for production. To achieve the required performance, optimization routines must be made available and efficient algorithms must be implemented to guarantee speed and good user interface, friendliness and portability of the software.

Our group at the University of Illinois has been involved during the past three years in the development of modeling and simulation techniques for interconnects and packages. In the parent project, the main emphasis of our work is directed toward the modeling of complex interconnect structures as well as the simulation of interconnects.

The development of efficient and accurate computer-aided design tools is essential for the implementation of high-speed digital circuits used in computer systems and communication networks. With increasing clock rates and reduced circuit sizes, electromagnetic phenomena such as crosstalk noise, distortion, ground bounce will become more pronounced in both circuit boards and chip environment. These effects seriously degrade the signal integrity of high-speed networks and compromise the overall network performance.

In many situations, one factor that contributes to the increased computation time in the calculation of the electrical parameters of the Green's function in the spatial domain, which represents the vector field produced by an infinitesimal dipole placed over the dielectric substrate layer backed by a ground plane. An efficient method to compute the 2-D and 3-D capacitance matrix of multiconductor interconnects in a multilayered dielectric medium was developed in our group. The method is applicable to conductors of arbitrary polygon shape embedded in a multilayered dielectric medium with possible ground planes on the top or bottom of the dielectric layers [2], [7]. The method has been extended to the computation of equivalent capacitance of via structures in multilayer environment [5].

In the time domain analysis, the ability to model fine features, e.g., wire bonds, is an important requirement and is unavailable in the conventional finite-difference time-domain (FDTD) approach unless a very high density of discretization is employed. The FDTD method is one of the most widely used techniques. In the FDTD, the derivative operators are replaced with the central difference operators, which preserves the second order accuracy. Hence, its extension to the general nonuniform grids is not possible without losing the second order accuracy or reformulating in terms of the curvilinear coordinates. However, in solving any practical problems nonuniform grids are highly desirable due to the limitation of computer resources.

An efficient way to implement the surface impedance boundary condition (SIBC) for the finite-difference time-domain FDTD method was introduced [4]. Surface impedance boundary conditions are first formulated for a lossy dielectric half-space in the frequency domain. The impedance function of a lossy medium is approximated with a series of first-order rational functions. Then the resulting time-domain convolution integrals are computed using recursive formulas which are obtained by assuming that the fields are piecewise linear in time. Thus the recursive formulas derived are second-order accurate. The preprocessing time is eliminated by performing a rational approximation on the normalized frequency-domain impedance. This approximation is independent of material properties.

Simulation of Interconnects

In the real world of electronic packaging, transmission lines are more likely to be nonuniform and may include discontinuities such as bends, tapers and transitions; hence, the standard simulation tools for uniform lines can no longer be used to analyze them. Presently, a number of methods are available for the simulation of coupled transmission lines that are used to model interconnects. In the past two years, we have carried out a systematic comparison of these methods with a view to developing an approach that would be optimal in terms of both accuracy and efficiency. This has led to the development of a transient simulation method based on the difference approximation which has the highly desirable feature that it can be conveniently incorporated in a circuit simulator [6]-[7], [10]-[13]. This approach not only outperforms the standard scattering parameter method, but is very accurate and computationally efficient as well. Software designers at Cadence Design Systems and Intel have recently implemented this method in the latest circuit simulators.

The problem of distributed line simulation was analyzed, and the optimal method, which results in the maximum efficiency, accuracy and practical applicability, was developed. The method is applicable to transmission lines characterized by frequency or time-domain data samples. The resulting line model can be directly used in a circuit simulator. The efficiency of the optimal method allows for the accurate transient simulation of real circuits containing thousands of lossy coupled frequency-dependent nonuniform lines surrounded by nonlinear active devices with virtually no increase in the simulation time compared to that for the simple replacement of interconnects with lumped resistors.

As components of the optimal method, the following novel techniques were introduced:

- The system model for uniform and nonuniform lines which simplifies analysis of distributed networks; the open-loop device model for uniform and nonuniform lines which relates voltages and currents at the line terminals via the simplest possible transfer functions and time-domain responses;

- The indirect numerical integration--a class of numerical integration methods, which has ideal accuracy, convergence and stability properties;

- The difference approximation, a general method for applying numerical integration to systems characterized by discrete data samples was developed and put in a matrix form.

- The matrix delay separation from the matrix propagation function, which avoids the use of frequency-dependent modal transformation matrices;

- The relaxation interpolation method, which allows for an accurate and efficient approximation of line responses in the time and frequency domains, automatically reduces the approximation order depending on the original function and eliminates spurious positive poles.

The complete set of frequency-domain relationships between the matrix Z, Y and S parameters were derived and the direct interpolation-based complex rational approximation method for transient simulation of macromodels for complicated multiport interconnects (such as IC packages and connectors) was developed. The direct interpolation-based method was applied to the automatic generation of lumped equivalent-circuit models of multiport EM systems (with Dan).

Approximation Techniques for Circuit Analysis

Our research has also been focused in developing a unified methodology of model-order reduction techniques for circuit and interconnects simulation. The following three classes of model-order reduction methods: moment-matching technique, Krylov subspace techniques, and reduced optimum approximation have been studied and their applications for efficient circuit simulations have been identified.

The moment-matching technique has been shown to be very effective for generating low order models for linear lumped and distributed systems. The method is useful for systems whose main features can be retained by the first few orders of reduced system models. These include the response estimations of linear lumped networks of medium complexity, wave propagation in transmission lines with short delays and diffusion process in p-n junctions [20].

Krylov subspace based methods such as Arnoldi algorithm and Lanczos algorithm are effective and robust in generating reduced-order model of large complex systems described by ordinary differential or difference equations. The methods are important in obtaining reduced-order models to systems that can be characterized by relatively higher

order models. The methods avoid the construction of ill-conditioned moment matrices and the loss of information contained by the eigenvalues of the systems with smaller magnitudes when higher models are sought. The methods are suitable for analyzing large, complex lumped networks.

An optimum approximation in conjuction with model order reduction techniques such as balanced representation and aggregation methods represents a very effective methodology for generating reduced-order models of complex interconnects (infinite dimension systems). The approximation method is applied to the distributed systems to drive high-order finite models as an intermediate stage and then using balanced transformation and aggregation method lower-order models are generated.

Publications

[1] K. S. Oh and José E. Schutt-Ainé, "Transient Analysis of Coupled Tapered Transmission Lines with Arbitrary Nonlinear Terminations," IEEE Trans. on Microwave Theory Tech., vol. MTT-41, pp. 268-273, February 1993.

[2] K. S. Oh, D. B. Kuznetsov and J. E. Schutt-Ainé "Capacitance Computations in a Multilayered Dielectric Medium Using Closed-Form Spatial Green's Functions, " IEEE Trans. Microwave Theory Tech., vol. MTT-42, pp. 1443-1453, August 1994.

[3] J. E. Schutt-Ainé and D. B. Kuznetsov, "Efficient transient simulation of distributed interconnects," Int. Journ. Computation Math. Electr. Eng. (COMPEL), vol. 13, no. 4, pp. 795-806, Dec. 1994.

[4] K. S. Oh and J. E. Schutt-Ainé, "An Efficient Implementation of Surface Impedance Boundary Conditions for the Finite Difference Time Domain Method, " IEEE Trans. Antennas Propagat., vol. AP-43, pp. 660-666, July 1995.

[5] K. S. Oh, J. E. Schutt-Ainé, Raj Mittra, and Bu Wang , "Computation of the Equivalent Capacitance of a Via in a Multilayered Board Using the Closed-Form Green's Function", IEEE Trans. Microwave Theory Tech. vol. MTT-44, pp. 347-349, February 1996.

[6] D. B. Kuznetsov and J. E. Schutt-Ainé, "The Optimal Transient Simulation of Transmission Lines," to be published in the IEEE Trans. Circuits Syst.-I.

[7] D. B. Kuznetsov and J. E. Schutt-Ainé, "Transmission line modeling and transient simulation," EMC Lab Technical Report No. 92-4, December 1992.

[8] H. Satsangi and J. E. Schutt-Ainé, "Implementation of Interconnect Simulation Tools in SPICE," EMC Lab technical Report No. 93-4, August 1993.

[9] K. S. Oh and J. E. Schutt-Ainé, "Efficient Modeling of Interconnects and Capacitive Discontinuities in High-Speed Digital Circuits," EMC Lab Technical Report No. EMC 95-1, June 1995.

[10] D. B. Kuznetsov and J. E. Schutt-Aine, "Indirect numerical integration," submitted for publication in IEEE Trans. Circuits Syst.

[11] D. B. Kuznetsov and J. E. Schutt-Aine, "Efficient circuit simulation of nonuniform transmission lines," submitted for publication in IEEE Trans. Microwave Theory Tech.

[12] D. B. Kuznetsov and J. E. Schutt-Aine, "Difference approximation," submitted for publication in IEEE Trans. Circuits Syst.

[13] D. B. Kuznetsov, K. S. Oh and J. E. Schutt-Aine, "Equivalent circuit modeling of electromagnetic systems," submitted for publication in IEEE Trans. Microwave Theory Tech.

[14] K. S. Oh, J. E. Schutt-Ainé and R. Mittra, "Conductance and Resistance Matrices of Multiconductor Transmission Lines in Multilayered Dielectric Medium" submitted to IEEE Trans. Microwave Theory Tech., January 1995.

[15] W. Beyene and J. E. Schutt-Ainé, "Asymptotic waveform evaluation analysis of diode switching characteristics," submitted to IEEE Transactions on Electron Devices.

[16] J. E. Schutt-Ainé and K. S. Oh, "Modeling Interconnections with Nonlinear Discontinuities," Proceedings of the 1993 IEEE-CAS International Symposium, pp. 2122-2124, May 1993.

[17] K. S. Oh and J. E. Schutt-Ainé, "Capacitance Computation in a Multilayered Dielectric Medium Using Closed-Form Spatial Green's Functions," 1993 IEEE-MTT-S International Symposium Digest, pp. 429-432, Atlanta, June 1993.

[18] J. E. Schutt-Ainé and D. B. Kuznetsov and "Efficient Transient Simulation of Distributed Interconnects, " Nasecode X Conference, Dublin, June 21-24, 1994.

[19] D. Kuznetsov, J. E. Schutt-Ainé and R. Mittra, "Optimal Transient Simulation of Distributed Lines," Proceedings of the IEEE 1995 Multi-Chip Module Conference, MCMC-95, pp. 164-169, February 1995.

[20] W. Beyene and J. E. Schutt-Ainé, "Accurate diode forward and reverse recovery model using asymptotic waveform evaluation," to appear in the International Symposium on Circuits and Systems, Atlanta, Georgia, May 12-15, 1996.

(a) M.S. Degrees Granted: 4

1. Dmitri Kuznetsov	1993
2. Hem Satsangi	1993
3. Kirk Ingemunson	1994

(b) Ph.D. Thesis Students Supervised 3

1. Kyung S. Oh
2. Dmitri Kuznetsov
3. Wendu Beyene

(c) Ph.D. Degrees Granted: 1

1. Kyung S. Oh	1992

ATTACHMENTS

Optimal Transient Simulation of Transmission Lines

Dmitri Borisovich Kuznetsov, *Student Member, IEEE,* and José E. Schutt-Ainé, *Member, IEEE*

Abstract— This paper presents an attempt to formulate a high-level description of the optimal transmission line simulation method. To formulate the optimal approach, most significant aspects of the problem are identified, and alternative approaches in each of the aspects are analyzed and compared to find the combination that results in the maximum efficiency, accuracy and applicability for the transient analysis of digital circuits. The practical implementation of the optimal method for uniform multiconductor lossy frequency-dependent lines characterized by samples of their responses is outlined. It is shown on an extensive set of runtime data that, based on the optimal approach, the accurate line modeling in a circuit simulator is as efficient as the simple replacement of interconnects with lumped resistors.

I. INTRODUCTION

THE PROBLEM of transmission line simulation gained special importance with the development of high-speed digital electronics. As transient times become faster, the transmission line behavior of electronic interconnects starts to significantly affect transient waveforms, and accurate modeling of on-board and even on-chip interconnects becomes an essential part of the design process. The complexity of contemporary digital circuits necessitates the simultaneous simulation of thousands of lossy coupled frequency-dependent lines surrounded by thousands of nonlinear active devices. Lines to be simulated may be characterized by measured or electromagnetically simulated samples of their responses.

There are two approaches to the interconnect simulation. The first approach creates macromodels for linear subcircuits that may contain many transmission lines and other linear elements [1], [2]. This paper discusses the second approach, in which each multiconductor line is treated as an individual circuit element.

The problem of the line simulation involves several areas of science, such as electromagnetics, computational mathematics, and circuit and system theories. The solution of the problem is straightforward in the sense that all of the components involved are well known and only have to be combined together. The integration of areas, however, is a difficulty that keeps the problem open and accounts for the diversity of developed methods.

This paper presents an original attempt to identify the components of the problem and to formulate a high-level description of the method that provides the maximum efficiency, accuracy and applicability for the transient analysis of digital

circuits. Such an approach allows one to more accurately assess and compare the performance of numerous and diverse line simulation methods.

The next section presents the formulation of the optimal approach and discusses many of the existing line simulation methods. Section III outlines the authors implementation of the optimal method and presents numerical verification of the method's accuracy and efficiency.

II. FORMULATION OF OPTIMAL APPROACH

To formulate the optimal approach, major aspects of the line simulation will be analyzed, *viz., the formulation, the line characterization, the line model,* and, *the transient simulation method* (see Fig. 1). Alternative approaches in each of the aspects will be compared to find the optimal combination that results in *the maximum efficiency, accuracy* and *practical applicability.*

A. Formulation

The formulation affects dimensions of the problem. One can distinguish between *time-and-space formulations* and *time-only formulations.*

Time-and-space formulations (such as segmentation models [3], [4]) are based on the voltage and current distributions inside the line. These formulations are multidimensional and computationally extensive.

Time-only formulations deal exclusively with the voltages and currents at the line terminals. These formulations are one-dimensional and more efficient. Consequently, to achieve the maximum efficiency, the line simulation should be based on a time-only formulation.

B. Line Characterization

As can be observed from the system diagram [5] shown in Fig. 2, a line with terminations forms a feedback system. Therefore, one can distinguish between *closed-* and *open-loop characterizations.*

Closed-loop characterizations (such as Z-, Y-, H- and S-parameter characterizations [6], [7]) include reflections from the terminations and lead to complicated oscillating transfer functions and transient characteristics (unit-step responses).

The open-loop characterization (direct characterization in terms of the propagation functions) separates forward and backward waves and results in the simplest transfer functions and transient characteristics (see Fig. 3). The complexity of the transfer functions and transient characteristics is an important factor affecting accuracy and efficiency of the transient simulation. Consequently, to attain the maximum efficiency and

Transmission Line Simulation

Formulation
- affects dimensions of the problem

Time-and-Space Formulations
- multidimensional, computationally inefficient

Time-Only Formulations
- one-dimensional, computationally efficient

Line Characterization
- affects complexity of the transfer functions, and transient and impulse characteristics used for the simulation

Closed-Loop Transfer Function Characterizations
(such as global Z-, Y-, H- and S-parameter characterizations)
- result in complex, oscillating transfer functions, transient and impulse characteristics

Open-Loop Transfer Function Characterization
(propagation function and characteristic admittance)
- results in simple, aperiodic transfer functions, transient and impulse characteristics

Line Model
- affects applicability of the resulting method

Noncircuit Models
- can not be directly placed in a circuit simulator, can not be used with efficiency for the transient simulation of real circuits

Circuit Models
- can be directly placed in a circuit simulator

Equivalent-Circuit Models
- have a larger number of nodes than the line they represent, are computationally inefficient

Device Models
- have the same number of nodes as the line they represent, are computationally efficient

Transient Simulation Technique
- affects computational efficiency and accuracy of the resulting method

Numerical Fourier and Laplace Transformations
- use system transfer functions
- computational complexity is worse than linear
- can not directly handle nonlinear and time-varying systems
- in addition to the discretization error, introduce frequency- and time-response truncation errors
- can not be directly used with recursive time-domain solvers employed by circuit simulators

Numerical Convolution
- uses system impulse responses
- computational complexity is worse than linear
- can not directly handle nonlinear and time-varying systems
- in addition to the discretization error, introduces impulse-response truncation error

Numerical Integration
- uses system differential equations
- computational complexity is linearly proportional to the number of time-steps
- can directly handle nonlinear and time-varying systems

Indirect
- has ideal accuracy, convergence and stability properties

Direct
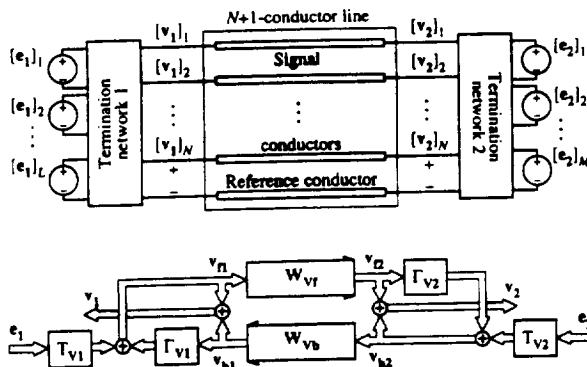
Fig. 1. Aspects of the transmission line simulation.

Fig. 2. System model for transmission lines. W_{vf} and W_{vb} represent the forward and backward matrix propagation functions for voltage waves; T_{v1}, T_{v2} and Γ_{v1}, Γ_{v2} stand for the near- and far-end matrix transmission and reflection coefficients.[1,2]

accuracy, the line simulation should be based on the open-loop characterization. The complete set of expressions for the open-loop functions for uniform lines is given in Appendix A.

C. Line Model

Line models can be divided into two large groups: *circuit* and *noncircuit*.

Noncircuit models can not be directly integrated into a circuit simulator. As a result, these models cannot be efficiently applied the transient analysis of real circuits containing

---

[1] Throughout the paper, capital boldface, small boldface and normal italic symbols denote matrices, vectors and scalars, respectively.

[2] Since only multiconductor lines will be considered, the modifier "matrix" will be omitted in the future for brevity.

thousands of nonlinear active devices. Examples of noncircuit models are the scattering-parameter model [6] and system model shown in Fig. 2.

Circuit models can be directly incorporated into a circuit simulator and are of prime practical interest. They relate voltages and currents at the line terminals and do not depend on the terminations. Circuit models can, in turn, be subdivided into *equivalent-circuit* and *device models*.

Equivalent-circuit models have a larger number of nodes than the line they represent. Examples of equivalent-circuit models are lumped and pseudo-lumped segmentation models [3], modal decomposition models for multiconductor lines [8], [3], [9], and equivalent-circuit modeling of the propagation function and characteristic impedance based on Padé synthesis [10].

Device models have the same number of nodes as the line they represent. A well-known example of device models is the method of characteristics [11]–[15]. The circuit simulation time is cubically proportional to the number of nodes and to the number of voltage and current variables. Consequently, to achieve the maximum efficiency and practical applicability, the line simulation should be based on a device model that does not require the introduction of current variables.

D. Transient Simulation Method

The transient simulation method is the prime factor affecting the efficiency of the line simulation. The selection of the transient simulation methods is confined to *the numerical Fourier* and *Laplace transformations, numerical convolution* and *numerical integration*.
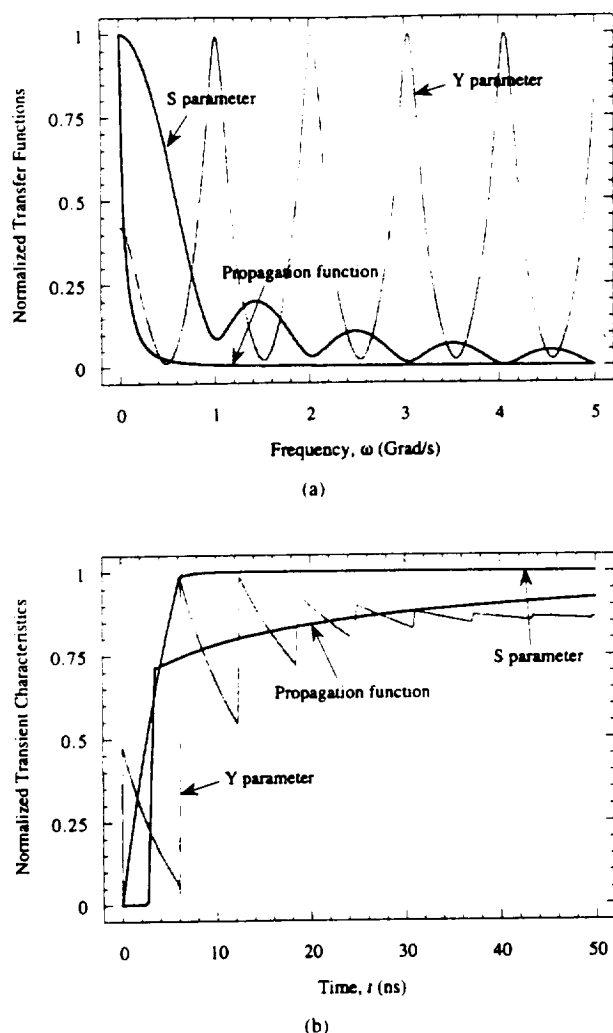
Fig. 3. Examples of (a) open- and closed-loop transfer functions and (b) transient characteristics. The scattering parameters correspond to the matched lossless reference system.

For *the transformation* and *convolution methods*, the computational complexity is higher than linear. These methods cannot directly handle nonlinear and time-varying systems, and, along with the discretization error, introduce time- and/or frequency-response truncation errors. In addition, the transformation methods cannot be directly used with recursive time-domain solvers employed by circuit simulators, that leads to relaxation techniques which additionally degrade the overall efficiency and accuracy [12]. Examples of the convolution-based techniques are the Spice model for lossy lines [9] and the scattering-parameter approach [6].

Numerical integration has linear computational complexity; it can directly handle nonlinear and time-varying systems, does not introduce truncation error, supports variable time-stepping and is compatible with recursive time-domain solvers. Numerical integration methods can be subdivided into *direct* and *indirect*.

Direct numerical integration is based on approximations for integrals or derivatives and includes such conventional methods as linear multistep formulas, Euler, Euler-Cauchy and Runge-Kutta techniques.

Indirect numerical integration [16] is based on the time-response invariant discrete synthesis, and has ideal accuracy, convergence and stability properties. Consequently, to achieve the maximum efficiency, accuracy and practical applicability, the line simulation should be based on indirect numerical integration. Indirect numerical integration covers as special cases techniques such as recursive convolution [13], [17], and approximation of the response of a linear network to an arbitrary piecewise linear input waveform used by some of the asymptotic waveform evaluation (AWE) methods [18].

To systems characterized with samples of their responses, numerical integration is applied via *the difference approximation method* [19]. The method is based on the approximation of the system response with the corresponding response of a system for which numerical integration formulas are already available. The complexity of the difference approximation method is only that of the approximation itself. As soon as a system response has been approximated, the numerical integration formulas are readily available directly in terms of the approximation parameters.

To attain the maximum efficiency and accuracy, the difference approximation should be applied in the domain of the system characterization. For transmission lines it usually is the frequency domain. The time-domain approximation should be used only when time-domain responses are available. The complete set of analytical expressions for the fundamental time-domain open-loop responses of two-conductor uniform constant-parameter lines is given in Appendix B. It also includes a new simple and accurate asymptotic approximation for the responses of propagation functions.

To improve accuracy, the delay should be separated from the propagation functions before the difference approximation is applied. The conventional frequency-domain method of delay separation for multiconductor lines is based on diagonalization with the frequency-dependent *modal transformation* matrices [14], [15], [17]. These matrices are nonminimum-phase functions of frequency with unstable time-domain responses, that limits the applicability of the modal transformation to special cases in which the matrices are constant [9], [20].

A novel *matrix delay separation method* [19] avoids the use of the frequency-dependent modal transformation matrices and is applicable to a general case of matrix transfer functions containing delay. For uniform lines, the formulas for the matrix delay separation from the propagation functions are included in Appendix A.

E. Approximation Methods

The choice of the approximation method for the difference approximation affects the overall efficiency, accuracy and reliability of the line simulation. Based on approximation criteria, approximation methods can be categorized into four major groups: *minimum maximum error based methods, least square based methods, interpolation methods*, and *series expansion based methods* (see Fig. 4).

Mini-max methods provide the highest accuracy, but result in the most inefficient and unreliable algorithms (nonlinear optimization).
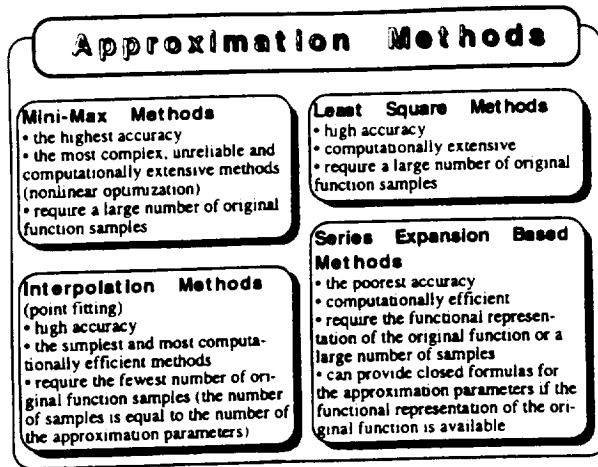
Fig. 4. Approximation methods.

TABLE I
COMPARISON OF APPROXIMATION METHODS

Approximation Method	Maximum Relative Error	Relative runtime
Mini-max approximation	0.0004%	200
Least squares approximation	0.002%	50
Interpolation	0.003%	1.0
Economized rational approximation	0.004%	2.0
Padé synthesis at zero	0.06%	1.3
Padé synthesis at infinity	0.3%	1.5

Least square methods provide high accuracy, but are still computationally extensive. The examples of least squares based methods for the time-domain difference approximation are Prony's method [21] and pencil-of-function method [22].

Series expansion based methods (such as Padé synthesis used for the AWE [23]–[25]) are computationally efficient, but provide the poorest accuracy.

Interpolation (point-fitting) [19] agrees exactly with the original function on a given set of samples. It provides high accuracy for simple functions, such as open-loop transmission-line responses, and is the most efficient among the approximation methods. It also requires the minimal number of the original function samples, which is important when the samples are obtained from electromagnetic simulations. Consequently, to achieve the maximum efficiency, the line simulation should be based on interpolation.

Table I presents the typical values of the maximum relative error in the full frequency range from zero to infinity and relative runtime for various approximation methods as applied to the third-order frequency-domain difference approximation of open-loop transmission-line functions. Economized rational approximation starts with the Padé synthesis, which is not accurate away from the expansion point, and then perturbs it to reduce the leading coefficient of error in a given approximation interval [23], [24].

As one can observe, interpolation provides accuracy comparable with that of the least square approximation, and

is 200 times more efficient than mini-max approximation. Interpolation is also up to two orders of magnitude more accurate and 30–50% more efficient than Padé synthesis. Note also that, because of the simplicity of the open-loop characterization, a very high accuracy is achieved with as low as third-order approximation and as few as seven samples of the original function used for the interpolation.

F. Summary of Optimal Approach

To summarize, the analysis of the problem showed that to achieve the maximum efficiency, accuracy and practical applicability, the line simulation should be based on

- time-only formulation;
- open-loop characterization;
- device model that does not require the introduction of current variables;
- indirect numerical integration;
- frequency-domain difference approximation based on the interpolation and matrix delay separation.

A method close to the optimal, but based on the time-domain difference approximation, was first proposed by Semlyen and Dabuleanu [17], and was further developed by Gruodis and Chang [15] to accommodate the frequency-domain approximation. The advantages of the approach were recognized only in recent years, and an increasing number of techniques close to optimal are published [13], [14], including techniques based on the AWE, recursive convolution and method of characteristics, and by researchers previously advocating transformation and direct convolution techniques. The applicability of the methods, however, had been limited by the lack of accurate, reliable and efficient frequency-domain approximation and delay separation techniques such as interpolation-based approximation methods and matrix delay separation [19], and by the lack of open-loop models for nonuniform lines.

The authors' implementation of the optimal method for uniform lines is outlined in the next section. The implementation of the method for nonuniform lines is described in [26].

III. IMPLEMENTATION OF OPTIMAL METHOD FOR UNIFORM LINES

A. Frequency-Domain Line Model for Transient Analysis

The frequency-domain element characteristic (for the transient analysis) which does not require the introduction of current variables and is suitable for the line modeling, is given by

$$\begin{cases} i_1(\omega) = Y_1(\omega)v_1(\omega) - j_1(\omega) \\ i_2(\omega) = Y_2(\omega)v_2(\omega) - j_2(\omega). \end{cases} \quad (1)$$

The conventions for the terminal voltages and currents are shown in Fig. 5. The expressions relating the matrix admittances Y_1 and Y_2 and vector current sources j_1 and j_2 to the transmission line characteristics are derived directly from the continuity conditions for the voltages and currents at the line terminals. To separate forward and backward waves and open the feedback loop, the current source j_1 must depend only on
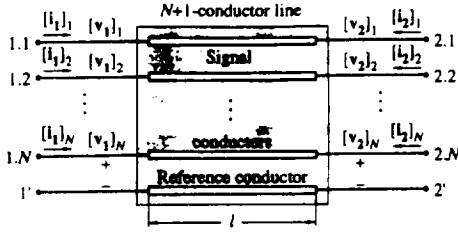
Fig. 5. Conventions for the voltages and currents at the line terminals.

the backward wave, and j_2 only on the forward wave. This condition uniquely defines Y_1, Y_2 and j_1, j_2 as follows:

$$Y_1(\omega) = Y_2(\omega) = Y_c(\omega) \tag{2}$$

and

$$\begin{cases} j_1(\omega) = 2i_{b1}(\omega) \\ j_2(\omega) = 2i_{f2}(\omega). \end{cases} \tag{3}$$

where Y_c stands for the characteristic admittance, and the forward and backward current waves, i_{f1}, i_{f2} and i_{b1}, i_{b2} are related as follows:

$$\begin{cases} i_{b1}(\omega) = W_{Ib}(\omega)[i_{b2}(\omega) = i_2(\omega) + i_{f2}(\omega)] \\ i_{f2}(\omega) = W_{If}(\omega)[i_{f1}(\omega) = i_1(\omega) + i_{b1}(\omega)]. \end{cases} \tag{4}$$

For uniform lines, the propagation functions for the forward and backward current waves are equal, $W_{If} = W_{Ib}$. The propagation function and characteristic admittance can be computed from the insertion loss data [15], scattering parameters [27], or distributed $RLGC$ parameters (see Appendix A).

As can be observed, for uniform lines, the open-loop device model (1)–(4) is equivalent to the generalized method of characteristics [12], [13], [15]. However, for nonuniform lines, the generalized method of characteristics no longer separates forward and backward waves and loses physical meaning [26].

B. Difference Approximation

To perform the transient analysis, indirect numerical integration [16] is applied to the propagation functions and characteristic admittances in the frequency-domain line model (1)–(4) by using the difference approximation method [19].

For the difference approximation in the parallel canonic form, samples of the frequency-domain transfer function are approximated with the rational polynomial function

$$\tilde{H}(j\omega) = \tilde{H}_\infty + \sum_{m=0}^{M} \frac{a_m}{1 + j\omega/\omega_{cm}}. \tag{5}$$

or samples of the time-domain unit-step response are approximated with the exponential series

$$\tilde{h}(t) = \tilde{H}_0 - \sum_{m=1}^{M} a_m e^{-\omega_{cm} t},$$

where $\tilde{H}_0$ and $\tilde{H}_\infty$ denote the initial and final values of the approximating transfer function $\tilde{H}(j\omega)$.

Once the approximation has been performed, indirect numerical integration formulas (discrete-time difference equations) are readily given in terms of the approximation parameters. For the step invariance the formulas are

$$\begin{cases} y(t_n) = \tilde{H}_\infty x(t_n) + \sum_{m=1}^{M} z_m(t_n) \\ z_m(t_n) = a_m(1 - e^{-\omega_{cm} T_n}) x(t_{n-1}) + e^{-\omega_{cm} T_n} z_m(t_{n-1}). \end{cases} \tag{6}$$

where x, y and z_m stand for the excitation, response and state variables, respectively, and $T_n = t_n - t_{n-1}$ is the time step at the nth transient iteration.

For the ramp invariance

$$\begin{cases} y(t_n) = \tilde{H}_0 x(t_n) - \sum_{m=1}^{M} z_m(t_n) \\ z_m(t_n) = d_m(T_n)(x(t_n) - x(t_{n-1})) + e^{-\omega_{cm} T_n} z_m(t_{n-1}). \end{cases} \tag{7}$$

where

$$d_m(T_n) = a_m \frac{1 - e^{-\omega_{cm} T_n}}{\omega_{cm} T_n}.$$

An alternative form of the ramp-invariant indirect numerical integration formula has the coefficients of the present-time sample of the excitation lumped together

$$\begin{cases} y(t_n) = \left(\tilde{H}_0 - \sum_{m=1}^{M} d_m(T_n) \right) x(t_n) - \sum_{m=1}^{M} z_m(t_n) \\ z_m(t_n) = (d_m(T_{n-1}) e^{-\omega_{cm} T_n} - d_m(T_n)) x(t_{n-1}) \\ \qquad + e^{-\omega_{cm} T_n} z_m(t_{n-1}). \end{cases} \tag{8}$$

This form is especially suitable for discretization of characteristic admittance, because, for admittances, the present- and past-time terms of the numerical integration formulas have different physical meanings.

Before the approximation, the delay is separated from the matrix propagation function using the matrix delay separation formulas from Appendix A, and is modeled separately using a low-order spline of the simulated time points. The difference approximation is applied to each element of the delayless propagation function and characteristic admittance matrices. For the characteristic admittances in (1), the excitations are the terminal voltages and the responses are the terminal currents. For the propagation functions in (4), the excitations and responses are the current waves.

Since the open-loop functions are aperiodic, they have to be approximated with only real poles, $-\omega_{cm}$. In addition, the poles have to negative to be assure stability.

To represent the original functions accurately with the minimum number of samples, the variation of the original function from sample to sample should be about the same. The following empirical formula for the sampling frequencies was found to provide good results

$$\omega_k = \omega_K \left(1 - \cos \frac{\pi k}{2K} \right). \qquad k = 0, 1, \cdots, K.$$

The end of the approximation interval, ω_K, should be chosen so that the original function would closely approach its

final value. This assures that the resulting indirect numerical integration formulas will be accurate in the full frequency and time ranges from zero to infinity.

C. Interpolation-Based Complex Rational Approximation Method for Frequency-Domain Difference Approximation

The method fits samples of a complex transfer function $H(\omega)$ with the rational polynomial function (5) at the set of arbitrary spaced frequencies $\{0, \omega_1, \omega_2, \cdots, \omega_K\}$. The method proceeds in three steps.

First, the real part of the original function is fit with the real part of the complex rational polynomial function, which is a real rational polynomial function of squared frequency [19]

$$Re(\tilde{H}(j\omega)) = \frac{c_0 + c_1\omega^2 + c_2(\omega^2)^2 + \cdots + c_M(\omega^2)^M}{1 + \beta_1\omega^2 + \beta_2(\omega^2)^2 + \cdots + \beta_M(\omega^2)^M}. \quad (9)$$

The following linear system of equations (10) (see bottom of the page) results from matching the real part of the original function with (9) at the set of frequencies and premultiplying both sides of each equation with the denominator For interpolation, $K = 2M$ and solving (10) produces a rational polynomial function which coincides with the real part of the original function at all of the sampling points. For a set of samples larger than $2M + 1$, the least square solution of (10) can be obtained. However, it minimizes the approximation error premultiplied by the denominator, which can lead to inaccurate approximation. Better results are achieved with the method of averages [28], which partitions the larger number of equations into $2M + 1$ subsets in the order of the increasing of ω. The equations within each subset are added up, which makes the system consistent. The method is effective in averaging out the noise in measured data.

After the real part has been approximated, the denominator of (9) is factored yielding the squared poles, $-\omega_{cm}^2$. Consequently, no unstable right-half-plane poles can be produced. However, there still can be spurious complex conjugate and purely imaginary poles, which are removed. The remaining real negative poles are used to formulate the equations for the partial expansion coefficients, a_m, of (5). As a result, the order M of (5) is less or equal to that of (9).

Matching the real and imaginary parts of the original transfer function $H(\omega)$ with the corresponding parts of (5) at the set of frequencies $\{0, \omega_1, \omega_2, \cdots, \omega_K\}$ leads to the following linear system of equations

$$A = \begin{pmatrix} \begin{bmatrix} 1 & 1 & \cdots & 1 \\ 1 & \dfrac{1}{1 + \omega_1^2/\omega_{c1}^2} & \cdots & \dfrac{1}{1 + \omega_1^2/\omega_{cM}^2} \\ & \vdots & & \\ 1 & \dfrac{1}{1 + \omega_K^2/\omega_{c1}^2} & \cdots & \dfrac{1}{1 + \omega_K^2/\omega_{cM}^2} \\ \hline 0 & \dfrac{-\omega_1/\omega_{c1}}{1 + \omega_1^2/\omega_{c1}^2} & \cdots & \dfrac{-\omega_1/\omega_{cM}}{1 + \omega_1^2/\omega_{cM}^2} \\ & \vdots & & \\ 0 & \dfrac{-\omega_K/\omega_{c1}}{1 + \omega_K^2/\omega_{c1}^2} & \cdots & \dfrac{-\omega_K/\omega_{cM}}{1 + \omega_K^2/\omega_{cM}^2} \end{bmatrix} \end{pmatrix}$$

$$\left(x = \begin{bmatrix} \tilde{H}_\infty \\ a_1 \\ a_2 \\ \vdots \\ a_M \end{bmatrix} \right) = b = \begin{bmatrix} H_0 \\ Re(H(\omega_1)) \\ \vdots \\ Re(H(\omega_K)) \\ \hline Im(H(\omega_1)) \\ \vdots \\ Im(H(\omega_K)) \end{bmatrix}. \quad (11)$$

For interpolation, $M = 2K$, and both real and imaginary parts of the original transfer function are matched exactly at all of the K frequency points and dc. For an arbitrary larger number of points, the least square solution of (11) is obtained from
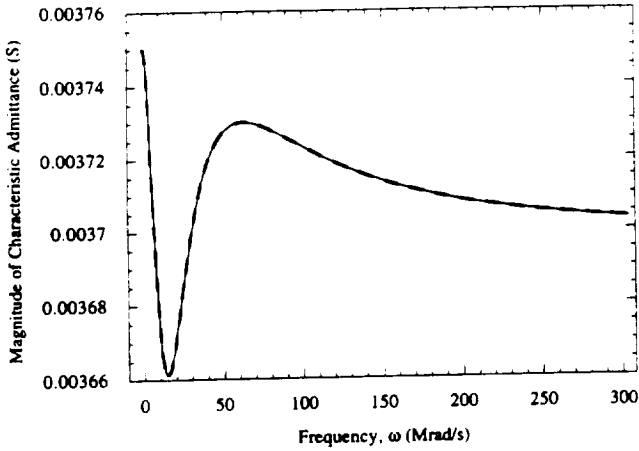
$$A^T A x = A^T b.$$

The total computational complexity of the approximation method is that of two real linear solutions and one polynomial factoring. The orders of the polynomial and linear systems depend only on the order of the approximation and not on the number of the original function samples. Since no iterative or relaxation techniques are involved, the method is free from convergence problems. The method can be extended to match exactly the initial and final values of the original function and to perform a complex-pole approximation [19].
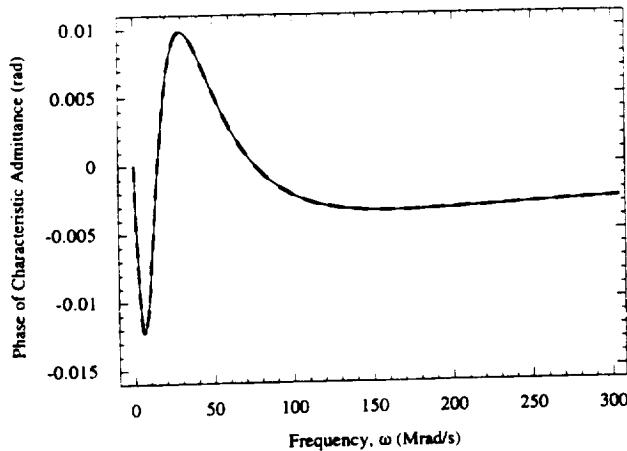
Fig. 6 shows an example of the fourth-order approximation of an open-loop transmission-line transfer function. As can be observed, although only nine samples of the original function were used, the approximation exhibits an excellent match in the full frequency range. In general, due to their simplicity, the open-loop functions can be accurately fit with the 3rd–9th-order approximation.

$$\begin{bmatrix} 1 & 0 & \cdots & 0 & 0 & \cdots & 0 \\ 1 & \omega_1^2 & \cdots & \omega_1^{2M} & -\omega_1^2 Re(H(\omega_1)) & \cdots & -\omega_1^{2M} Re(H(\omega_1)) \\ & & \vdots & & & \vdots & \\ 1 & \omega_K^2 & \cdots & \omega_K^{2M} & -\omega_K^2 Re(H(\omega_K)) & \cdots & -\omega_K^{2M} Re(H(\omega_K)) \end{bmatrix} \begin{bmatrix} c_0 \\ \vdots \\ c_M \\ \beta_1 \\ \vdots \\ \beta_M \end{bmatrix} = \begin{bmatrix} H_0 \\ Re(H(\omega_1)) \\ \vdots \\ Re(H(\omega_K)) \end{bmatrix} \quad (10)$$

$$\text{(14)}$$

(the KCL-at-node Modified Nodal Approach stamp matrix equation, with blocks $\hat{\mathbf{Y}}_1$ and $\hat{\mathbf{Y}}_2$)

Fig. 6. An example of the 4th-order complex rational approximation. The original function is shown by the thin continuous curves and the approximating function by the thick dashed curves.

D. Companion Model

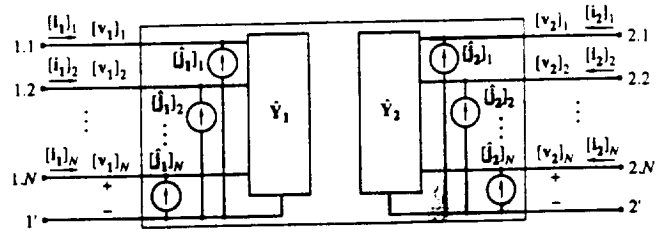By applying the difference approximation to the propagation function and characteristic admittance, the frequency-domain

Fig. 7. Companion model for a transmission line.

element characteristic (1) is transformed into the following discrete-time element characteristic, or companion model

$$\begin{cases} i_1(t_n) = \hat{Y}_1(t_n)v_1(t_n) - \hat{j}_1(t_n) \\ i_2(t_n) = \hat{Y}_2(t_n)v_2(t_n) - \hat{j}_2(t_n). \end{cases} \quad (12)$$

The circuit-diagram interpretation of the companion model is shown in Fig. 7.

The admittances $\hat{Y}_1$ and $\hat{Y}_2$ represent present-time coefficients in the indirect numerical integration formulas for the admittances Y_1 and Y_2. The current sources $\hat{j}_1$ and $\hat{j}_2$ combine the currents j_{Y_1} and j_{Y_2}, which correspond to the remaining parts of the numerical integration formulas for the admittances, and j_1 and j_2, which are given by the discretized (3) and (4)

$$\begin{cases} \hat{j}_1(t_n) = -j_{Y_1}(t_n) + j_1(t_n) \\ \hat{j}_2(t_n) = -j_{Y_2}(t_n) + j_2(t_n). \end{cases} \quad (13)$$

Equations (3) and (4) do not contribute to the admittance part of the companion model because the propagation functions contain a delay.

The Modified Nodal Approach (MNA) stamp corresponding to the companion model (12) is (see (14) at the top of the page).

In the circuit simulator during the transient analysis, the lines are represented by the tables of numbers (14), which are recursively updated at each time iteration using numerical integration. The left-hand side of the stamp (14) has to be updated only when the value of the time step changes. If the step-invariant indirect numerical integration formulas (6) are

$$
\text{KCL at node:}
\begin{array}{c}
1.1 \\ \vdots \\ 1.N \\ 1' \\ 2.1 \\ \vdots \\ 2.N \\ 2'
\end{array}
\left[
\begin{array}{ccc|c|ccc|c}
& & & -\sum_{j=1}^{N}[\mathbf{Y}_{11}]_{1j} & & & & -\sum_{j=1}^{N}[\mathbf{Y}_{12}]_{1j} \\
& \mathbf{Y}_{11} & & \vdots & & \mathbf{Y}_{12} & & \vdots \\
& & & -\sum_{j=1}^{N}[\mathbf{Y}_{11}]_{Nj} & & & & -\sum_{j=1}^{N}[\mathbf{Y}_{12}]_{Nj} \\ \hline
-\sum_{i=1}^{N}[\mathbf{Y}_{11}]_{i1} & \cdots & -\sum_{i=1}^{N}[\mathbf{Y}_{11}]_{iN} & \sum_{i=1}^{N}\sum_{j=1}^{N}[\mathbf{Y}_{11}]_{ij} & -\sum_{i=1}^{N}[\mathbf{Y}_{12}]_{i1} & \cdots & -\sum_{i=1}^{N}[\mathbf{Y}_{12}]_{iN} & \sum_{i=1}^{N}\sum_{j=1}^{N}[\mathbf{Y}_{12}]_{ij} \\ \hline
& & & -\sum_{j=1}^{N}[\mathbf{Y}_{21}]_{1j} & & & & -\sum_{j=1}^{N}[\mathbf{Y}_{22}]_{1j} \\
& \mathbf{Y}_{21} & & \vdots & & \mathbf{Y}_{22} & & \vdots \\
& & & -\sum_{j=1}^{N}[\mathbf{Y}_{21}]_{Nj} & & & & -\sum_{j=1}^{N}[\mathbf{Y}_{22}]_{Nj} \\ \hline
-\sum_{i=1}^{N}[\mathbf{Y}_{21}]_{i1} & \cdots & -\sum_{i=1}^{N}[\mathbf{Y}_{21}]_{iN} & \sum_{i=1}^{N}\sum_{j=1}^{N}[\mathbf{Y}_{21}]_{ij} & -\sum_{i=1}^{N}[\mathbf{Y}_{22}]_{i1} & \cdots & -\sum_{i=1}^{N}[\mathbf{Y}_{22}]_{iN} & \sum_{i=1}^{N}\sum_{j=1}^{N}[\mathbf{Y}_{22}]_{ij}
\end{array}
\right]
\left[
\begin{array}{c}
V_{1,1} \\ \vdots \\ V_{1,N} \\ V_{1'} \\ V_{2,1} \\ \vdots \\ V_{2,N} \\ V_{2'}
\end{array}
\right]
=
\left[
\begin{array}{c}
0 \\ \vdots \\ 0 \\ 0 \\ 0 \\ \vdots \\ 0 \\ 0
\end{array}
\right]
\tag{16}
$$

used, the LHS of the stamp becomes independent of the time step, and only the right-hand side vector has to be updated.

Since the terminal currents are not introduced as variables, the values of i_1 and i_2 in (4) are computed from (12).

E. Line Model for AC and DC Analyses

For ac and dc analyses, the complexity of the transfer functions is not important, and the element characteristic that does not require the introduction of current variables and is suitable for the ac/dc modeling of transmission lines is the Y-parameter characteristic

$$
\begin{cases}
i_1(\omega) = \mathbf{Y}_{11}(\omega)\mathbf{v}_1(\omega) + \mathbf{Y}_{12}(\omega)\mathbf{v}_2(\omega) \\
i_2(\omega) = \mathbf{Y}_{21}(\omega)\mathbf{v}_1(\omega) + \mathbf{Y}_{22}(\omega)\mathbf{v}_2(\omega).
\end{cases}
\tag{15}
$$

The Y-parameters are related to the open-loop functions as follows:

$$
\begin{aligned}
\mathbf{Y}_{11}(\omega) &= \mathbf{Y}_{22}(\omega) \\
&= \mathbf{Y}_c(\omega) + 2[\mathbf{I} - \mathbf{W}_I^2(\omega)]^{-1}\mathbf{W}_I^2(\omega)\mathbf{Y}_c(\omega). \\
\mathbf{Y}_{12}(\omega) &= \mathbf{Y}_{21}(\omega) = -2[\mathbf{I} - \mathbf{W}_I^2(\omega)]^{-1}\mathbf{W}_I(\omega)\mathbf{Y}_c(\omega),
\end{aligned}
$$

where $\mathbf{I}$ is the identity matrix. The expressions were derived by eliminating j_1 and j_2 from (1)–(4), and transforming them to the form of (15).

The dc model is merely the ac model at zero frequency. For the limiting case of lines with zero distributed conductance, $G = 0$, the dc values of the Y-parameters are

$$
\mathbf{Y}_{11}(0) = \mathbf{Y}_{22}(0) = -\mathbf{Y}_{12}(0) = -\mathbf{Y}_{21}(0) = \frac{1}{l}\mathbf{R}^{-1}.
$$

The MNA stamp corresponding to (15) is (see (16) at the top of the page).

F. Initial Conditions for Transient Analysis

The dc model is used to perform the operating-point (op) analysis before the transient simulation. The op solution is then used as the initial conditions for the transient analysis. The initial conditions for the indirect numerical integration are the dc values of the state variables, which are related to the dc

value of the excitation, x_0, as follows: $z_m(t_0) = a_m x_0$ for the step-invariant case (6), $z_m(t_0) = 0$ for the ramp-invariant case (7), and $z_m(t_0) = -d_m(T_1)x_0$ for the ramp-invariant case (8). The dc values of i_{f1} and i_{b2}, which serve as excitations for the propagation functions in (4), have to be expressed in terms of the terminal voltages obtained from the op analysis. Resolving (1)–(4) leads to

$$
\begin{cases}
i_{f1}(0) = [\mathbf{I} - \mathbf{W}_I^2(0)]^{-1}[\mathbf{Y}_c(0)\mathbf{v}_1(0) \\
\qquad - \mathbf{W}_I(0)\mathbf{Y}_c(0)\mathbf{v}_2(0)] \\
i_{b2}(0) = [\mathbf{I} - \mathbf{W}_I^2(1)]^{-1}[\mathbf{Y}_c(0)\mathbf{v}_2(0) \\
\qquad - \mathbf{W}_I(0)\mathbf{Y}_c(0)\mathbf{v}_1(0)].
\end{cases}
$$

For the limiting case of $G = 0$, the expressions become

$$
i_{f1}(0) = -i_{b2}(0) = \frac{1}{2l}\mathbf{R}^{-1}[\mathbf{v}_1(0) - \mathbf{v}_2(0)].
$$

G. Optimal Line Simulation Algorithm

For an MNA-based simulator, the optimal line simulation algorithm is as follows:

1) Before the transient analysis:
   a) Perform op analysis of the circuit to find the initial conditions for the transient analysis. Use the ac/dc model (15)–(16).
   b) For each line in the circuit, perform the difference approximation of each element of the propagation function and characteristic admittance matrices.
2) At each time iteration: Recursively update the line stamps using the indirect numerical integration formulas obtained at step 1(b) and companion model (12)–(14).

Since the method introduces neither additional nodes nor current variables, the optimal line modeling does not increase at all the circuit solution time. The only additional time is required to perform a low-order interpolation once in the beginning of the simulation, and for a low-order numerical integration. As shown in the next section, this time is negligibly small compared to the circuit solution time.

TABLE II
RELATIVE RUNTIMES

Number of Nodes	Circuit Description	Relative Runtime[a]				
		Lines Modeled with Lumped Resistors[b]	Lines Modeled with the Optimal Method			
			Total Circuit Simulation[c]	Indirect Numerical Integration[d]	Difference Approximation[d]	
					Frequency Domain	Time Domain[e]
10	2 two-conductor lines, 1 four-conductor line (lines and excitation sources only)	0.937	1.00	0.0927	0.0793	0.0550
10	2 two-conductor lines, 12 MOSFETs	1.00	1.00	$9.66 \cdot 10^{-3}$	$9.47 \cdot 10^{-3}$	$6.57 \cdot 10^{-3}$
100	20 two-conductor lines, 10 four-conductor lines (lines and excitation sources only)	0.999	1.00	$2.06 \cdot 10^{-3}$	$1.75 \cdot 10^{-3}$	$1.21 \cdot 10^{-3}$
1000	200 two-conductor lines, 100 four-conductor lines (lines and excitation sources only)	1.00	1.00	$1.64 \cdot 10^{-5}$	$1.39 \cdot 10^{-5}$	$9.64 \cdot 10^{-6}$

[a] For 1000 time points.

[b] One resistor per signal conductor.

[c] Does not include the difference approximation time.

[d] Seventh-order.

[e] Time-domain difference approximation was performed by the relaxation interpolation method [19]. The runtime includes automatic determination of the approximation interval and interpolation points.

H. Numerical Results

The optimal method has been adopted in several industrial and commercial circuit simulators, and, in numerous real-life simulation exercises, proved to be reliable, accurate and efficient. Table II presents relative runtime data for circuits of various types and sizes. As can be observed, even for the worst case of a small circuit consisting only of lines, the optimal model is virtually as efficient as the simple replacement of interconnects with lumped resistors. The resistive model was chosen for the comparison because it represents the limiting case in the simplicity and computational efficiency of the interconnect modeling.

Fig. 8 shows verification of the optimal model accuracy with the Spice3e2 lossy multiconductor line model [9]. A simple network was chosen as an example to reduce the influence of factors other than the line model on the simulation accuracy. A variable, third-to-fifth-order frequency-domain difference approximation was applied. As can be observed, the compared waveforms are indistinguishable. In fact, the accuracy of the optimal method depends exclusively on the accuracy of the difference approximation which is very high (see Table I). The runtime for the optimal model was three orders of magnitude shorter than that for the Spice model, which is, in turn, an order of magnitude faster than segmentation models.

IV. CONCLUSION

From a novel analysis, based on identification of the most significant aspects of the problem and comparison of alternative approaches in each of the aspects, it was shown that to achieve the maximum efficiency, accuracy and practical applicability, the line simulation should be based on: a time-only formulation, open-loop characterization, device model that does not require the introduction of current variables, in-
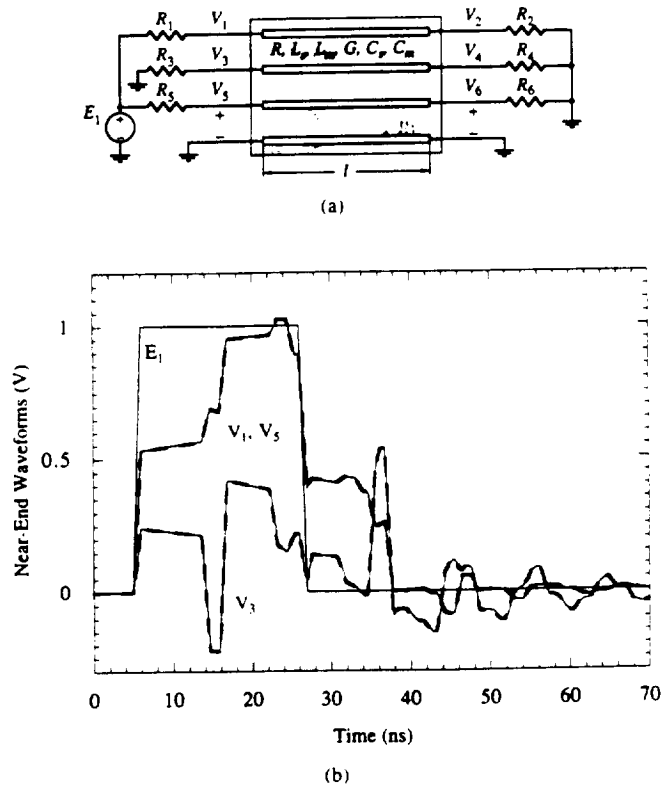

(a)

(b)

Fig. 8. (a) The network configuration and (b) comparison of the transient waveforms generated using the optimal line model installed in an MNA-based circuit simulator (thick broken curves) and Spice3e2 (thin continuous curves). $R_1 = R_5 = 50\ \Omega$. $R_2 = R_6 = 1\ k\Omega$. $R_3 = R_4 = 10\ M\Omega$. self-inductance $L_s = 418$ nH/m. self-capacitance $C_s = 94$ pF/m. mutual inductance $L_m = 125$ nH/m. mutual capacitance $C_m = 22$ pF/m. $R = 15\ \Omega/m$. $G = 0$. $l = 0.677$ m (all signal conductors are the same).

direct numerical integration, and frequency-domain difference approximation based on the interpolation and matrix delay separation.

TABLE III

Name of Function	Function for Current Waves[a]		Function for Voltage Waves[a]	
	In Standard Basis	In Modal Basis	In Standard Basis	In Modal Basis
Admittance and impedance per unit length	$Y(\omega) = G(\omega) + j\omega C(\omega)$ $= M_I(\omega)\, Y_m(\omega)\, M_V^{-1}(\omega)$	$Y_m(\omega)$ $= M_I^{-1}(\omega)\, Y(\omega)\, M_V(\omega)$	$Z(\omega) = R(\omega) + j\omega L(\omega)$ $= M_V(\omega)\, Z_m(\omega)\, M_I^{-1}(\omega)$	$Z_m(\omega)$ $= M_V^{-1}(\omega)\, Z(\omega)\, M_I(\omega)$
Modal transformation matrices	$M_I(\omega)$ $= \mathrm{Eigenvectors}(Y(\omega)\, Z(\omega)),$ $\hat{M}_I = M_I(\infty)$ $= \mathrm{Eigenvectors}(C(\infty)\, L(\infty))$	$M_I^{-1}(\omega) = M_V^T(\omega),$ $\hat{M}_I^{-1} = \hat{M}_V^T$	$M_V(\omega)$ $= \mathrm{Eigenvectors}(Z(\omega)\, Y(\omega)),$ $\hat{M}_V = M_V(\infty)$ $= \mathrm{Eigenvectors}(L(\infty)\, C(\infty))$	$M_V^{-1}(\omega) = M_I^T(\omega),$ $\hat{M}_V^{-1} = \hat{M}_I^T$
Characteristic admittance and impedance	$Y_c(\omega) = K_I(\omega)\, Z^{-1}(\omega)$ $= K_I^{-1}(\omega)\, Y(\omega) = Z_c^{-1}(\omega)$ $= M_I(\omega)\, Y_{cm}(\omega)\, M_V^{-1}(\omega)$	$Y_{cm}(\omega) = \left(Z_m^{-1}(\omega)\, Y_m(\omega)\right)^{\frac{1}{2}}$ $= K_{Im}^{-1}(\omega)\, Y_m(\omega) = Z_{cm}^{-1}(\omega)$ $= M_I^{-1}(\omega)\, Y_c(\omega)\, M_V(\omega)$	$Z_c(\omega) = K_V(\omega)\, Y^{-1}(\omega)$ $= K_V^{-1}(\omega)\, Z(\omega) = Y_c^{-1}(\omega)$ $= M_V(\omega)\, Z_{cm}(\omega)\, M_I^{-1}(\omega)$	$Z_{cm}(\omega) = \left(Y_m^{-1}(\omega)\, Z_m(\omega)\right)^{\frac{1}{2}}$ $= K_{Vm}^{-1}(\omega)\, Z_m(\omega) = Y_{cm}^{-1}(\omega)$ $= M_V^{-1}(\omega)\, Z_c(\omega)\, M_I(\omega)$
Propagation constant[b]	$K_I(\omega) = \left(Y(\omega)\, Z(\omega)\right)^{\frac{1}{2}}$ $= Y(\omega)\, Y_c^{-1}(\omega)$ $= M_I(\omega)\, K_{Im}(\omega)\, M_I^{-1}(\omega)$	$K_{Im}(\omega) = \left(Y_m(\omega)\, Z_m(\omega)\right)^{\frac{1}{2}}$ $= Y_m(\omega)\, Y_{cm}^{-1}(\omega)$ $= \mathrm{Eigenvalues}(K_I(\omega))$ $= M_I^{-1}(\omega)\, K_I(\omega)\, M_I(\omega)$ $= K_{Vm}(\omega)$	$K_V(\omega) = \left(Z(\omega)\, Y(\omega)\right)^{\frac{1}{2}}$ $= Z(\omega)\, Z_c^{-1}(\omega)$ $= M_V(\omega)\, K_m(\omega)\, M_V^{-1}(\omega)$	$K_{Vm}(\omega) = \left(Z_m(\omega)\, Y_m(\omega)\right)^{\frac{1}{2}}$ $= Z_m(\omega)\, Z_{cm}^{-1}(\omega)$ $= \mathrm{Eigenvalues}(K_V(\omega))$ $= M_V^{-1}(\omega)\, K_V(\omega)\, M_V(\omega) =$ $= K_{Im}(\omega)$
Propagation delay[b]	$T_I = \left(C(\infty)\, L(\infty)\right)^{\frac{1}{2}} l$ $= K_I(\infty)\, l = \hat{M}_I\, T_{Im}\, \hat{M}_I^{-1}$	$T_{Im} = K_{Im}(\infty)\, l$ $= \mathrm{Eigenvalues}(T_I)$ $= \hat{M}_I^{-1}\, T_I\, \hat{M}_I = T_{Vm}$	$T_V = \left(L(\infty)\, C(\infty)\right)^{\frac{1}{2}} l$ $= K_V(\infty)\, l = \hat{M}_V\, T_{Vm}\, \hat{M}_V^{-1}$	$T_{Vm} = K_{Vm}(\infty)\, l$ $= \mathrm{Eigenvalues}(T_V)$ $= \hat{M}_V^{-1}\, T_V\, \hat{M}_V = T_{Im}$
Propagation function[b]	$W_I(\omega) = e^{-K_I(\omega) l}$ $= M_I(\omega)\, W_{Im}(\omega)\, M_I^{-1}(\omega)$ $= Y_c(\omega)\, W_V(\omega)\, Z_c(\omega)$ $= \hat{W}_I(\omega)\, e^{-j\omega T_I}$ $= \hat{W}_I(\omega)\, \hat{M}_I\, e^{-j\omega T_{Im}}\, \hat{M}_I^{-1}$	$W_{Im}(\omega) = e^{-K_{Im}(\omega) l}$ $= M_I^{-1}(\omega)\, W_I(\omega)\, M_I(\omega)$ $= W_{Vm}(\omega)$	$W_V(\omega) = e^{-K_V(\omega) l}$ $= M_V(\omega)\, W_{Vm}(\omega)\, M_V^{-1}(\omega)$ $= Z_c(\omega)\, W_I(\omega)\, Y_c(\omega)$ $= \hat{W}_V(\omega)\, e^{-j\omega T_V}$ $= \hat{W}_V(\omega)\, \hat{M}_V\, e^{-j\omega T_{Vm}}\, \hat{M}_V^{-1}$	$W_{Vm}(\omega) = e^{-K_{Vm}(\omega) l}$ $= M_V^{-1}(\omega)\, W_V(\omega)\, M_V(\omega)$ $= W_{Im}(\omega)$
Delayless propagation function[b]	$\hat{W}_I(\omega) = W_I(\omega)\, e^{j\omega T_I}$		$\hat{W}_V(\omega) = W_V(\omega)\, e^{j\omega T_V}$	
Transmission coefficient[c]	$T_I(\omega) = \left(I + Y_t(\omega)\, Z_c(\omega)\right)^{-1}$ $= Y_c(\omega)\, T_V(\omega)\, Z_t(\omega)$		$T_V(\omega) = \left(I + Z_t(\omega)\, Y_c(\omega)\right)^{-1}$ $= Z_c(\omega)\, T_I(\omega)\, Y_t(\omega)$	
Reflection coefficient[c]	$\Gamma_I(\omega) = \left(I + Y_t(\omega)\, Z_c(\omega)\right)^{-1}$ $\cdot\left(I - Y_t(\omega)\, Z_c(\omega)\right)$ $= Y_c(\omega)\, \Gamma_V(\omega)\, Z_c(\omega)$		$\Gamma_V(\omega) = \left(Z_t(\omega)\, Y_c(\omega) + I\right)^{-1}$ $\cdot\left(Z_t(\omega)\, Y_c(\omega) - I\right)$ $= Z_c(\omega)\, \Gamma_I(\omega)\, Y_c(\omega)$	

[a] Voltage and current functions are related via the following duality replacement rules: $V \leftrightarrow I$, $Z \leftrightarrow Y$, $R \leftrightarrow G$, $L \leftrightarrow C$.

[b] Boldface $(.)^{\frac{1}{2}}$ and $e^{(.)}$ denote matrix squre root and matrix exponential, respectively.

[c] For a Thevenin's termination $Z_t(\omega)$.

The practical implementation of the optimal method for multiconductor lossy frequency-dependent lines characterized by discrete samples of their responses was outlined, including extraction of initial conditions from op analysis and the line model for ac/dc analysis. The complete set of expressions for the open-loop transmission-line functions was given, including new formulas for the matrix delay separation from the propagation functions, which avoid the use of frequency-dependent modal transformation matrices. The complete set of analytical expressions for the fundamental open-loop time-domain responses of two-conductor lines was presented, including a new simple and accurate asymptotic approximation for the responses of propagation function. The novel interpolation-based complex rational approximation method was introduced, and ramp- and step-invariant indirect numerical formulas were given in terms of the approximation parameters.

TABLE IV

Name of Function	G	Transient Characteristic, $h(t)$	Impulse Characteristic, $g(t)$
Propagation function, $W(\omega)$[a]	Arbitrary G	$h_w(t) = \left(e^{-\alpha} + a \int_\tau^t e^{-\beta t} \dfrac{I_1(b\sqrt{t^2-\tau^2})}{\sqrt{t^2-\tau^2}}\, dt \right) u(t-\tau)$	$g_w(t) = e^{-\alpha}\delta(t) + a\, e^{-\beta t}\dfrac{I_1(b\sqrt{t^2-\tau^2})}{\sqrt{t^2-\tau^2}}\, u(t-\tau)$
	$G=0$	$h_w(t) \approx \left(1 - \dfrac{2a}{\sqrt{2\pi b(t+d)}}\right)u(t-\tau)$[b]	$g_w(t) \approx e^{-\alpha}\delta(t) + \dfrac{a}{(2\pi b(t+d))^{3/2}}\, u(t-\tau)$[b]
Characteristic admittance, $Y_c(\omega)$[c]	Arbitrary G	$h_Y(t) = Y_0\left(e^{-\beta t} I_0(bt) + \dfrac{G}{C}\int_0^t e^{-\beta t} I_0(bt)\, d\tau\right)$	$g_Y(t) = Y_0\left\{\delta(t) + e^{-\beta t}\left[\left(\dfrac{G}{C}-\beta\right)I_0(bt) + b\,I_1(bt)\right]\right\}$
	$G=0$	$h_Y(t) = Y_0\, e^{-\beta t} I_0(\beta t)$	$g_Y(t) = Y_0\left\{\delta(t) + \beta\, e^{-\beta t}\left[I_1(\beta t) - I_0(\beta t)\right]\right\}$
Transmission coefficient for voltage waves, $T_v(\omega)$[c, d]	Arbitrary G	$h_T(t) = \dfrac{Z_0}{R_t^2 - Z_0^2}\left\{-Z_0\left[\dfrac{R}{cL} + \left(1-\dfrac{R}{cL}\right)e^{-ct}\right]\right.$ $\left. + R_t\left[e^{-\beta t}I_0(bt) + (2\beta - c)e^{-ct}\int_0^t e^{(\beta-c)\tau}I_0(bt)\, d\tau\right.\right.$ $\left.\left. + \dfrac{RG}{LC}\int_{\tau=0}^t e^{-c\tau}\int_{\tau=0}^\tau e^{(\beta-c)\tau}I_0(bt)\, d\tau\, d\tau'\right]\right\}$	$g_T(t) = \dfrac{Z_0}{R_t + Z_0}\delta(t) + \dfrac{Z_0}{R_t^2 - Z_0^2}\left\{Z_0\left(c-\dfrac{R}{L}\right)e^{-ct}\right.$ $+ R_t\left[e^{-\beta t}\left[(\beta-c)I_0(bt) + b\,I_1(bt)\right]\right.$ $\left.\left. + \left(c(c-2\beta) + \dfrac{RG}{LC}\right)e^{-ct}\int_0^t e^{(\beta-c)\tau}I_0(bt)\, d\tau\right]\right\}$
	$G=0$	$h_T(t) = \dfrac{Z_0}{R_t^2 - Z_0^2}\left\{-Z_0\left[\dfrac{R}{cL} + \left(1-\dfrac{R}{cL}\right)e^{-ct}\right]\right.$ $\left. + R_t\left[e^{-\beta t}I_0(bt) + (2\beta - c)e^{-ct}\int_0^t e^{(\beta-c)\tau}I_0(bt)\, d\tau\right]\right\}$	$g_T(t) = \dfrac{Z_0}{R_t + Z_0}\delta(t) + \dfrac{Z_0}{R_t^2 - Z_0^2}\left\{Z_0\left(c-\dfrac{R}{L}\right)e^{-ct}\right.$ $+ R_t\left[e^{-\beta t}\left[(\beta-c)I_0(bt) + b\,I_1(bt)\right]\right.$ $\left.\left. + c(c-2\beta)e^{-ct}\int_0^t e^{(\beta-c)\tau}I_0(bt)\, d\tau\right]\right\}$
Reflection coefficient, $\Gamma(\omega)$[a]		$h_\Gamma(t) = 1 - 2h_T(t)$	$g_\Gamma(t) = \delta(t) - 2g_T(t)$

N o t e : $u(t)$ is the unit-step function, $\alpha = \frac{1}{2}\left(GZ_0 + \frac{R}{Z_0}\right)l$, $a = \frac{1}{2}\left|GZ_0 - \frac{R}{Z_0}\right|l$, $\beta = \frac{1}{2}\left(\frac{G}{C}+\frac{R}{L}\right)$, $b = \frac{1}{2}\left|\frac{G}{C}-\frac{R}{L}\right|$,

$c = -\dfrac{R}{L}\dfrac{Z_0^2}{R_t^2 - Z_0^2}$, $d = \dfrac{4a^2}{2\pi b(1-e^{-\alpha})^2}$, $\tau = \sqrt{CL}\, l$, $Y_0 = \sqrt{\frac{C}{L}}$, and $Z_0 = \sqrt{\frac{L}{C}}$. For $G=0$: $\alpha = a = \dfrac{Rl}{2Z_0}$ and $\beta = b = \dfrac{R}{2L}$.

[a] In the case of two-conductor lines, this functions are the same for both voltage and current waves.

[b] Approximation based on the asymptotic expansion of the modified Bessel function $I_1(x)$. It is within 1% accurate in the full time range.

[c] Expressions for the corresponding dual (voltage/current) functions can be obtained via the duality replacement rules (see Appendix A).

[d] For a Thevenin's termination R_t.

The optimal method is compatible with recursive time-domain solvers employed by circuit simulators and supports variable time-stepping. The method has been adopted in several industrial and commercial circuit simulators. and, in numerous real-life simulation exercises, proved to be reliable and accurate. It was shown on an extensive set of runtime data that, based on the optimal approach, accurate line modeling in a circuit simulator is as efficient as a simple replacement of interconnects with lumped resistors.

APPENDIX A
OPEN-LOOP TRANSMISSION-LINE TRANSFER FUNCTIONS

See Table III.

APPENDIX B
TIME-DOMAIN OPEN-LOOP RESPONSES OF CONSTANT-PARAMETER TWO-CONDUCTOR LINES

See Table IV.

ACKNOWLEDGMENT

REFERENCES

[1] T. Dhaene. L. Martens. and D. De Zutter. "Transient simulation of arbitrary nonuniform interconnection structures characterized by scattering

parameters." *IEEE Trans. Circuits Syst.*, vol. 39, pp. 928–937, Nov. 1992.

[2] J. E. Bracken, V. Raghavan, and R. A. Rohrer, "Interconnect simulation with asymptotic waveform evaluation (AWE)," *IEEE Trans. Circuits Syst.*, vol. 39, pp. 869–878, Nov. 1992.

[3] T. Dhaene and D. De Zutter, "Selection of lumped element models for coupled lossy transmission lines," *IEEE Trans. Computer-Aided Design*, vol. 11, pp. 805–815, July 1992.

[4] K. S. Oh and J. E. Schutt-Aine, "Transient analysis of coupled, tapered transmission lines with arbitrary nonlinear terminations," *IEEE Trans. Microwave Theory Tech.*, vol. 41, pp. 268–273, Feb. 1993.

[5] D. B. Kuznetsov, "Transmission line modeling and transient simulation," M.S. thesis, Univ. Illinois at Urbana, 1993.

[6] J. E. Schutt-Aine and R. Mittra, "Nonlinear transient analysis of coupled transmission lines," *IEEE Trans. Circuits Syst.*, vol. 36, pp. 959–967, Jul. 1989.

[7] I. Maio, S. Pignari, and F. Canavero, "Influence of the line characterization on the transient analysis of nonlinearly loaded lossy transmission lines," *IEEE Trans. Circuits Syst.*, vol. 41, pp. 197–209, Mar. 1994.

[8] F. Romeo and M. Santomauro, "Time-domain simulation of n coupled transmission lines," *IEEE Trans. Microwave Theory Tech.*, vol. MTT-35, pp. 131–137, Feb. 1987.

[9] J. S. Roychowdhury and D. O. Pederson, "Efficient transient simulation of lossy interconnect," in *Proc. 28th ACM/IEEE Design Automat. Conf.*, 1991, pp. 740–745.

[10] F.-Y. Chang, "Transient analysis of lossy transmission lines with arbitrary initial potential and current distributions," *IEEE Trans. Circuits Syst.*, vol. 39, pp. 180–198, Mar. 1992.

[11] F. H. Branin, Jr., "Transient analysis of lossless transmission lines," *Proc. IEEE*, vol. 55, pp. 2012–2013, Nov. 1967.

[12] F.-Y. Chang, "Transient simulation of nonuniform coupled lossy transmission lines characterized with frequency-dependent parameters, Part I: Waveform relaxation analysis," *IEEE Trans. Circuits Syst.*, vol. 39, pp. 585–603, Aug. 1992.

[13] F.-Y. Chang, "Transient simulation of frequency-dependent nonuniform coupled lossy transmission lines," *IEEE Trans. Compon. Pack. Manufact. Technol.*, vol. 17, pp. 3–14, Feb. 1994.

[14] J. E. Bracken, V. Raghavan, and R. A. Rohrer, "Extension of the asymptotic waveform evaluation technique with the method of characteristics," in *Tech. Dig. IEEE Int. Conf. Computer-Aided Design*, 1992, pp. 71–75.

[15] A. J. Gruodis and C. S. Chang, "Coupled lossy transmission line characterization and simulation," *IBM J. Res. Develop.*, vol. 25, pp. 25–41, Jan. 1981.

[16] D. B. Kuznetsov and J. E. Schutt-Aine, "Indirect numerical integration," to be published.

[17] A. Semlyen and A. Dabuleanu, "Fast and accurate switching transient calculations on transmission lines with ground return using recursive convolutions," *IEEE Trans. Power Appar. Syst.*, vol. PAS-94, pp. 561–569, Mar./Apr. 1975.

[18] T. K. Tang, M. S. Nakhla, and R. Griffith, "Analysis of lossy multiconductor transmission lines using the asymptotic waveform evaluation technique," *IEEE Trans. Microwave Theory Tech.*, vol. 39, pp. 2107–2116, Dec. 1991.

[19] D. B. Kuznetsov and J. E. Schutt-Aine, "Difference approximation," to be published.

[20] C. R. Paul, "On uniform multimode transmission lines," *IEEE Trans. Microwave Theory Tech.*, pp. 556–558, Aug. 1973.

[21] S. L. Marple, Jr., *Digital Spectral Analysis.* Englewood Cliffs, NJ: Prentice-Hall, 1987, pp. 303–349.

[22] Y. Hua and T. K. Sarkar, "Generalized pencil-of-function method for extracting poles of an EM system from its transient response," *IEEE Trans. Antennas Propagat.*, vol. 37, pp. 229–234, Feb. 1989.

[23] C.-E. Froberg, *Numerical Mathematics: Theory and Computer Applications.* Menlo Park, CA: Benjamin/Cummings, 1985.

[24] A. Ralston and P. Rabinowitz, *A First Course in Numerical Analysis.* 2nd ed. New York: McGraw-Hill, 1978.

[25] L. T. Pillage and R. A. Rohrer, "Asymptotic waveform evaluation for timing analysis," *IEEE Trans. Computer-Aided Design*, vol. 9, pp. 352–366, Apr. 1990.

[26] D. B. Kuznetsov and J. E. Schutt-Aine, "Efficient circuit simulation of nonuniform transmission lines," to be published.

[27] J. E. Schutt-Aine, "Modeling and simulation of high-speed digital circuit interconnections," Ph.D. dissertation, Univ. Illinois at Urbana, 1988.

[28] I. N. Bronshteyn and K. A. Semendyaev. *Spravochnik po matematike.* Moscow: Nauka, 1967, p. 578. (in Russian).

Dmitri Borisovich Kuznetsov (S'95) was born on June 26, 1966, in Moscow, U.S.S.R. He received the Dipl. Ing. degree *summa cum laude*, in electronics engineering with a specialization in space electronics from the Moscow Electrotechnical Institute of Telecommunication, Department of Automatics, Telemechanics and Electronics, in 1988. He received the M.S. degree in 1993 from the University of Illinois at Urbana and is currently pursuing the Ph.D. degree.

From 1987 to 1991 he worked as an electronics engineer at the Space Research Institute, Academy of Sciences of the U.S.S.R., Moscow, on the design, manufacturing, testing, maintenance and repair of computer graphics systems. From 1988 to 1991 he attended the post-graduate school of the Space Research Institute, specializing in the information and measuring systems in space research. Since 1991 he has conducted research in computational electronics, transient simulation, and transmission line modeling at the Department of Electrical and Computer Engineering, University of Illinois at Urbana.

Jose E. Schutt-Aine (M'88) received the B.S. degree from the Massachusetts Institute of Technology in 1981, and the M.S. and Ph.D. degrees from the University of Illinois in 1984 and 1988, respectively.

Following his graduation from MIT he spent two years with the Hewlett-Packard Microwave Technology Center in Santa Rosa, CA, where he worked as a device application engineer. While pursuing his graduate studies at the University of Illinois, he held summer positions at GTE Network Systems in Northlake, Illinois. He is presently serving on the faculty of the Department of Electrical and Computer Engineering at the University of Illinois as an Associate Professor. His interests include microwave theory and measurements, electromagnetics, high-speed digital circuits, solid-state electronics, circuit design, and electronic packaging.

Capacitance Computations in a Multilayered Dielectric Medium Using Closed-Form Spatial Green's Functions

Kyung Suk Oh, *Student Member, IEEE*, Dmitri Kuznetsov, and Jose E. Schutt-Aine, *Member, IEEE*

Abstract— An efficient method to compute the 2-D and 3-D capacitance matrices of multiconductor interconnects in a multilayered dielectric medium is presented. The method is based on an integral equation approach and assumes the quasi-static condition. It is applicable to conductors of arbitrary polygonal shape embedded in a multilayered dielectric medium with possible ground planes on the top or bottom of the dielectric layers. The computation time required to evaluate the space-domain Green's function for the multilayered medium, which involves an infinite summation, has been greatly reduced by obtaining a closed-form expression, which is derived by approximating the Green's function using a finite number of images in the spectral domain. Then the corresponding space-domain Green's functions are obtained using the proper closed-form integrations. In both 2-D and 3-D cases, the unknown surface charge density is represented by pulse basis functions, and the delta testing function (point matching) is used to solve the integral equation. The elements of the resulting matrix are computed using the closed-form formulation, avoiding any numerical integration. The presented method is compared with other published results and showed good agreement. Finally, the equivalent microstrip crossover capacitance is computed to illustrate the use of a combination of 2-D and 3-D Green's functions.

I. INTRODUCTION

IN recent years, the characterization of microstrip discontinuities in a multilayered dielectric medium by equivalent circuits has gained special interest due to the modern development of VLSI technology. For an inhomogeneous structure the modes are hybrid, and the full-wave analysis must be considered. However, the quasi-static approximation is sufficiently correct when the transverse components of the electric and magnetic fields are predominant over the longitudinal components; in other words, the transverse dimensions of microstrip lines are much smaller than the wavelength. Based on this quasi-static approximation, we present an efficient method to compute the 2-D and 3-D capacitance matrices of multiconductor interconnects in a multilayered dielectric medium.

Under the quasi-TEM approximation, the capacitance calculation follows from the solution of Laplace's equation with appropriate boundary conditions. Various methods have been employed to obtain the solution in two-dimensional space [1]-[9]. Two commonly used techniques for both 2-D

and 3-D capacitance calculations in multilayered structures are the integral equation method [10], [11] and the domain methods, such as the finite difference and finite element methods [12], [13]. In the domain methods, the unknown potential distribution is solved to compute the capacitance over an entire domain by either directly approximating the differential equation with the finite difference equation (FD) or using the equivalent variational expression in conjunction with the method of subareas (FEM). The major disadvantage of the domain methods is that the unknown potential distribution to be sought is over the entire geometry considered, including the dielectric regions; hence, it may be computationally inefficient for the open geometry case even with the use of absorbing boundary conditions to truncate the open geometry. On the other hand, the integral equation approach first obtains the Green's function for a layered medium using image theory, which consists of rather slowly converging infinite series, and solves for the charge density on the conductor surfaces using this Green's function as its kernel. As noted in [2] for N layers, the expression for the Green's function would consist of $N - 1$ infinite series. Alternatively, the free-space Green's function is used in [2], [3] to avoid infinite series, but additional unknown charges on the dielectric interface and ground planes, on top of the unknown charges on the conductor surface, must be included. Hence, the dimension of the resulting moment matrix is substantially increased.

Yet another approach to avoid an infinite summation is to solve the integral equation in the spectral domain (SDA), where the Green's function is in a closed-form expression; however, this approach can not be applied to general problems, e.g., conductor with a finite thickness. In this paper, the Green's function for the layered medium is approximated in the spectral domain using exponential functions, which is equivalent to a finite number of weighted real images in the space domain. Although complex-valued exponentials, which are often used in a nonquasi-TEM analysis [14], can also be employed to reduce the number of weighted images [15], real-valued exponentials are sufficient to approximate for quasi-TEM applications, and it further avoids the use of expensive complex operations. Since the spectral-domain representations of the Green's function for 2-D and 3-D cases are identical, the approximation is only performed once for both cases, and then the equivalent weighted images in the spectral domain are directly used to evaluate the Green's functions in the space domain.
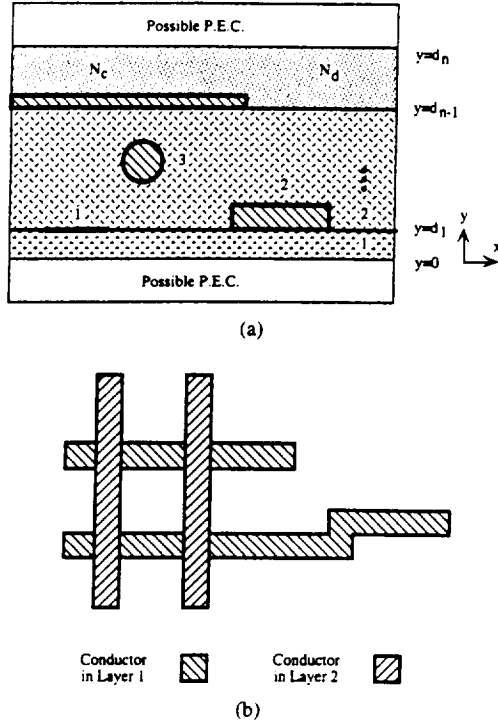
(a)

(b)

Fig. 1. (a) Cross-sectional and (b) planar views of possible configurations of multiconductors in a multilayered medium. The two figures are not related.

II. GENERAL STATEMENT OF THE PROBLEM

The general geometries of systems of multiconductors embedded in a multilayered medium are illustrated in Fig. 1; (a) shows a possible cross-sectional view while (b) shows a possible planar view. An arbitrary number N_d of nonmagnetic dielectric layers are backed by two optional ground planes with possible top or bottom locations, and within these layers an arbitrary number N_c of perfect conductors are placed throughout the layers with arbitrary orientations and possible discontinuities. The geometries of the dielectric layers are assumed to be uniform in the x- and z-directions, and the cross sections and planar geometries of the conductors can be arbitrary as long as their boundaries can be described with a piecewise linear function.

The integral equation relating the electrostatic potential $V(r)$ to the charge density $\rho(r)$ is

$$V(r) = \int_\Omega G(r, r')\rho(r')dr' \qquad (1)$$

where $G(r, r')$ is the Green's function for the multilayered medium, and Ω denotes the surfaces or cross-sectional boundaries of conductors for 2-D or 3-D problems, respectively. The capacitance can be computed by solving this integral equation for the charge density $\rho(r')$ with various settings of voltages on the conductors. We will first concentrate on the determination of the Green's function $G(r, r')$.

III. APPROXIMATION OF THE SPECTRAL-DOMAIN GREEN'S FUNCTION

Consider a unit point charge located at the mth layer at (x_0, y_0, z_0) (Fig. 2). By definition, the 3-D Green's function
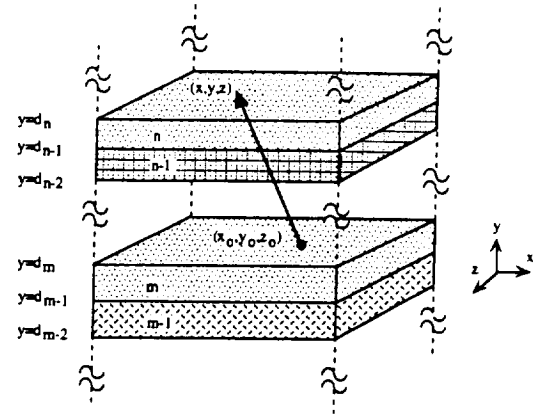

Fig. 2. the geometric configuration used for determining the Green's function.

satisfies Poisson's differential equation:

$$\nabla^2 G^{3D}(x, y, z \mid x_0, y_0, z_0) = \frac{1}{\varepsilon}\delta(x - x_0)\delta(y - y_0)\delta(z - z_0) \qquad (2)$$

with the appropriate boundary conditions at the possible ground planes and dielectric interfaces. Noting that the dielectric medium is uniform in two directions, we can represent the Green's function and the point source in the spectral domain in terms of its transforms in the x- and z-directions. The space-domain and the spectral domain Green's functions are then related by

$$G^{3D}(x, y, z \mid x_0, y_0, z_0)$$
$$= \frac{1}{(2\pi^2)}\int_{-\infty}^{+\infty}\int_{-\infty}^{+\infty} d\alpha d\beta e^{-j\alpha(x-x_0)-j\beta(z-z_0)}$$
$$\times \tilde{G}^{3D}(\alpha, y, \beta \mid x_0, y_0, z_0) \qquad (3a)$$

$$\tilde{G}^{3D}(\alpha, y, \beta \mid x_0, y_0, z_0)$$
$$= \int_{-\infty}^{+\infty}\int_{-\infty}^{+\infty} dx dz e^{j\alpha(x-x_0)+j\beta(z-z_0)}$$
$$\times G^{3D}(x, y, z \mid x_0, y_0, z_0) \qquad (3b)$$

where $\tilde{G}^{3D}(\alpha, y, \beta \mid x_0, y_0, z_0)$ is the 3-D spectral-domain Green's function and α and β are the transform constants associated with the x and z directions, respectively. Then, (2) can be written as

$$\left(\frac{\partial^2}{\partial y^2} - \alpha^2 - \beta^2\right)\tilde{G}^{3D}(\alpha, y, \beta \mid x_0, y_0, z_0) = \frac{1}{\varepsilon}\delta(y - y_0). \qquad (4)$$

The general solution of the above equation is given by

$$\tilde{G}^{3D}(\gamma, y \mid r_0) = \frac{A_{m,n}e^{-\gamma y} + B_{m,n}e^{\gamma y}}{2\varepsilon_m\gamma}, \quad \gamma = \sqrt{\alpha^2 + \beta^2} \qquad (5)$$

where the first subscript m denotes the layer where the source is located (source point), while the second subscript n denotes the layer where the Green's function is evaluated (observation point). The same expression can be obtained by Fourier transforming $G^{2D}(x, y \mid x_0, y_0)$ in the x-direction

with the transform variable γ. Furthermore, since the unknown coefficients $A_{m,n}$ and $B_{m,n}$ are to be determined using the boundary conditions in the y-direction only, it is easily seen that the expressions for $\tilde{G}^{2D}$ and $\tilde{G}^{3D}$ must be identical under our Fourier transformations. Thus, in what follows, we will omit the superscripts for the spectral-domain Green's functions. Applying the boundary conditions at the dielectric interface and ground planes, (5) can be written as

$$\tilde{G}(\gamma, y \mid r_0) = \frac{A_{m,n}^+}{2\varepsilon_m \gamma}\left(e^{-\gamma 0y} + \tilde{\Gamma}_{n,n+1}e^{-2\gamma d_n + \gamma y}\right) \quad y \geq y_0 \tag{6a}$$

$$\tilde{G}(\gamma, y \mid r_0) = \frac{A_{m,n}^-}{2\varepsilon_m \gamma}\left(e^{+\gamma y} + \tilde{\Gamma}_{n,n-1}e^{+2\gamma d_n - \gamma y}\right) \quad y \leq y_0 \tag{6b}$$

where

$$A_{m,n}^+ = A_{m,m}^+ \prod_{j=m}^{n-1} S_{j,j+1}^+$$

$$A_{m,n}^- = A_{m,m}^- \prod_{j=n+1}^{m} S_{j,j-1}^- \tag{7}$$

$$S_{j,j+1}^+ = \frac{T_{j,j+1}}{1 - \Gamma_{j+1,j}\tilde{\Gamma}_{j+1,j+2}e^{2\gamma(d_j - d_{j+1})}}$$

$$S_{j,j-1}^- = \frac{T_{j,j-1}}{1 - \Gamma_{j-1,j}\tilde{\Gamma}_{j-1,j-2}e^{2\gamma(d_{j-1} - d_j)}} \tag{8}$$

$$\tilde{\Gamma}_{j,j+1} = \frac{\Gamma_{j,j+1} + \tilde{\Gamma}_{j+1,j+2}e^{2\gamma(d_j - d_{j+1})}}{1 + \Gamma_{j,j+1}\tilde{\Gamma}_{j+1,j+2}e^{2\gamma(d_j - d_{j+1})}}$$

$$\tilde{\Gamma}_{j,j-1} = \frac{\Gamma_{j,j-1} + \tilde{\Gamma}_{j-1,j-2}e^{2\gamma(d_{j-2} - d_{j-1})}}{1 + \Gamma_{j,j-1}\tilde{\Gamma}_{j-1,j-2}e^{2\gamma(d_{j-2} - d_{j-1})}} \tag{9a}$$

$$\Gamma_{i,j} = \frac{\varepsilon_i - \varepsilon_j}{\varepsilon_i + \varepsilon_j} \qquad T_{i,j} = \frac{2\varepsilon_i}{\varepsilon_i + \varepsilon_j}. \tag{9b}$$

Here, $\tilde{\Gamma}_{j,j+1}$ is the generalized reflection coefficient, which is the ratio of the amplitudes of voltages at $y = d_n$ due to the image charges located above and below the jth layer. $\tilde{\Gamma}_{j,j+1}$ takes the value of 0 or -1 if the jth layer is a half space, or the $(j+1)$th layer is a ground plane, respectively. The unknowns to be determined are $A_{m,m}^+$ and $A_{m,m}^-$. Using the facts that, at $y = y_0$, (6a) and (6b) must be equal and that the normal component of the displacement field must be discontinuous by

the charge density at $y = y_0$, we can obtain expressions for $A_{m,m}^+$ and $A_{m,m}^-$ as follows:

$$A_{m,m}^+ = M_m\left[e^{+\gamma y_0} + \tilde{\Gamma}_{m,m-1}e^{-2\gamma d_{m-1} - \gamma y_0}\right] \tag{10a}$$

$$A_{m,m}^- = M_m\left[e^{-\gamma y_0} + \tilde{\Gamma}_{m,m+1}e^{-2\gamma d_m + \gamma y_0}\right] \tag{10b}$$

where

$$M_m = \left[1 - \tilde{\Gamma}_{m,m-1}\tilde{\Gamma}_{m,m+1}e^{+2\gamma(d_{m-1} - d_m)}\right]^{-1}. \tag{11}$$

Now to approximate the Green's function with respect to γ but independently of y and y_0, we rearrange these expressions by factoring out all y and y_0 dependencies as follows in (12a) and (12b), shown at the bottom of the page. where

$$K_{m,n,1}^+ = M_m\tilde{\Gamma}_{n,n+1}\prod_{j=m}^{n-1} S_{j,j+1}^+$$

$$K_{m,n,2}^+ = M_m\tilde{\Gamma}_{n,n+1}\tilde{\Gamma}_{m,m-1}\prod_{j=m}^{n-1} S_{j,j+1}^-$$

$$K_{m,n,3}^+ = M_m\prod_{j=m}^{n-1} S_{j,j+1}^+$$

$$K_{m,n,4}^+ = M_m\tilde{\Gamma}_{m,m-1}\prod_{j=m}^{n-1} S_{j,j+1}^+ \tag{13a}$$

$$K_{m,n,1}^- = M_m\tilde{\Gamma}_{m,m+1}\prod_{j=n+1}^{m} S_{j,j-1}^-$$

$$K_{m,n,2}^- = M_m\prod_{j=n+1}^{m} S_{j,j-1}^-$$

$$K_{m,n,3}^- = M_m\tilde{\Gamma}_{m,m+1}\tilde{\Gamma}_{n,n-1}\prod_{j=n+1}^{m} S_{j,j-1}^-$$

$$K_{m,n,4}^- = M_m\tilde{\Gamma}_{n,n-1}\prod_{j=n+1}^{m} S_{j,j-1}^-. \tag{13b}$$

The determination of the closed-form space-domain Green's function can now be preceded by the approximation of the coefficient functions $K_{m,n,i}^{\pm}$ of the exponential terms.

A physically intuitive approach to approximate the potential due to a charge in the layered medium is the use of a finite number of the weighted image charges in the homogenous medium, which is equivalent to approximating the coefficient functions $K_{m,n,i}^{\pm}$ with exponential functions. The equivalence

$$\tilde{G}(\gamma, y \mid r_0) = \frac{1}{2\varepsilon_m \gamma}\left(K_{m,n,1}^+ e^{\gamma(y+y_0-2d_n)} + K_{m,n,2}^+ e^{\gamma(+y-y_0+2(d_{m-1}d_n))} + K_{m,n,3}^+ e^{\gamma(-y+y_0)}\right.$$

$$\left. + K_{m,n,4}^+ e^{\gamma(-y-y_0+2d_{m-1})}\right) \quad y \geq y_0 \tag{12a}$$

$$\tilde{G}(\gamma, y \mid r_0) = \frac{1}{2\varepsilon_m \gamma}\left(K_{m,n,1}^- e^{\gamma(y+y_0-2d_m)} + K_{m,n,2}^- e^{\gamma(+y-y_0)} + K_{m,n,3}^+ e^{\gamma(-y+y_0-2(d_{n-1}-d_m))}\right.$$

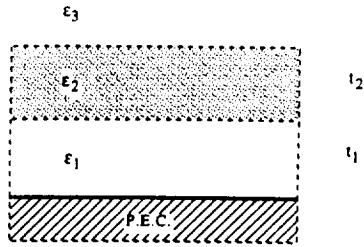$$\left. + K_{m,n,4}^- e^{\gamma(-y-y_0+2d_{n-1})}\right) \quad y \leq y_0 \tag{12b}$$

Fig. 3. The geometry used to test the approximated Green's function.

Fig. 4. Comparison of approximated and exact Green's functions in the spectral domain.

between the weighted image charges and exponential functions will be shown below in (15) and (16). In EM analyses, the complex-valued exponentials are often used for pole-zero modeling of signals, such as an electromagnetic-scatterer response. The least-square formulation of this exponential approximation results in nonlinear equations and can only be solved by iterative methods, such as gradient descent procedures or the Newton method. Due to the computational inefficiency of these algorithms, some other suboptimal noniterative techniques are also proposed: the least-squares Prony method and the generalized pencil-of-function (GPOF) method [16], [17]. Although these algorithms are noniterative, their computation involves matrix inversions and a polynomial factoring or a solution of the generalized eigenvalue problem, which are still computationally inefficient compared to the proposed method. By taking into account the specific properties of the coefficient functions $K^{\pm}_{m,n,i}$, which are real-valued and nonoscillatory, we can utilize more simple and efficient methods than the universal approximation techniques mentioned above; in particular, real exponentials are sufficient to approximate the coefficient functions and avoid any complex operations[1]. Thus, we have devised a simple relaxation algorithm based on curve fitting. The details of the procedure are given in Appendix A. Although this method is simple and iterative in nature, it converges to reasonable accuracy in a few iterations, and requires less computation time as compared to those for the previously mentioned methods.

In general, the coefficient functions $K^{\pm}_{m,n,i}$ have asymptotic values, and an analytical extraction of these values should be performed to increase the accuracy of the approximated functions or to reduce the computation time. The expressions for these asymptotic values can be easily obtained numerically or analytically. Furthermore, some of these coefficient functions are often zero, one, or symmetry of the others and these properties can also be explored to reduce the computation time.

It can be seen that there exists a pole at $\gamma = 0$ for a case with a presence of both top and bottom ground planes, and $K^{\pm}_{m,n,i}$ can no longer be approximated with exponential functions. To remove the singularity for this case, one can subtract the original Green's function by the Green's function for a homogenous case. Then, the remain part can be approximated as before, and for the homogeneous Green's function a closed-form or a fast converging summation form can be used in the space domain [18]. The detailed discussion of a stripline case for the 2-D case is given in Appendix B.

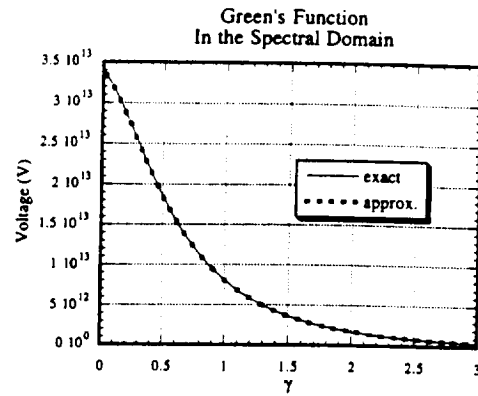[1] The complex-valued exponentials can be viewed as the *complex images* in the space domain in this paper.

The Green's function for the structure shown in Fig. 3 is approximated and compared with the exact Green's function in the spectral domain. The dielectric constants ϵ_1, ϵ_2, and ϵ_3 are taken to be $2\epsilon_0, 5\epsilon_0$, and ϵ_0, accordingly. The thicknesses of the layers t_1 and t_2 are 0.6 mm and 1.0 mm, and the observation and source points, y and y_0, are 0.6 mm and 1.6 mm, respectively. A maximum number of eleven exponentials were used to approximate the Green's function. As shown in Fig. 4, the approximated results agree with the original one, and the maximum relative error was 0.0003. It is important to observe that although the exponential approximation might fail for the large argument case due to its fast decaying nature, by extracting the asymptotic value and the exponential factor from the coefficient function, the limiting behavior of the overall approximated Green's function would still remain accurate.

After approximating the Green's function in the spectral domain, one can obtain the expressions for 2-D and 3-D spatial Green's functions using the following identities:

$$\frac{1}{r} = \frac{1}{\sqrt{x^2 + y^2 + z^2}}$$
$$= \frac{1}{2\pi} \int_{-\infty}^{+\infty} \int_{-\infty}^{+\infty} d\alpha d\beta e^{-j(\alpha x + \beta z)} \frac{e^{-\gamma|y|}}{\gamma} \quad (14a)$$

$$-\ln(\rho) = -\ln\left(\sqrt{x^2 + y^2}\right)$$
$$= \frac{1}{2\pi} \int_{-\infty}^{+\infty} d\gamma e^{-j\gamma x} \frac{e^{-|\gamma y|}}{|\gamma|}. \quad (14b)$$

The above identities can be easily derived by considering the potential due to the unit point or line charges[2]. Thus, in the space domain, the approximated Green's function for 2-D and 3-D cases, in general, can be written as

$$G^{3D}(r \mid r_0) = \frac{1}{4\pi\epsilon_m} \sum_{j=1}^{4} f_j^{3D,\pm}(r \mid r_0) \quad (15a)$$

$$G^{2D}(\rho \mid \rho_0) = -\frac{1}{2\pi\epsilon_m} \sum_{j=1}^{4} f_j^{2D,\pm}(\rho \mid \rho_0). \quad (15b)$$

Again, the superscripts $+$ and $-$ are used to denote the cases for $y \geq y_0$ and $y \leq y_0$, respectively. For $j = 1$ and $y \geq y_0$,

[2] Equation (14a) can be viewed as the static version of Weyl's identity.
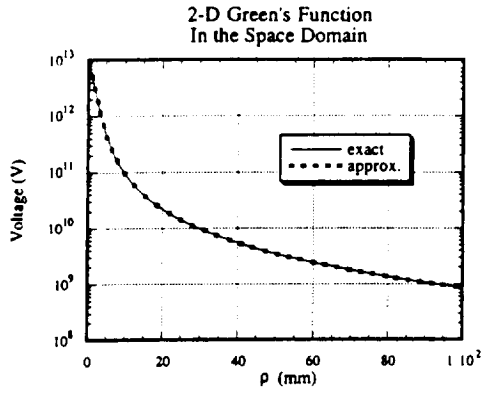
**2-D Green's Function
In the Space Domain**

Fig. 5. Comparison of approximated and exact Green's functions in the space domain.

the expressions for $f_j^{3D,+}(r \mid r_0)$ and $f_j^{2D,+}(r \mid r_0)$ are given by (16a) and (16b), shown at the bottom of the page. Here, $K_{m,n,j}^{+,\infty}$ denotes the asymptotic value of $K_{m,n,j}^{+}$ and we have assumed that $K_{m,n,j}^{+}$ is approximated by

$$K_{m,n,j}^{+}(\gamma) = \sum_{i=1}^{N_{m,n,j}^{+}} C_{m,n,j}^{+,i} e^{a_{m,n,j}^{+,i}\gamma}, \quad j = 1,2,3,4 \quad (17)$$

where $N_{m,n,j}^{+}$ is the number of exponential functions used to approximate $K_{m,n,j}^{\pm}$. The approximated Green's function is also compared in the space domain for the 2-D case. The same structure is used as in the previous one with $\epsilon_2 = \epsilon_1 = 2\epsilon_0$, and y and y_0 were 0.6 mm and 1.6 mm, respectively. A maximum number of exponentials used in the approximation was five. The exact Green's function is obtained by applying the image principle in the space domain. Fig. 5 shows the comparison. The maximum relative error was 0.0033.

Finally, we note that considering the forms of (15) and (16) it can be seen that the exponentials used to approximate the Green's function in the spectral domain correspond to the weighted images in the space domain.

IV. SOLUTION METHOD FOR THE INTEGRAL EQUATION

Once we obtain the approximated Green's function, the integral (1) can now be solved by the moment method. First, discretizing the surface or the cross section of each conductor with polygonal-type elements, the unknown charge density can

be expanded with the pulse basis functions over the discretized elements. Then, applying the point matching technique to each cell, (1) for 3-D problems becomes

$$V_i = \sum_{k=1}^{N_T} q_k \int\!\!\int_{s_k} G(x_i, y_i, z_i \mid x, y, z) ds; \quad i = 1, 2, \ldots, N_T. \quad (18)$$

Here, q_k is the unknown coefficient to be determined, and N_T is the total number of cells used to discretize conductors. s_k is the surface of the kth cell, and point matching is applied at the center of the ith cell (x_i, y_i, z_i). The similar equation can be also obtained for 2-D problems. Assuming that all possible ground planes are held with the same potential and the ith cell is in the jth conductor, V_i is the voltage difference between the jth conductor and the ground plane; in the case of no ground plane, any one of the existing conductors can be chosen to be the ground reference to define the voltage. For the capacitance computation, V_i takes the value of 1 or 0 depending on the excitation of the jth conductor.

With manipulations in y, y_i, and the terms due to the exponential approximation, the surface integration in (18) can be put into the following forms:

$$\int\!\!\int_s \frac{ds'}{\sqrt{(x-x')^2 + (y-y')^2 + (z-z')^2}} = \int\!\!\int \frac{ds'}{|\mathbf{r} - \mathbf{r}'|}$$
$$= \int\!\!\int \frac{ds'}{R}. \quad (19a)$$

Similarly, for 2-D problems we have

$$\int_c \ln\left(\sqrt{(x-x')^2 + (y-y')^2}\right) dl' = \int_c \ln(|\rho - \rho'|) dl'$$
$$= \int_c \ln(P) dl'. \quad (19b)$$

The evaluations of (19a) and (19b) over an arbitrary polygonal patch and a line segment are well-known and the closed-form formulas are given in [19].

Now solving the system of linear equations obtained from (18) will give the unknown charge distribution in terms of its basis function. It is important to point out that without the closed-form expression of the Green's function, the integration (19) must be performed, theoretically, an infinite number of

$$f_1^{3D,+}(r \mid r_0) = K_{m,n,1}^{+,\infty} \frac{1}{\sqrt{(x-x_0)^2 + (y+y_0-2d_n)^2 + (z-z_0)^2}}$$

$$+ \sum_{i=1}^{N_{m,n,1}^{+}} C_{m,n,1}^{+,i} \frac{1}{\sqrt{(x-x_0)^2 + (y+y_0-2d_n+a_{m,n,1}^{+,i})^2 + (z-z_0)^2}} \quad (16a)$$

$$f_1^{2D,+}(\rho \mid \rho_0) = K_{m,n,1}^{+,\infty} \cdot \ln\left(\sqrt{(x-x_0)^2 + (y+y_0-2d_n)^2}\right)$$

$$+ \sum_{i=1}^{N_{m,n,1}^{+}} C_{m,n,1}^{+,i} \cdot \ln\left(\sqrt{(x-x_0)^2 + (y+y_0-2d_n+a_{m,n,1}^{+,i})^2}\right). \quad (16b)$$

TABLE I

Computation			Delabare et al. [4]		
141.38	-21.493	-0.9924	142.09	-21.765	-0.8920
-21.491	92.951	-17.844	-21.733	93.529	-18.098
-0.9023	-17.844	87.495	-0.8900	-18.097	87.962

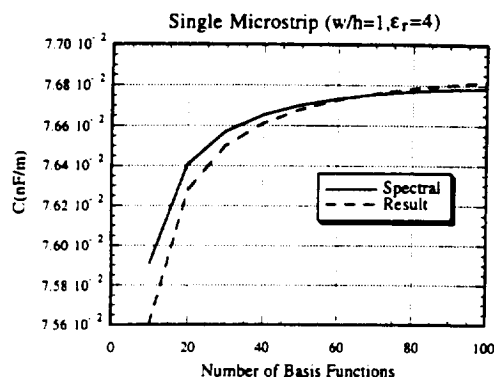(Computation matrix and Delabare matrix both in (pF/m))

Single Microstrip (w/h=1,ε_r=4)

Fig. 6. Comparison of the present method with the spectral domain approach as a function of the number of basis functions.
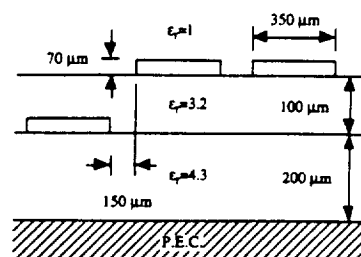

Fig. 7. Three conductors in a layered medium. All dimensions of conductors and spacings are identical.
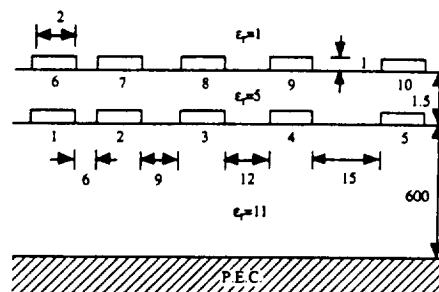

Fig. 8. Ten conductors in a layered medium. All dimensions of conductors and spacings are identical, and all units are in micrometer.

TABLE II

307.13	-41.2	-11.34	-6.28	-5.351	-218.8	-4.966	-1.385	-0.814	-0.729
-41.20	319.6	-28.04	-7.79	-4.987	-5.025	-216.95	-3.54	-0.985	-0.666
-11.34	-28.04	310.5	-24.29	-8.587	-1.366	-3.503	-218.4	-3.18	-1.148
-6.279	-7.79	-24.29	303.5	-24.73	-0.798	-0.946	-3.164	-219.4	-3.345
-5.351	-4.988	-8.588	-24.73	290.5	-0.708	-0.627	-1.12	-3.325	-221.3
-218.8	-5.01	-1.363	-0.796	-0.709	231.7	-2.074	-0.393	-0.182	-0.134
-4.954	-216.97	-3.494	-0.944	-0.628	-2.074	232.0	-1.19	-0.255	-0.135
-1.382	-3.532	-218.4	-3.157	-1.12	-0.393	-1.19	231.8	-0.8752	-0.242
-0.813	-0.982	-3.174	-219.5	-3.32	-0.182	-0.255	-0.875	231.6	-0.763
-0.729	-0.665	-1.145	-3.34	-221.4	-0.134	-0.135	-0.242	-0.763	231.3

times. For most practical problems, the time to construct the matrix of the linear equation (moment matrix) takes the major portion of the computation time. We have significantly reduced this computation time by approximating the Green's function with a finite number of exponentials.

V. NUMERICAL EXAMPLES

A computer program was developed based on the above algorithm, and it is capable of handling an arbitrary number of dielectric layers and conductors and designed to read mesh data from a conventional mesh generator to allow computation of the complex geometries and meshes. The algorithm is tested for both 2-D and 3-D problems, and the equivalent crossover capacitance of two orthogonal microstrip lines is computed based on the integral equation with both 2-D and 3-D Green's functions.

A. 2-D Problems

First, a simple microstrip capacitance is computed to verify the method, and the results are compared with those for the spectral domain approach (SDA) in Fig. 6. The spectral domain method used for comparison solves the integral equation iteratively in conjunction with the minimization in the boundary condition error. A more complex geometry, a three-conductor system in a layered medium, shown in Fig. 7, is also computed. The number of basis functions used was 50 for each conductor. In both cases, the maximum number of exponentials used to approximate the coefficient function $K^{\pm}_{m,n,i}$ was 7. Comparison with the results in [4] is shown in Table I. In [4], the spectral-domain Green's function is numerically integrated to obtain the corresponding space-domain Green's function using a Gaussian quadrature formula in conjunction with analytical asymptotic extraction.

A ten-conductor transmission line system above a thick dielectric substrate, shown in Fig. 8, is also considered. The total number of 300 basis functions was used to represent the unknown charges, and nine exponentials were used to approximate each coefficient function of the Green's function. Table II shows the computed results. The same structure is considered in [3] using the free-space Green's function with the basis functions which incorporate the edge singularities of the charge near the corners of the conductors. In [3], data are obtained using 160 and 190 basis functions for conductors and dielectric interfaces, respectively. The methods used in [2] and [4] are also employed to compute the same structure in [3]. According to [3], the methods used in [2] and [4] resulted in nonphysical values, for instance, negative self-capacitance values. The method used in [4] took the CPU times of 89611.19 s on an IBM RS-6000 station with 300 basis functions, whereas, the method in [3] took 458.67 s. On the same machine, our method took only 85.7 s of CPU time.

For the final 2-D example, a multilayered stripline case, shown in Fig. 9, is also analyzed. Fifty basis functions are used to discretize each conductor. We have obtained the values
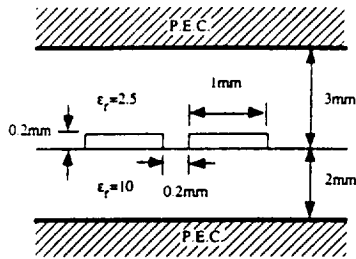
Fig. 9. Two conductors in a layered medium with two ground planes. Dimensions of conductors are identical.

TABLE III

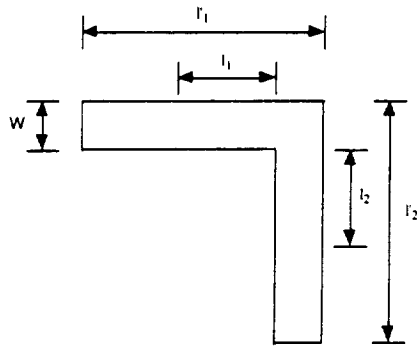|	Computation	Silvester et al. [20]	Gupta et al [21]
C_{ex} (fF)	65.3	72	67.65
$C_{normalized}$ $(C_{ex} / (C_{unif} * h))$	0.359	0.386	0.363

Fig. 10. Geometry of the test microstrip bend.

$C_{11} = C_{22} = 217.07$ pF/m and $C_{12} = C_{21} = -107.76$ pF/m. Data obtained from the Ansoft Maxwell software are $C_{11} = C_{22} = 217.65$ pF/m and $C_{12} = C_{21} = -108.24$ pF/m.
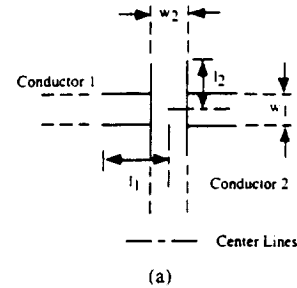
Fig. 11. (a) Planar and (b) cross-sectional views of the microstrip crossover.

B. Equivalent Capacitance for a Microstrip Bend

In this numerical example, we will use the 3-D Green's function to calculate the equivalent capacitances for a right-angle bend of a microstrip line. Although the equivalent capacitance or excess capacitance due to the right-angle bend discontinuities has been well-studied [20], [21], it is considered here again to verify the present method. An accurate characterization of a microstrip bend involves the semi-infinite microstrip lines which, in turn, requires different expressions for the Green's function. However, since the effects of the discontinuity are localized, it is expected that the equivalent capacitances can still be accurately calculated by truncating the semi-infinite lines with finite lengths.

Referring to Fig. 10, the excess capacitance C_{ex} can be defined by

$$C_{ex} = \lim_{\substack{l'_{1,2} \to \infty \\ l_{1,2} \to l'_{1,2}}} [C_T - C_{unif}(l_1 + l_2)] \qquad (20)$$

where C_T is the total lumped capacitance and C_{unif} is the capacitance per unit length for the uniform microstrip line. Setting V to 1 in (18), (20) can be directly written in terms of charges:

$$C_{ex} = Q_{ex} = \lim_{\substack{l'_{1,2} \to \infty \\ l_{1,2} \to l'_{1,2}}} [Q_T - Q_{unif}(l_1 + l_2)]. \qquad (21)$$

Here, Q_T is the total charge on the conductor, and Q_{unif} is the charge per unit length for the uniform line. The excess

capacitance was computed for $w = 1.5$ mm, $h = 3$ mm and $\epsilon_r = 4.5$, and $l_{1,2}$ and $l'_{1,2}$ were 5 w and 20 w, respectively. A total of 456 nonuniform cells were used to mesh the geometry, and C_{unif}, which was calculated using the 2-D Green's function, was found to be 62.12 pF/m. Table III compares the program results with those obtained from [20], [21]. The result from [21] contains a maximum error of 5%, while [20] contains 4% according to their analysis. The graph reading error must also be considered in [20].

C. Equivalent Capacitance for a Microstrip Crossover

In the following, we seek the equivalent capacitances for a microstrip crossover. Fig. 11 shows the geometry of the crossover considered, and Fig. 12 shows the equivalent circuit representation. In Fig. 12, two lines are uncoupled except c^m at the location of the crossover. Here, instead of constructing the integral equation in terms of the total charges, as we did for a microstrip bend case, we will formulate the integral equation in terms of the excess charges. The major drawback of the prior approach is that since the excess charge due to the discontinuities is usually much smaller than the total charge, the final accuracy in terms of the excess charge is much worse than the accuracy obtained for solving the total charge.

Based on the equivalent circuit representation in Fig. 12, the integral equations after applying the boundary conditions
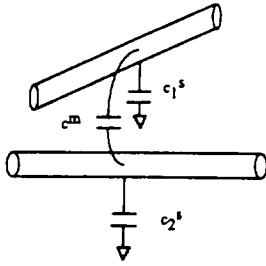
Fig. 12. Equivalent circuit representation for the microstrip crossover shown in Fig. 11.

TABLE IV

	$\varepsilon_{r1} = 2$, and $\varepsilon_{r2} = 2$	$\varepsilon_{r1} = 4$, and $\varepsilon_{r2} = 2$
c^m	69.17 (fF)	59.748 (fF)
c_1^f	-55.40 (fF)	-48.580 (fF)
c_2^f	-58.94 (fF)	-53.968 (fF)

on the surfaces of the conductors can be written as follows:

$$
\begin{bmatrix} V \\ 0 \end{bmatrix} = \begin{bmatrix} \langle G_{11}^{3D}, q_{11}^T \rangle + \langle G_{21}^{3D}, q_{12}^T \rangle \\ \langle G_{12}^{3D}, q_{11}^T \rangle + \langle G_{22}^{3D}, q_{12}^T \rangle \end{bmatrix}
$$
$$
= \begin{bmatrix} \langle G_{11}^{2D}, q_{11}^{unif} \rangle + \langle G_{11}^{3D}, q_{11}^{ex} \rangle + \langle G_{21}^{3D}, q_{12}^{ex} \rangle \\ \langle G_{12}^{2D}, q_{11}^{unif} \rangle + \langle G_{12}^{3D}, q_{11}^{ex} + \langle G_{22}^{3D}, q_{12}^{ex} \rangle \end{bmatrix}
$$
$$(22a)$$

$$
\begin{bmatrix} 0 \\ V \end{bmatrix} = \begin{bmatrix} \langle G_{11}^{3D}, q_{21}^T \rangle + \langle G_{21}^{3D}, q_{22}^T \rangle \\ \langle G_{12}^{3D}, q_{21}^T \rangle + \langle G_{22}^{3D}, q_{22}^T \rangle \end{bmatrix}
$$
$$
= \begin{bmatrix} \langle G_{21}^{2D}, q_{22}^{unif} \rangle + \langle G_{11}^{3D}, q_{21}^{ex} \rangle + \langle G_{21}^{3D}, q_{22}^{ex} \rangle \\ \langle G_{22}^{2D}, q_{22}^{unif} \rangle + \langle G_{12}^{3D}, q_{21}^{ex} \rangle + \langle G_{22}^{3D}, q_{22}^{ex} \rangle \end{bmatrix}.
$$
$$(22b)$$

Here, the superscript T denotes the total quantity on the line while the superscript unif denotes the quantity per unit length of an isolated line. The integrations over the Green's functions are symbolically written by $\langle \cdot, \cdot \rangle$, and the excitation voltage is assumed to be 1. The subscript ij used in the Green's functions G_{ij} denotes that the source is located at the ith conductor, and the boundary condition is applied at the jth conductor. The subscript ij used in the charge density functions q_{ij} denotes that q_{ij} is the charge density at the jth conductor with excitation at the ith conductor. Now noting that $\langle G_{ii}^{2D}, q_{ii}^{unif} \rangle$ is equal to V, we can rewrite (22) as follows:

$$
\begin{bmatrix} 0 \\ -\langle G_{12}^{2D}, q_{11}^{unif} \rangle \end{bmatrix} = \begin{bmatrix} \langle G_{11}^{3D}, q_{11}^{ex} \rangle + \langle G_{21}^{3D}, q_{12}^{ex} \rangle \\ \langle G_{12}^{3D}, q_{11}^{ex} \rangle + \langle G_{22}^{3D}, q_{12}^{ex} \rangle \end{bmatrix} \quad (23a)
$$

$$
\begin{bmatrix} -\langle G_{21}^{2D}, q_{22}^{unif} \rangle \\ 0 \end{bmatrix} = \begin{bmatrix} \langle G_{11}^{3D}, q_{21}^{ex} \rangle + \langle G_{21}^{3D}, q_{22}^{ex} \rangle \\ \langle G_{12}^{3D}, q_{21}^{ex} \rangle + \langle G_{22}^{3D}, q_{22}^{ex} \rangle \end{bmatrix}. \quad (23b)
$$

Since the excess charges are expected to be localized, we can truncate the domain of the basis functions used to expand the excess charge density over distances l_1 and l_2 from the crossover junction (see Fig. 11(a)). Now using pulse basis functions and the point matching technique, (23) can be put into the following matrix form:

$$
\begin{bmatrix} V_{11} & 0 \\ 0 & V_{22} \end{bmatrix} \begin{bmatrix} 0 & q_{22}^{unif} \\ q_{11}^{unif} & 0 \end{bmatrix} = \begin{bmatrix} M_{11} & M_{12} \\ M_{21} & M_{22} \end{bmatrix} \begin{bmatrix} q_{11}^{ex} & q_{21}^{ex} \\ q_{12}^{ex} & q_{22}^{ex} \end{bmatrix}
$$
$$(24a)$$

TABLE V
COMPARISON OF RESULTS FOR FIG. 11 WITH $\varepsilon_{r1} = \varepsilon_{r2} = 2$

	Papatheodorou et al. [10]	Computation
c^m over $h_1 c_2'$	1.672	1.776
$\frac{c_1^f}{h_1 c_1'}$	-1.345	-1.321
$\frac{c_2^f}{h_1 c_2'}$	-1.296*	-1.513

* This entry is incorrect, and it can be verified by considering [10, Fig. 4].

where

$$
[V_{11}]_{ij} = -\int_{cj} G_{11}^{2D}(\rho_i \mid \rho')dl'
$$

$$
[V_{22}]_{ij} = -\int_{cj} G_{12}^{2D}(\rho_i \mid \rho')dl' \quad (24b)
$$

$$
M_{klij} = \int_s \int_j G_{lk}^{3D}(r_i \mid r')ds' \quad (24c)
$$

$$
q_{ij}^{ex} = \left[q_{ij,1}^{ex}, q_{ij,2}^{ex}, \ldots, q_{ij,N_{3D,i}}^{ex} \right]'
$$

$$
q_{ii}^{unif} = \left[q_{ii,1}^{unif}, q_{ii,2}^{unif}, \ldots, q_{ii,N_{2D,i}}^{unif} \right]'. \quad (24d)
$$

Here, $[A]_{ij}$ is the jth element of the ith row of the matrix A, and $N_{3D,i}$ and $N_{2D,i}$ are the number of patches and the number of segments used to discretize the surface and the cross section of the ith conductor, respectively. q_{ii}^{unif} can be obtained by solving the 2-D problems for each isolated microstrip with the excitation voltage set equal to 1. Then (24) can be solved for the excess charges. Finally the equivalent excess capacitance can be found by

$$
c_{ij}^{ex} = \sum_{k=1}^{N_{3D,i}} \text{Area}_{ik} \cdot q_{ij,k}^{ex} \quad (25)
$$

where Area_{ik} is the area of the kth patch in the ith conductor.

For a numerical example, the same structure used in [10] is considered, where h_1 and h_2 were 4 mm and 6 mm, the widths of both strips were 0.04 h_1, respectively, l_1 and l_2 were 10 h_2, and 800 nonuniform patches and 40 pulse basis functions are used to solve the 2-D and 3-D problems, accordingly. Two different dielectric configurations are considered and the results are shown in Table IV. The maximum number of exponentials used for each coefficient function was seven for
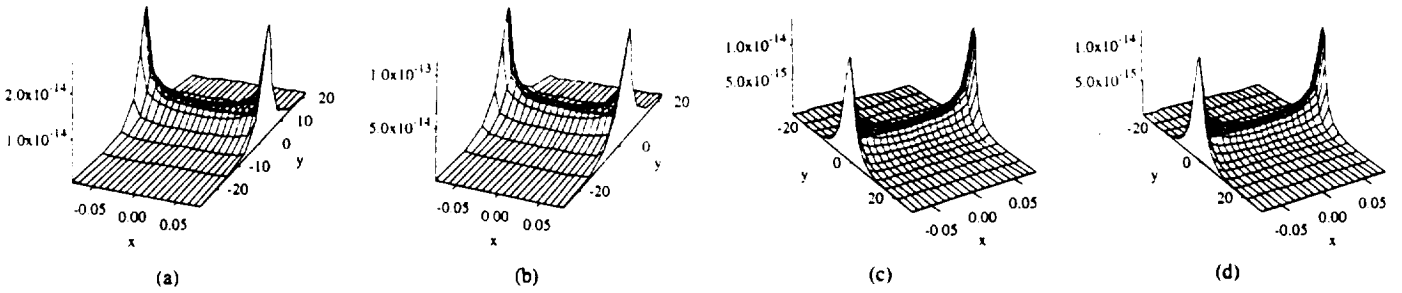
Fig. 13. Plots of the magnitudes of the excessive charge distributions for (a) q_{11}^{er}, (b) q_{21}^{er}, (c) q_{12}^{er}, and (d) q_{22}^{er} with $\epsilon_{r1} = 4$, and $\epsilon_{r2} = 2$. x and y denote the transverse and the longitudinal, respectively.

both cases. The result with $\varepsilon_{r1} = \varepsilon_{r2} = 2$ are compared with the results from [10] in Table V. In Table V, c_1' and c_2' are the capacitances per unit length of the isolated wire lines with radii equal to 0.25 w and $\varepsilon_{r1} = \varepsilon_{r2} = 1$. In [10], l_1 and l_2 were 10 h_1; hence, their value of c^m is expected to be smaller than ours as shown in Table V. The 3-D plots of excess charges are shown in Fig. 13. The Green's function used in [10] is based on the image principle in the space domain and involves an infinite summation. According to [10], only ten terms were sufficient to evaluate the infinite summation for this particular structure, where lines are extremely narrow. However, for wider microstrip lines, the number of terms to compute the infinite summation will be much larger; this can be easily seen from the expression of the Green's function in [10].

VI. CONCLUSION AND FUTURE WORK

In the design of VLSI circuits, the capacitance computation plays an important role, and the present method can be conveniently combined with CAD tools. Since the Green's function depends only on the processing parameters, such as the thickness and number of dielectric layers, the dielectric constants, and location of ground planes, the Green's function approximation has to be performed only when the processing parameters are changed. Then, the approximation result can be used to compute capacitance parameters throughout the design period.

In the computation of parasitic or excess capacitances, semi-infinite microstrip lines are often encountered, and to have accurate results, as mentioned earlier, the integral equation is often formulated in terms of the excessive charges which, in turn, requires the *Green's function* due to the semi-infinite lines. The authors are currently studying the generalization of the present method for such a Green's function in a layered medium.

APPENDIX A

THE REAL-VALUED EXPONENTIAL APPROXIMATION BASED ON THE RELAXATION OF CURVE FITTING

First, we will assume that a function $y(x)$ to be approximated is real valued and nonoscillatory and, furthermore, that its asymptotic value is zero. The latter assumption can easily be satisfied if the function is limited at infinity. Our goal is to

find the right-hand side of

$$y(x) \cong f_a(x) = \sum_{i=1}^{N} f_i(x) = \sum_{i=1}^{N} C_i e^{\lambda_i x} \qquad (A1)$$

Let w us for a moment assume that each first-order function f_i approximates the original function y at some interval around one of the approximation points and is decreasing fast enough so that its value is negligibly small at the approximation points corresponding to larger values of the argument x. Then, we can safely determine one of the first-order functions, say f_1, by neglecting contributions due to the other first-order functions, which are as yet unknowns to be determined. The parameters of f_1 can be easily obtained by curve fitting two values of y for some large value of x. In a similar manner, we can find the parameters of the other first-order functions; however, this time we have to take into account contributions due to the previous ones which are already known.

From the above argument, given 2N approximation points, the equations used to determine the parameters for the ith first-order function are then written by

$$\lambda_i = \frac{2\pi \ln \left(y_i(2x_{2i-1})/y_i(x_{2i}) \right)}{x_{2i} - x_{2i-1}} \qquad (A2)$$

$$C_i = e^{-\lambda_i x_{2i-1}} y_i(x_{2i-1}) \qquad (A3)$$

where

$$y_i(x_j) = y_{i-1}(x_j) - f_{i-1}(x_j); \quad j = 1, \ldots, 2N. \qquad (A4)$$

In the above, $y_0(x_j)$ is equal to $y(x_j)$. Let us now consider the case in which the value of a first-order function is not negligible at the other approximation points. In this case, if we perform the above procedure, there will be some difference between the original and the approximated function since we have ignored contributions due to some of the first-order functions. In such a case, to reduce this difference, we can iterate the above procedure including the contributions due to all other first-order functions which were obtained from the previous iteration. Thus, for the kth iteration, (A4) must be modified as

$$y_i^{(k)}(x_j) = y(x_j) - \sum_{l=1}^{i-1} f_l^{(k)}(x_j) - \sum_{l=i+1}^{N} f_l^{(k-1)}(x_j);$$

$$j = 1, \ldots, 2N. \qquad (A5)$$

$$y(x) = \frac{e^{-2x}}{\sqrt{1+x}} + e^{-x}$$

(a)

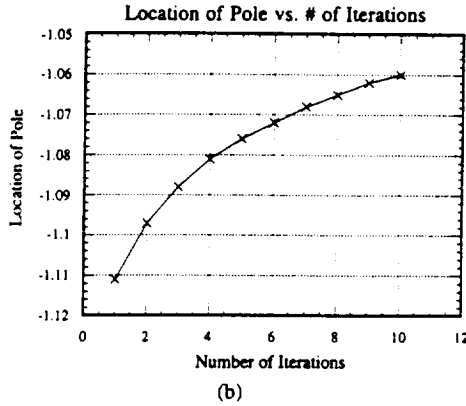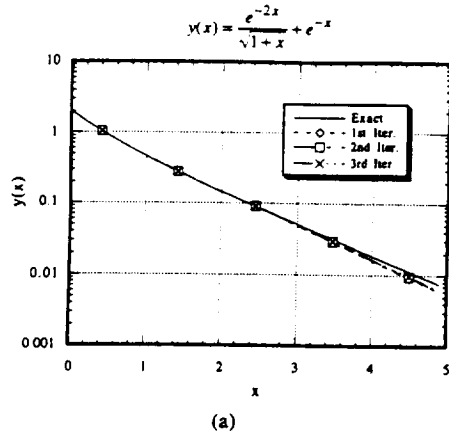Location of Pole vs. # of Iterations

Number of Iterations

(b)

Fig. 14. (a) Comparison of approximated and exact values of (A6). (b) Convergence of the location of the smallest pole (-1) with the number of iterations.

It can easily be shown that if $y(x)$ had N distinct eigenvalues, by iterating the above procedure, the approximated function will converge to the original function. However, in general, the approximating function will never be exact and the iteration must be stopped at some point at which the approximated function is *optimal* in the sense of curve fitting. Since our curve-fitting algorithm, most likely, has the biggest relative error for the values of x between x_{2N-1} and x_{2N}, one can check the approximated value with the exact value at any point in this interval for the convergence criterion. In some cases, if the desired accuracy can not be achieved, then one should increase the number of exponentials. This case can be determined by checking the difference between the computed parameters of $f_i^{(k)}$ and $f_i^{(k-1)}$.

The described method allows one to find the parameters of an approximating function one-by-one directly without solving a system of nonlinear or linear equations and does not require an original function to be monotonic. Moreover, the limiting values of the approximated function match exactly with the original function.

Finally, to demonstrate the method, the following testing function is approximated and the results are shown in Fig. 14:

$$y(x) = \frac{e^{-2x}}{\sqrt{1+x}} + e^{-x}. \tag{A6}$$

As illustrated in Fig. 14(b), to find the exact location of the pole at -1, we need a large number of iterations; however, since our goal is to approximate the overall function, only a few iterations were needed to approximate the function. To locate the poles exactly, one should use other methods such as those based on pencil of functions or the Prony approximation.

APPENDIX B

STRIP TRANSMISSION LINE CASE

Solving Poisson's equation with separation of variables, the Green's function for the strip transmission line case with the distance h between two ground planes can be written as follows (see [22]):

$$G(x, y \mid x', y') = \frac{1}{\pi \epsilon} \sum_{n=1}^{\infty} \frac{1}{n} \sin \left(\frac{n\pi y}{h} \right)$$
$$\times \sin \left(\frac{n\pi y'}{h} \right) e^{-(n\pi |x-x'|/h)}. \tag{A7}$$

The above expression for the Green's function can be easily integrated analytically over the pulse basis function analytically. This summation is quickly converging, and only a few first terms are needed; for instance, four digits of accuracy can be obtained using less than five terms for $|x - x'|/h > 0.5$. However, when $|x - x'|/h$ is small, the summation converges rather slowly, and the use of this Green's function expression should be avoided. In such cases, we can use the following closed-form Green's function:

$$G(x, y \mid x', y') = \frac{1}{4\pi \epsilon} \ln \left[\frac{\sinh^2 \left[\frac{\pi(x-x')}{2h} \right] + \sin^2 \left[\frac{\pi(y+y')}{2h} \right]}{\sinh^2 \left[\frac{\pi(x-x')}{2h} \right] + \sin^2 \left[\frac{\pi(y-y')}{2h} \right]} \right]. \tag{A8}$$

This expression for the Green's function can be obtained using the conformal mapping and the method of images [18]. The major disadvantage of this expression is that the closed-form integration over the pulse basis function is unappealing; hence, the numerical integration scheme is unavoidable. Therefore, this form of the Green's function must be only used when $|x - x'|/h$ is small. As shown in [1], to integrate (A7) numerically, it is convenient to rewrite this expression by extracting the singularity as

$$G(x, y \mid x', y') = \frac{1}{4\pi \epsilon} \ln \left[(x - x')^2 + (y - y')^2 \right]$$
$$+ g(x, y \mid x', y') \tag{A9}$$

$$g(x, y \mid x', y') = \frac{1}{4\pi \epsilon} \ln \left[\frac{\left[(x - x')^2 + (y - y')^2 \right] \left[\sinh^2 \left[\frac{\pi(x-x')}{2h} \right] + \sin^2 \left[\frac{\pi(y+y')}{2h} \right] \right]}{\sinh^2 \left[\frac{\pi(x-x')}{2h} \right] + \sin^2 \left[\frac{\pi(y-y')}{2h} \right]} \right] \tag{A10}$$

where (A10), shown at the bottom of the previous page. Now the first term in (A8) can be analytically integrated using (20(b)), and the second term can be integrated numerically.

ACKNOWLEDGMENT

REFERENCES

[1] W. T. Weeks, "Calculation of coefficients of capacitance of multiconductor transmission lines in the presence of a dielectric interface," *IEEE Trans. Microwave Theory Tech.*, vol. MTT-18, pp. 35–43, Jan. 1970.

[2] C. Wei, R. F. Harrington, J. R. Mautz, and T. K. Sarkar, "Multiconductor transmission lines in multilayered dielectric media," *IEEE Trans. Microwave Theory Tech.*, vol. MTT-32, pp. 439–450, Apr. 1984.

[3] G. W. Pan, G. Wang, and B. K. Gilbert, "Edge effect enforced boundary element analysis of multilayered transmission lines," *IEEE Trans. Circuits Syst.*, vol. 39, pp. 955–963, Nov. 1992.

[4] W. Delbare and D. D. Zutter, "Space-domain Green's function approach to the capacitance calculation of multiconductor lines in multilayered dielectrics with improved surface charge modeling," *IEEE Trans. Microwave Theory Tech.*, vol. 37, pp. 1562–1568, Oct. 1989.

[5] E. Yamashita, "Variational method for the analysis of microstrip-like transmission lines," *IEEE Trans. Microwave Theory Tech.*, vol. MTT-16, pp. 529–535, May 1964.

[6] H. A. Wheeler, "Transmission line properties of parallel wide strips by a conformal mapping approximation," *IEEE Trans. Microwave Theory Tech.*, vol. MTT-12, pp. 280–289, May 1964.

[7] J. Svacina, "Analysis of multilayer microstrip lines by a conformal mapping method," *IEEE Trans. Microwave Theory Tech.*, vol. 40, pp. 769–772, Apr. 1992.

[8] A. Farrar and A. T. Adams, "Multilayer microstrip transmission lines," *IEEE Trans. Microwave Theory Tech.*, vol. MTT-12, pp. 889–891, Oct. 1974.

[9] W. E. Matzke, B. Heinemann, and R. Telschow, "On the calculation of the capacitance coefficients for VLSI multilevel metallization lines by using domain methods," *IEEE Trans. Electron. Devices*, vol. ED-36, pp. 447–449, Feb. 1989.

[10] S. Papatheodorou, R. F. Harrington, and J. R. Mautz, "The equivalent circuit of a microstrip crossover in a dielectric substrate," *IEEE Trans. Microwave Theory Tech.*, vol. 38, pp. 135–140, Feb. 1990.

[11] H. Nelis, E. Deprettere, and P. Dewilde, "An efficient method for modelling VLSI interconnections," *European Conf. Circuit Theory Design*, Sept. 1989, pp. 94–98.

[12] W. Veit, H. Diestel and R. Pregla, "Coupling of crossed planar multiconductor systems," *IEEE Trans. Microwave Theory Tech.*, vol. 38, pp. 265–269, Mar. 1990.

[13] A. H. Zemanian, R. P. Tewarson, C. P. Ju, and J. F. Jen, "Three-dimensional capacitance computations for VLSI/ULSI interconnections," *IEEE Trans. Computer-Aided Design*, vol. CAD-8, pp. 1319–1326, Dec. 1989.

[14] M. I. Aksun and R. Mittra, "Derivation of closed-form Green's functions for a general microstrip geometry," *IEEE Trans. Microwave Theory Tech.*, vol. 40, pp. 2055–2062, Nov. 1992.

[15] Y. L. Chow, J. J. Yang, and G. E. Howard, "Complex images for electrostatic field computation in multilayered media," *IEEE Trans. Microwave Theory Tech.*, vol. 39, pp. 1120–1125, July 1991.

[16] S. L. Marple, *Digital Spectral Analysis.* Englewood Cliffs, NJ: Prentice-Hall, 1987.

[17] Y. Hua and T. K. Sarkar, "Generalized pencil-of-function method for extracting poles of an EM system from its transient response," *IEEE Trans. Antennas Propagat.*, vol. 37, pp. 229–234, Feb. 1989.

[18] P. M. Morse, *Methods of Theoretical Physics*, vol. 2. New York: McGraw-Hill, 1953.

[19] D. R. Wilton, S. M. Rao, A. W. Glisson, D. H. Schaubert, O. M. Al-Bundak *et al.*, "Potential integrals for uniform and linear source distributions on polygon and polyhedral domains," *IEEE Trans. Antennas Propagat.*, vol. AP-32, pp. 276–281, Mar. 1984.

[20] P. Silvester and P. Bendedek, "Correction to 'Microstrip discontinuity capacitances for right-angle bends, T junctions, and crossings'," *IEEE Trans. Microwave Theory Tech.*, vol. MTT-23, p. 456, May 1975.

[21] K. C. Gupta, R. Gary, and R. Chadha, *Computed-Aided Design of Microwave Circuits.* Norwood, MA: Artech House, 1987.

[22] R. E. Collin, *Field Theory of Guided Waves*, 2nd ed. New York: IEEE, 1991.

Kyung S. Oh (S'91) was born in Pusan, South Korea, in 1965. He received the B.S. and M.S. degrees in electrical engineering from the University of Illinois, Champaign in 1990 and 1992, respectively. He is presently studying in the Graduate School of Electrical Engineering at the University of Illinois, where he has been engaged in research on modeling and simulation of high speed digital circuits.

Dmitri B. Kuznetsov was born June 26, 1966, in Moscow, U.S.S.R. He received the Dipl. Eng. in electronics engineering from the Moscow Electrotechnical Institute of Telecommunication, Department of Automatics, Telemechanics and Electronics, in 1988. He received the M.S. degree in electrical and computer engineering from the University of Illinois, Champaign in 1993, where he is pursuing the Ph.D. degree.

From 1987 to 1991, he worked as an electronics engineer at the Space Research Institute, Academy of Sciences of the U.S.S.R., Moscow, on the design, manufacturing, testing, maintenance and repair of computer graphics system. From 1988 to 1991, he attended the postgraduate school of the Space Research Institute specializing in the information and measuring systems in space research.

Jose E. Schutt-Aine (M'82) received the B.S. degree from Massachusetts Institute of Technology, Cambridge, and the M.S. and Ph.D. degrees from the University of Illinois in 1984 and 1988, respectively.

Following his graduation from MIT, he spent two years with Hewlett-Packard Microwave Technology Center in Santa Rosa, CA, where he worked as a device application engineer. While pusuing his graduate studies at the University of Illinois, he held summer positions at GTE Network Systems in Northlake, IL. He is presently serving on the faculty of the Department of Electrical and Computer Engineering at the University of Illinois an Assistant Professor. His research interests include microwave theory and measurements, electromagetics, high-speed digital circuits, solid-state electronics, circuit design and electronic packaging.

Computation of the Equivalent Capacitance of a Via in a Multilayered Board Using the Closed-Form Green's Function

Kyung S. Oh, Jose E. Schutt-Aine, Raj Mittra, and Bu Wang

Abstract— A method based on the quasi-static approximation for computing the equivalent capacitance of a via is presented in this paper. The geometry of a via consists of traces, pads and a perfectly conducting cylindrical rod; the via is buried in a multilayered dielectric medium with optional reference (ground) planes. The total number of traces, pads, and ground planes can be arbitrary, as well as the angles and cross sections. The method is based on the excess charge formulation of an integral equation applied in conjunction with the recently developed closed-form Green's function.

I. INTRODUCTION

Although a via is one of the most common discontinuities encountered in high-speed integrated circuits, it has not received as much attention as some of the other discontinuities, e.g., open-end terminations, bends, and junctions. This is due mainly to the nonplanar and complex three-dimensional (3-D) geometry of the via, which has often been simplified in the works published previously [1]–[3]. For instance, a via penetrating through a single reference (ground) plane with two wire traces has been considered in [1], and without any traces in [2], while a via above a reference plane with two wire traces but without a through-hole reference plane between these traces has been investigated in [3]. A novel equivalent network model, which accounts for the frequency dependence, has been proposed in [4] and has also been applied to the problem of coupling between two adjacent vias in [5]. In [1] and [3], an integral equation has been formulated in terms of the excess charge distribution to compute the equivalent (excess) capacitance. In this paper, this excess charge formulation is further generalized for vias with more complex geometries than has been analyzed hitherto and is applied in conjunction with the closed-form Green's function to analyze vias embedded in multilayered dielectric media.

A closed-form Green's function for a multilayered dielectric medium was first introduced in [6]. This Green's function utilizes a finite number of complex images and avoids the evaluation of a nested infinite series expression required in the computation of the exact Green's function for a layered medium. In [7], a closed-form Green's function based on weighted real images was proposed and was used to compute the equivalent circuit of a strip crossover. In [8], this closed-form Green's function based on weighted real images was further generalized to handle a semi-infinite line and then applied to compute various strip junction discontinuities. In this paper, the closed-form Green's function discussed in [8] is employed to compute the equivalent circuit for a via in a multilayered dielectric medium.

II. GENERAL STATEMENT OF THE PROBLEM

To illustrate the geometries of vias considered in this paper, a via comprised of three traces and one reference ground plane is shown in Fig. 1(a). In general, a via can pass through N_g reference (ground) planes and N_t traces, and N_p pads can be attached to the via where
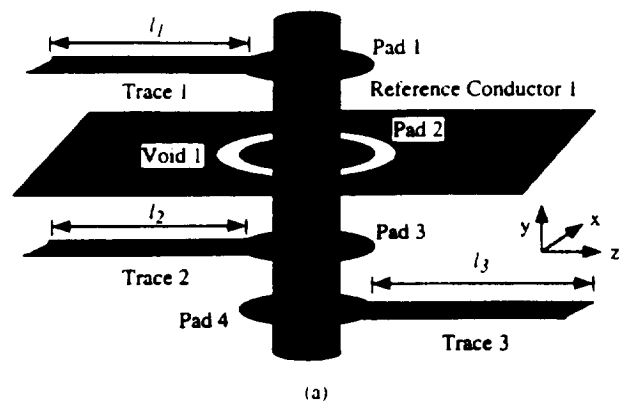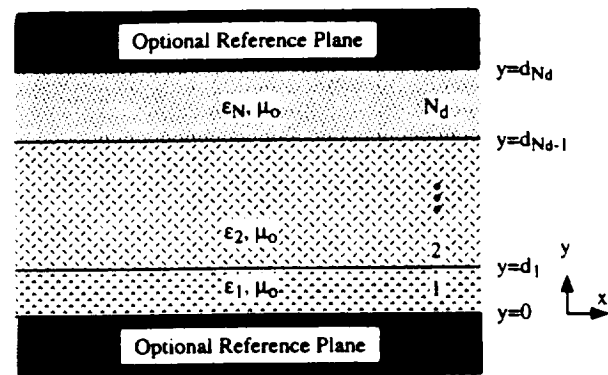
Fig. 1. (a) The geometry of a via, and (b) its surrounding multilayered medium.

N_g, N_t, and N_p are all arbitrary. The vias are embedded in a multilayered medium consisting of N_d (arbitrary) dielectric layers, which can be backed by two optional reference planes as shown in Fig. 1(b). To distinguish between these optional reference planes and those associated with the via, we will reserve the term "reference plane" to designate an optional top or bottom reference plane, and use the term "reference conductor" to denote other reference planes. It is evident that the reference conductors must have perforations to avoid any contact with the vias; however, the two optional reference planes are assumed to be solid. To simplify the numerical computation, we assume that all of the conductors are infinitely thin and that the shapes of all the pads and perforations in the reference conductors are circular.

A quasi-static equivalent circuit representation of the via shown in Fig. 1 is given in Fig. 2. This paper will only address the problem of computing the total equivalent capacitance C. The method to compute the equivalent inductance of a via can be found in [9].

In Section III, an integral equation is formulated in terms of the excess charge distribution using the closed-form Green's function, and the method of moments (MoM) is subsequently employed to determine the unknown charge distribution. A detail discussion of the closed-form Green's function and the corresponding expression can be found in [8]. In Section IV, several numerical examples are presented to verify the proposed method.

III. FORMULATION OF AN INTEGRAL EQUATION

An impressed potential on conductors results in free charge accumulation on the surfaces of conductors, and the electrostatic potential

TABLE 1
EQUIVALENT CAPACITANCES FOR VIAS SHOWN IN FIG. 3. UNITS ARE IN pF

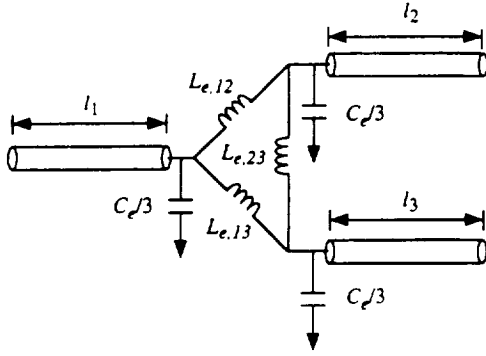|	Fig. 3(a)		Fig. 3(b)	
	$\varepsilon_1=\varepsilon_2=\varepsilon_0$	$\varepsilon_1=4\varepsilon_0,\ \varepsilon_2=\varepsilon_0$	$\varepsilon_1=\varepsilon_2=4\varepsilon_0$	$\varepsilon_1=4.5\varepsilon_0,\ \varepsilon_2=5.4\varepsilon_0$
Computed Result	0.3841	1.233	9.952	12.31
Others	0.3701 [3]	1.28 [3]	6.35 [1]	7.85 [1]

Fig. 2.   A equivalent circuit representation of the via shown in Fig. 1(a).

$o(r)$ at any point except inside conductors is then related to this surface charge density $q(r)$ via the following integral equation

$$o(r) = \int_\Omega G^{3D}(r \mid r')q(r')dr' = \langle G^{3D}, q \rangle \qquad (1)$$

where Ω denotes the surfaces of all conductors, including the via and reference conductors. $G^{3D}(r \mid r')$ is the 3-D closed-form Green's function for a multilayered medium, and it accounts for polarization charges on dielectric interfaces and free charges on the surfaces of reference planes [8]. The integration is symbolically written as $\langle \cdot, \cdot \rangle$ to simplify the notation. Next, the charge distribution over the whole structure analyzed is decomposed into $q_v(r), q_p'(r), q_l'(r)$, and $q_q'(r)$ where $q_v(r)$ is the charge density on the surface of a via hole, and $q_p'(r), q_l'(r)$, and $q_q'(r)$ are the charge densities on the ith pad, trace, and reference conductor, respectively. Equation (1) can be rewritten as

$$o(r) = \langle G^{3D}, q_v \rangle + \sum_{i=1}^{N_p} \langle G^{3D}, q_p' \rangle$$
$$+ \sum_{i=1}^{N_t} \langle G^{3D}, q_l' \rangle + \sum_{i=1}^{N_q} \langle G^{3D}, q_q' \rangle. \qquad (2)$$

Next, the charge density $q_l'(r)$ is further decomposed into the uniform charge density $q_l^{unif,i}(r)$ and the excess charge density $q_l^{excess,i}(r)$

$$q_l'(r) = q_l^{unif,i}(r) + q_l^{excess,i}(r). \qquad (3)$$

Here, $q_l^{unif,i}(r)$ is the uniform charge density on the ith trace under the assumptions that it is infinite in both directions, no other traces are present, and the reference conductors have no perforations; this charge density is computed by solving an appropriate two-dimensional (2-D) problem. Since the reference conductors become uniform planes without any perforations for this 2-D problem, the potential distribution on the region above the reference conductor is not affected by the region below it and vice versa. To solve for $q_l^{unif,i}(r)$, it is then expedient to introduce a new medium surrounding the ith trace. As a consequence, the medium employed

in the 2-D problem is generally different from that of the 3-D via problem, and could, in fact, be different for each trace. Once the appropriate medium has been chosen, $q_l^{unif,i}(r)$ can be obtained by using the method described in [7]. The resulting $q_l^{unif,i}(r)$ yields the capacitance per unit length for the ith transmission line in the equivalent circuit representation shown in Fig. 2.

In the process of determining $q_l^{unif,i}(r)$, the 2-D closed-form Green's function $G^{2D,i}(\rho \mid \rho_0)$ is used to formulate an integral equation for a 2-D problem [7]. However, in the integral (2) for computing the equivalent capacitance problem, the uniform charge density $q_l^{unif,i}(r)$ resides on the ith trace, which is only a semi-infinite line. It is therefore necessary to employ $G^{semi,i}(r \mid r_0, \xi)$ to compute the potential due to $q_l^{unif,i}(r)$ [8]. Using (3), (2) can be rewritten as

$$o(r) - \sum_{i=1}^{N_t} \langle G^{semi,i}, q_l^{unif,i} \rangle$$

$$= \langle G^{3D}, q_v \rangle + \sum_{i=1}^{N_p} \langle G^{3D}, q_p' \rangle$$

$$+ \sum_{i=1}^{N_t} \langle G^{3D}, q_l^{excess,i} \rangle + \sum_{i=1}^{N_q} \langle G^{3D}, q_q' \rangle. \qquad (4)$$

If we set the via potential to be o_0 with respect to the reference conductors and planes, $o(r)$ becomes o_0 on the surfaces of the via hole, pads, and traces, and is equal to 0 on the surfaces of reference conductors. Hence, once $q_l^{unif,i}(r)$ has been determined, all of the quantities associated with the left-hand side of (4) can be considered to be known at the surface of the conductors, and the method of moments can be applied to solve (4). The various integrations appearing in (4) can be evaluated analytically for pulse-type basis functions using closed-form formulas given in [8].

Once the unknown charge distributions have been determined, the equivalent (excess) capacitance C, can be obtained by using the following expression which involves the integrals of these charge distributions

$$C \cdot o_0 = \int_{\Omega_v} q_v(r')dr' + \sum_{i=1}^{N_p} \int_{\Omega_{p,i}} q_p'(r')dr'$$

$$+ \sum_{i=1}^{N_t} \int_{\Omega_{t,i}} q_l^{excess,i}(r')dr' + \sum_{i=1}^{N_q} \int_{\Omega_{q,i}} q_q'(r')dr' \qquad (5)$$

where Ω_v is the surface of a via hole. $\Omega_{p,i}, \Omega_{t,i}$, and $\Omega_{q,i}$ are the surfaces of the ith pad, trace, and reference conductor, respectively.

IV. NUMERICAL EXAMPLES

We will now present two numerical examples to illustrate the application of the method presented above to the computation of the equivalent capacitances of two via structures, one with a reference plane and the other with a reference conductor. The detailed geometries of the two via structures are shown in Fig. 3. The computed
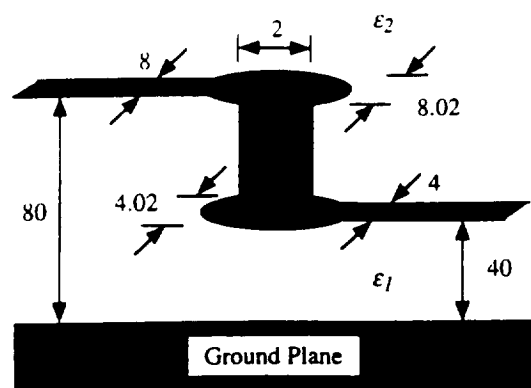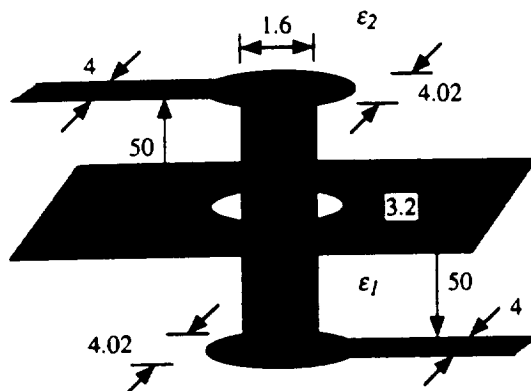
Fig. 3. (a) A two-trace via with a reference plane and (b) a two-trace via with a reference conductor. All dimensions are in mm.

excess capacitances for Fig. 3(a) with 1) $\varepsilon_1 = \varepsilon_2 = \varepsilon_0$ and 2) $\varepsilon_1 = 4\varepsilon_0$ and $\varepsilon_2 = \varepsilon_0$; for Fig. 3(b) with 3) $\varepsilon_1 = \varepsilon_2 = 4\varepsilon_0$ and 4) $\varepsilon_1 = 4.5\varepsilon_0$ and $\varepsilon_2 = 5.4\varepsilon_0$ are listed in Table I along with data obtained from [1] and [3]. In [1] and [3], the strips were replaced by the equivalent wires of radii which are one-fourth of the widths of the strips. In our computation, the lengths of all traces have been truncated to $2.5h$, whereas the width of the reference conductor has been truncated to $1.5l$, with h and l being the height of a via hole and the length of the traces. The truncation of traces and reference conductors is valid since the excess charge distribution decays rapidly as we move away from the center of a via. A total of 263 and 687 unknowns were used for the vias shown in Figs. 3(a) and (b), respectively. As shown in Table I, the data for the via shown in Fig. 3(a) agree well with the published results. However, the data for the via shown in Fig. 3(b) are considerably different from the results reported elsewhere. Unfortunately, no experimental result for this structure is available to establish the relative accuracy of these results associated with Fig. 3(b).

V. CONCLUSION

A method to compute the equivalent capacitance of a via, which is based on an integral equation formulated in terms of the excess charge formulation, has been presented in this paper. The method is

applicable to via geometries with or without through-hole reference conductors. The recently developed closed-form Green's function was employed to circumvent the time-consuming evaluation of a nested infinite series, required in the evaluation [3].

REFERENCES

[1] T. Wang, R. F. Harrington, and J. R. Mautz, "Quasi-static analysis of a microstrip via through a hole in a ground plane," *IEEE Trans. Microwave Theory Tech.*, vol. 36, pp. 1008–1013. June 1988.

[2] P. Kok and D. De Zutter, "Capacitance of a circular symmetric model of a via hole including finite ground plane thickness," *IEEE Trans. Microwave Theory Tech.*, vol. 39, pp. 1229–1234, July 1991.

[3] T. Wang, J. R. Mautz, and R. F. Harrington, "The excess capacitance of a microstrip via in a dielectric substrate," *IEEE Trans. Computed-Aided Design*, vol. 9, pp. 48–56, Jan. 1990.

[4] Q. Gu, Y. E. Yang, and M. A. Tassoudji, "Modeling and analysis of vias in multilayered integrated circuits," *IEEE Trans. Microwave Theory Tech.*, vol. 41, pp. 206–214, Feb. 1993.

[5] Q. Gu, M. A. Tassoudji, S. Y. Poh, R. T. Shin, and J. A. Kong, "Coupled noise analysis for adjacent vias in multilayered digital circuits," *IEEE Trans. Circuit Syst.*, vol. 41, pp. 796–804, Dec. 1994.

[6] Y. L. Chow, J. J. Yang, and G. E. Howard, "Complex images for electrostatic field computation in multilayered media," *IEEE Trans. Microwave Theory Tech.*, vol. 40, pp. 1120–1125, July 1991.

[7] K. S. Oh, D. Kuznetsov, and J. E. Schutt-Aine, "Capacitance computations in a multilayered dielectric medium using closed-form spatial Green's functions," *IEEE Trans. Microwave Theory Tech.*, vol. 42, pp. 1443–1453, Aug. 1994.

[8] K. S. Oh, "Efficient modeling of interconnections and capacitive discontinuities in high-speed digital circuits," Ph.D. dissertation, Univ. of IL at Urbana-Champaign, 1995.

[9] A. R. Djordjevic and T. K. Sarkar, "Computation of inductance of simple vias between two striplines above a ground plane," *IEEE Trans. Microwave Theory Tech.*, vol. 33, pp. 265–269, Mar. 1985.

Analysis of Edge Coupled Strip Inset Dielectric Guide

Z. Fan and Y. M. M. Antar

Abstract—The edge coupled strip inset dielectric guide is analyzed using the extended spectral domain approach. This structure, as compared to microstrip line, has several interesting features and can be very useful for microwave and millimeter wave applications. Validity of the approach is established by comparing numerical results with measured data. As many structural and material parameters can be chosen, a wide fundamental mode bandwidth and a broad range of characteristic impedances can be achieved, leading to great flexibility. The dispersion in fundamental mode propagation constants and impedances is found to be very low. With suitable choice of different permittivities for two dielectric layers, the same propagation constants for two fundamental modes can be obtained. This property is desirable for directional coupler applications.

I. INTRODUCTION

Microstrip line has been the most popular transmission medium used for constructing microwave and millimeter wave circuits [1]. It is well known that one of the problems with open microstrip circuits is the excitation of surface waves from discontinuities in the circuits

EFFICIENT TRANSIENT SIMULATION OF DISTRIBUTED INTERCONNECTS

Jose E. Schutt-Aine and Dmitri Kuznetsov
Electrical and Computer Engineering,
University of Illinois,
Urbana, IL 61801,
USA

I. Introduction

The electrical performance of high-speed integrated circuits and digital networks strongly depends on the behavior of interconnects between various components of these systems. The prediction of such performance can only be achieved by the used of computer-aided design and simulation tools. The simulation of high-speed digital circuits has gained a significant role in the past few years since it is critical in the evaluation of noise levels, signal corruption and signal delay in fast switching circuits. This paper explores the various aspects and techniques for transmission line simulation; in particular, two different methods are described: the scattering parameter method and the optimal method.

Two main aspects in the solution procedure must be distinguished, namely the line model and the transient simulation scheme. In the transient simulation step, the time-domain representation of the line model is obtained to yield the transient solution.

Two different classes of models can be employed: circuit models and non-circuit models. Non circuit models cannot be directly implemented into a circuit simulator. Circuit models can be directly incorporated into a circuit simulator; they relate voltages and currents at the line terminals and are independent of the terminations.

Further, two types of line characterization can be identified, namely closed-loop and open-loop characterizations. A closed-loop characterization such as Z- Y- H- and S- parameter characterizations results in complex oscillating transfer functions and transient characteristics. An open-loop characterization—in terms of the propagation functions— separates forward and backward waves and results in simple transfer functions and transient characteristics.

II. Scattering Parameters

Scattering parameters have been extensively used in microwave applications for the

measurement of high-frequency circuits as well as circuit analysis. The advantages of the scattering parameter approach reside in the flexibility in the choice of the reference system which can be adjusted to match certain characteristics of the network under study and simplify the analysis and the computations [1]-[3]. A direct consequence of this property is the greater computational stability and the simplicity of the closed-form solutions. More specifically, lossless and lossy transmission lines can be analyzed in conjunction with nonlinear terminations to yield solutions in which backward and forward waves are separated (see Fig. 1).
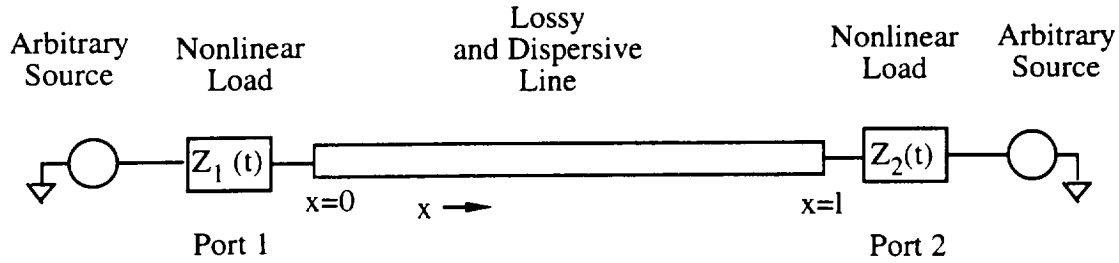

Fig. 1.

Consider a transmission line of length 1 with complex characteristic impedance Z_c and propagation velocity v. This transmission line is connected to two ideal lossless reference lines as shown in Fig. 2, it can then be described in the frequency domain through its scattering parameters using

$$B_1 = S_{11}A_1 + S_{12}A_2 \qquad (1a)$$

$$B_2 = S_{21}A_1 + S_{22}A_2 \qquad (1b)$$

where A_1 and A_2 are the incident voltage waves in the reference line of characteristic impedance Z_0. B_1 and B_2 are the reflected waves due to A_1 and A_2 respectively. It can be shown that

$$S_{11} = S_{22} = \frac{(1 - e^{-2j\omega l/v})\rho}{1 - e^{-2j\omega l/v}\rho^2} \qquad S_{12} = S_{21} = \frac{(1 - \rho^2)e^{-j\omega l/v}}{1 - e^{-2j\omega l/v}\rho^2} \qquad (2)$$

where

$$\rho = \frac{Z_c - Z_0}{Z_c + Z_0} \qquad (3)$$

In the time domain this correlates to (lowercase characters for time-domain variables)

$$b_1(t) = s_{11}(t)*a_1(t) + s_{12}(t)*a_2(t) \qquad (4a)$$

$$b_2(t) = s_{21}(t)*a_1(t) + s_{22}(t)*a_2(t) \qquad (4b)$$

where $s_{ij}(t)$ is the time-domain Green's function associated with S_{ij}. These equations are combined with the terminal conditions

$$a_1(t) = T_1(t)g_1(t) + \Gamma_1(t)b_1(t) \qquad (5a)$$

$$a_2(t) = T_2(t)g_2(t) + \Gamma_2(t)b_2(t) \qquad (5b)$$
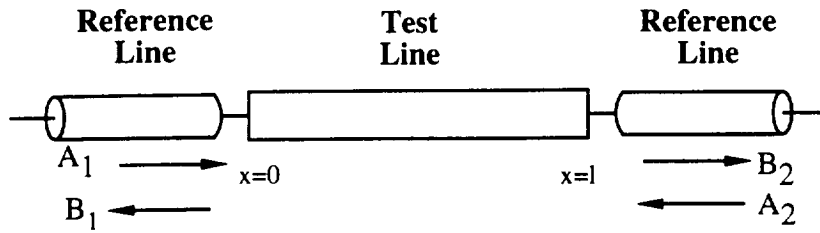

Fig. 2.

where $T_1(t)$, $T_2(t)$ are the transmission coefficients, $\Gamma_1(t)$ and $\Gamma_2(t)$ are the reflection coefficients and $g_1(t)$ and $g_2(t)$ are the time-domain expressions for the voltage sources. $T_1(t)$, $T_2(t)$, $\Gamma_1(t)$ and $\Gamma_2(t)$ are time-dependent and are related to the terminations $Z_1(t)$ and $Z_2(t)$ of Fig. 1 which may be the time-domain representations of reactive elements or linearized active circuits. The convolution operation is defined as

$$s_{ij}(t)*a_j(t) = \int_0^t s_{ij}(t-\tau)*a_j(\tau)d\tau \qquad (6)$$

When time is discretized the convolution becomes

$$s_{ij}(t)*a_j(t) = \sum_{\tau=1}^{t} s_{ij}(t-\tau)a_j(\tau)\Delta\tau \qquad (7)$$

where $\Delta\tau$ is the time step.
we isolate the term containing $a_j(t)$

$$s_{ij}(t) * a_j(t) = s_{ij}(0)a_j(t) + \sum_{\tau=1}^{t-1} s_{ij}(t-\tau)a_j(\tau)\Delta\tau \tag{8}$$

we then define the history term as

$$H_{ij}(t) = \sum_{\tau=1}^{t-1} s_{ij}(t-\tau)a_j(\tau)\Delta\tau : \quad \text{History} \tag{9}$$

Define $s'_{ij}(0) = s_{ij}(0)\Delta\tau$ we finally obtain

$$b_1(t) = s'_{11}(0)a_1(t) + s'_{12}(0)a_2(t) + H_{11}(t) + H_{12}(t) \tag{10a}$$

$$b_2(t) = s'_{21}(0)a_1(t) + s'_{22}(0)a_2(t) + H_{21}(t) + H_{22}(t) \tag{10b}$$

When combined with the termination conditions of (5), the solution for the independent waves can be extracted to yield

$$a_1(t) = \frac{[1-\Gamma_2(t)s'_{22}(0)]\,[T_1(t)g_1(t)+\Gamma_1(t)M_1(t)]}{\Delta(t)} + \frac{\Gamma_1(t)s'_{12}(0)[T_2(t)g_2(t)+\Gamma_2(t)M_2(t)]}{\Delta(t)} \tag{11a}$$

$$a_2(t) = \frac{[1-\Gamma_1(t)s'_{11}(0)]\,T_2(t)g_2(t)+\Gamma_2(t)M_2(t)]}{\Delta(t)} + \frac{\Gamma_2(t)s'_{21}(t)(0)[T_1(t)g_1(t)+\Gamma_1(t)M_1(t)]}{\Delta(t)} \tag{11b}$$

$$\Delta(t) = [1-\Gamma_1(t)s'_{11}(0)]\,[1-\Gamma_2(t)s'_{22}(0)] - \Gamma_1(t)s'_{12}(0)\Gamma_2(t)s'_{21}(0) \tag{11c}$$

with $M_1(t) = H_{11}(t) + H_{12}(t)$ and $M_2(t) = H_{21}(t) + H_{22}(t)$. The total voltages and currents at the ports can be recovered from the voltage waves using the relations

$$v_1(t) = a_1(t) + b_1(t) \tag{12a}$$

$$v_2(t) = a_2(t) + b_2(t) \tag{12b}$$

$$i_1(t) = \frac{a_1(t)}{Z_o} - \frac{b_1(t)}{Z_o} \tag{12c}$$

$$i_2(t) = \frac{a_2(t)}{Z_o} - \frac{b_2(t)}{Z_o} . \tag{12d}$$

In general, the frequency domain scattering parameters can be calculated from the line

parameters using equations (2); next an inverse Fourier transform permits to extract the time-domain Green's functions which can then be used to calculate the voltage waves. Most of the computations reside in the evaluation of the convolution history terms as expressed by (9).

III. The Optimal Method

In [4] the problem of distributed line simulation was analyzed to develop the optimal method, resulting in the maximum efficiency, accuracy and practical applicability with respect to the transient simulation of digital circuits. The method handles, in the same straightforward manner, uniform and nonuniform multiconductor lines with constant and frequency-depend parameters, including real lines characterized with frequency- or time-domain data samples. Moreover, an excellent simulation accuracy in the full frequency/time range, from zero to infinity, is attained with the minimal number of the data samples. The resulting line model can be directly used in a circuit simulator; the method supports variable time stepping and has linear computational complexity. The efficiency of the optimal method allows for an accurate simulation of realistic circuits, containing thousands of multiconductor nonuniform frequency-depend lines and nonlinear active devices, with virtually no increase in the simulation time compared to the simple replacement of interconnects with lumped resistors.

As shown in [4] and [5], to achieve the maximum efficiency, accuracy and practical applicability, transient simulation of distributed lines should be based on:

- a time-only formulation;
- the open-loop characterization;
- a device model which does not require to introduce current variables;
- indirect numerical integration;
- the difference approximation based on interpolation.

The detailed description of the optimal method and its application to uniform and nonuniform coupled lines can be found in [5]-[9]. Here, we shall confine ourselves to a single uniform line case.

For single uniform lines, the open-loop element characteristic is given by

$$I_1 = Y_c(\omega)V_1 - G_1, \tag{13a}$$

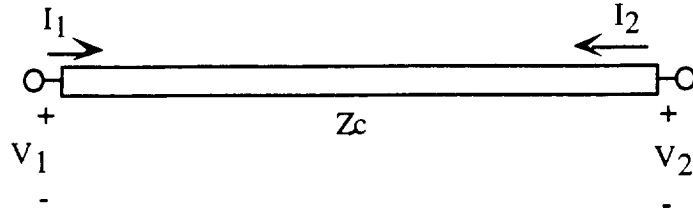$$I_2 = Y_c(\omega)V_2 - G_2, \tag{13b}$$

Fig. 3. Conventions for the voltages and currents at the line terminals.
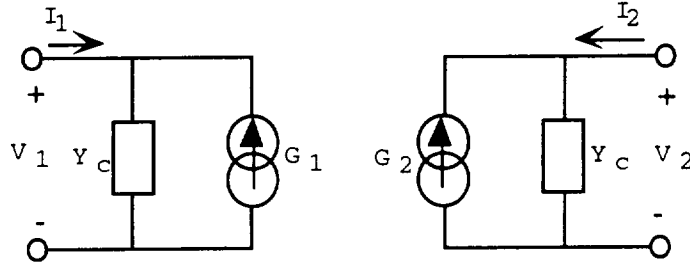

Fig. 4. A circuit-diagram interpretation of the line element characteristic.

where

$$G_1 = e^{-\gamma l} [2I_2 + G_2],$$ (14a)

$$G_2 = e^{-\gamma l} [2I_1 + G_1],$$ (14b)

$Y_c = 1/Z_c$ is the complex characteristic admittance of the line, and $e^{-\gamma l}$ is the propagation function. Conventions for the terminal voltages and currents are shown in Fig. 3. Figure 4 shows a circuit-diagram interpretation of the element characteristic (13).

The difference approximation [6] is a general method for applying numerical integration to systems whose differential equations are not available (such as systems characterized with discrete samples of their time- or frequency-domain responses, or transcendental transfer functions). The first step of the difference approximation consists of approximating the responses with the corresponding responses of a system with known differential equations. For instance, for the scalar frequency-domain difference approximation in the parallel canonic form, we express the propagation function in terms of rational function as

$$e^{-\gamma l} \cong \left[A_1 + \sum_{i=1}^{L} \frac{a_{1i}}{1 + j\omega / \omega_{c1i}} \right] e^{-j\omega\tau}, \tag{15}$$

where τ is the propagation delay, A_1 is the final value, the a_i's and ω_{ci}'s are the cut-off frequencies and partial-expansion coefficients respectively. We also approximate $Y_c(\omega)$ as

$$Y_c(\omega) \cong \left[A_2 + \sum_{i=1}^{L} \frac{a_{2i}}{1 + j\omega / \omega_{c2i}} \right]. \tag{16}$$

Note that there is no delay term since the transfer relationship of the impedance is instantaneous.

We use interpolation-based methods [6], [9] to perform the approximation. One of the methods—the relaxation interpolation method in the parallel form—approximates the original function in terms of a sum of basis functions

$$g(\omega) = \sum_{i=1}^{L} \phi_i(\omega), \tag{17}$$

where $g(\omega)$ is the function to be approximated and $\phi_i(\omega)$ are the basis functions. It is assumed that the finite values of the basis functions and the finite value the original function are zero. Let each basis function approximate the original function at some interval around one of the approximation points and be decreasing so fast that its value is negligibly small at the approximation points corresponding to larger values of the argument. For the first basis function this assumes

$$\phi_1(\omega_1) \cong g(\omega_1). \tag{18}$$

Now, we can write for the next basis function

$$\phi_2(\omega_2) \cong g(\omega_2) - \phi_1(\omega_2), \tag{19}$$

and more generally

$$\phi_i(\omega_i) \cong g(\omega_i) - \sum_{j=1}^{i-1} \phi_j(\omega_i). \tag{20}$$

After the first pass, we can repeat the above procedure, taking into account all the basis functions obtained from the first pass:

$$\phi_i(\omega_i) \cong g(\omega_i) - \sum_{\substack{j=1 \\ j \neq i}}^{L} \phi_j(\omega_i). \tag{21}$$

After this second pass, the difference between the original and approximating functions will be reduced, because an influence of all the terms was accounted more accurately during the calculation of the approximation parameters. The procedure may be repeated to achieve a desired accuracy.

The following summarizes the steps involved in applying the real-part parallel relaxation interpolation method to $Y_c(\omega)$. In this case, $Y_c(\omega)$ is being approximated as

$$Y_c(\omega) \cong \left[A + \sum_{i=1}^{L} \frac{a_i}{1 + j\omega/\omega_{ci}} \right]. \tag{22}$$

Let g be the real part of Y_c, then

$$g(\omega) \cong \left[A + \sum_{i=1}^{L} \frac{a_i}{1 + \omega^2/\omega_{ci}^2} \right]. \tag{23}$$

1. Choose approximation interval: 2L+1 frequency points.

2. Sample original function at the frequencies $\omega_k = \omega_{max} \left[\dfrac{k}{2L} \right]^7$, $k = 0, 1, ..., 2L$.

3. Reverse the order of the samples.

4. Initialize $a_i = 0$, $\omega_i = 1$, $i = 1, 2, ..., L$.

REPEAT until a desired accuracy tolerance is attained

$$A = g(\omega_{max}) - \sum_{j=1}^{L} \frac{a_j}{1 + \omega_{max}^2/\omega_{cj}^2}, \tag{24}$$

FOR

i runs as 1, 2, ..., L

$$\omega_i^2 = \frac{\theta_i(\omega_{2i})\omega_{2i}^2 - \theta_i(\omega_{2i-1})\omega_{2i-1}^2}{\theta_i(\omega_{2i-1}) - \theta_i(\omega_{2i})}, \tag{25}$$

$$a_i = \theta_i(\omega_{2i})\left(1 + \frac{\omega_{2i}}{\omega_{ci}^2}\right), \tag{26}$$
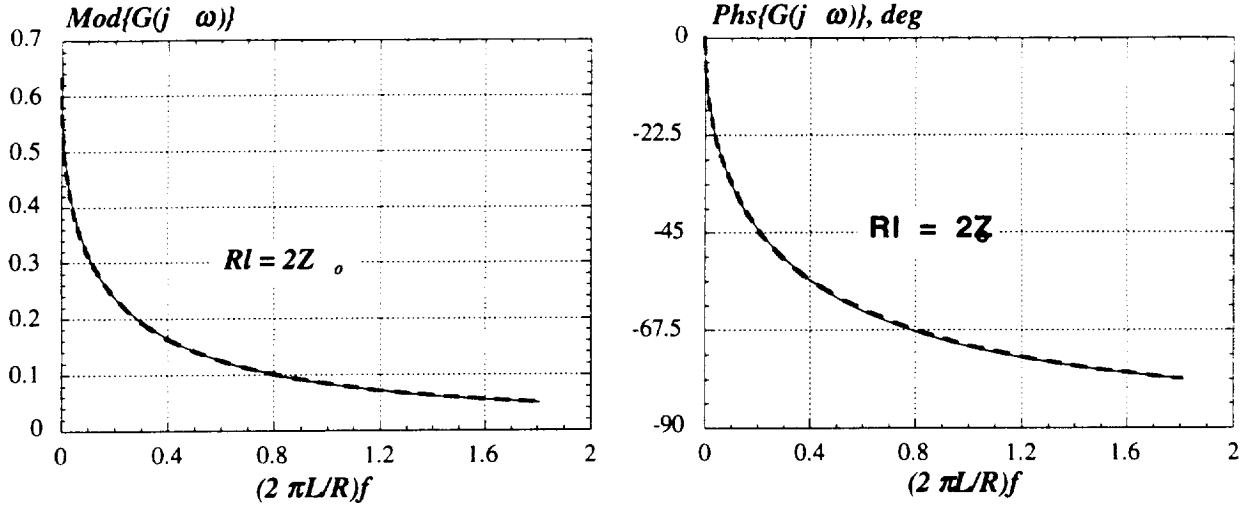
where

Fig. 5. Comparison of the original (thin continuous curves) and approximate (thick dashed curves) functions.

$$\theta_i(\omega_k) = g(\omega_k) - A - \sum_{\substack{j=1 \\ j \neq i}}^{L} \frac{a_j}{1 + \omega_k^2 / \omega_{cj}^2}, \tag{27}$$

End of FOR loop,
End of REPEAT loop.

Figure 5 shows a typical 5th-order approximation of the dynamic part of the propagation function.

The indirect numerical integration [7] is a class of numerical integration methods based on the analytical relationship between the continuous and discrete domains. It has ideal accuracy, convergence and stability properties. The approximate rational polynomial transfer functions represent systems described with finite-order ordinary differential equations, and can be discretized, and simulated recursively in the time-domain using numerical integration. For instance, for a system with the transfer function of the form

$$\tilde{H}(f) \cong \left[A + \sum_{i=1}^{L} \frac{a_i}{1 + j\omega / \omega_{ci}} \right] e^{j\omega\tau}, \tag{28}$$

the step-response invariant indirect numerical integration formulas in the parallel canonic form are given by

$$y[nT] = Ax[(n-k)T] + \sum_{i=1}^{L} y_{pi}[nT], \tag{29}$$

where

$$y_{pi}[nT] = a_i(1 - e^{-\omega_{ci}T})x[(n-k-1)T] + e^{-\omega_{ci}T}y_{pi}[(n-1)T], \tag{30}$$

x is the excitation, y is the system response, T is the time step and k is the discrete-time delay.

After the characteristic admittances and propagation functions have been discretized, the frequency-domain element characteristic (13) turns into the discrete-time element characteristic—the companion model—which is used by a circuit simulator to represent distributed lines, and is recursively updated at each time iteration via numerical integration formulas.

Figure 6 presents the comparison of the simulation results obtained with the optimal method and segmentation method (separating delays and losses). The network and line parameters are: R1=50 Ω, R2=1 kΩ, C=39 pF/m, L=539 nH/m, R=125 Ω/m, G=0, l=0.675 m. The following voltage pulse with linear rise and fall was taken for the excitation: E1=4 V (start time t_s=5 ns, rise time t_r=1 ns, pulse width t_w=20 ns, fall time t_f=1 ns), E2=0. The time-step T=0.5 ns. As can be observed, the results are in excellent agreement.

IV. Conclusions

Two methods of distributed line simulation were discussed—the scattering-parameter method and the optimal method. The scattering-parameter method permits a straightforward implementation of voltage wave solutions but is computationally expensive as a result of convolution calculations. The optimal method results in the maximum efficiency, accuracy and practical applicability with respect to the transient analysis of digital circuits. The optimal line model can be directly used in a circuit simulator, and lines can be characterized with frequency or time-domain data samples. The efficiency of the optimal method allows for an accurate simulation of real circuits, containing thousands of multiconductor nonuniform frequency-depend lines and nonlinear active devices, with virtually no increase in the simulation time compared to the replacement of interconnects with lumped resistors.
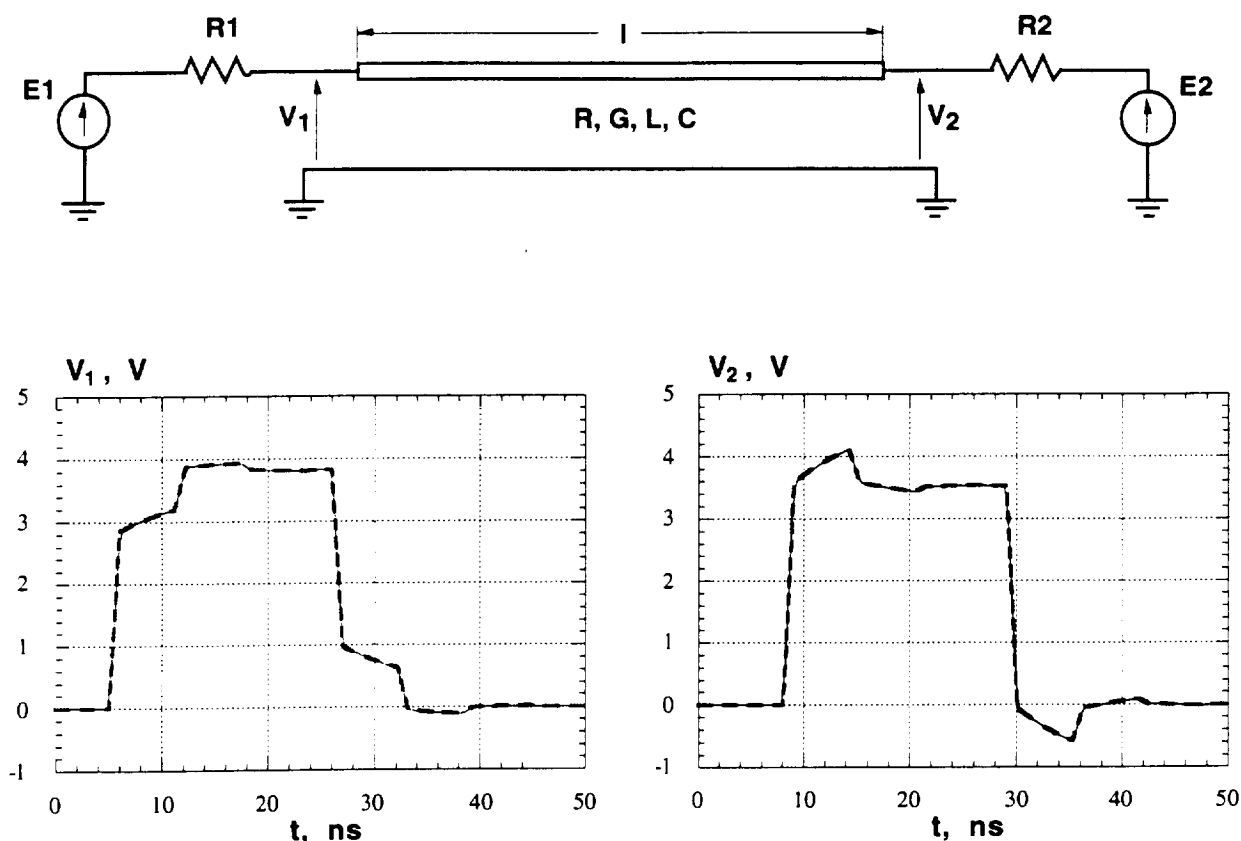
Fig. 6. Network configuration and comparison of the simulated waveforms obtained using the segmentation method (thin continuous curves) and the optimal method (thick dashed curves).

References

[1] J. E. Schutt-Ainé and R. Mittra, "Scattering Parameter Transient Analysis of Transmission Lines Loaded with Nonlinear Terminations," *IEEE Trans. Microwave Theory Tech.*, vol. MTT-36, pp. 529-536, March 1988.

[2] J. E. Schutt-Ainé and R. Mittra, "Transient Analysis of Coupled Lossy Transmission Lines with Nonlinear Terminations,"" *IEEE Trans. Circuit Syst.*, vol. CAS-36, pp. 959-967, July 1989.

[3] J. E. Schutt-Ainé, "Scattering Parameters for the Simulation of Transmission-Line Networks," *1990 IEEE-CAS International Symposium Proceedings*, pp. 2693-2695, New Orleans, May 1990

[4] D. B. Kuznetsov, *Transmission Line Modeling and Transient Simulation*, MS thesis. Urbana, IL: University of Illinois at Urbana-Champaign, 1993.

[5] D. B. Kuznetsov and J. E. Schutt-Ainé. "The optimal transient simulation of distributed lines, Part I: Formulation of the optimal method," submitted for publication in *IEEE Trans. Circuits Syst.—I: Fundamental Theory and Applications*.

[6] D. B. Kuznetsov and J. E. Schutt-Ainé. "The optimal transient simulation of distributed lines, Part II: Difference Approximation," submitted for publication in

IEEE Trans. Circuits Syst.—I: Fundamental Theory and Applications.

[7] D. B. Kuznetsov and J. E. Schutt-Ainé. "Indirect numerical integration," submitted for publication in *IEEE Trans. Circuits Syst.—I: Fundamental Theory and Applications.*

[8] D. B. Kuznetsov and J. E. Schutt-Ainé. "The optimal transient simulation of nonuniform distributed lines," submitted for publication in *IEEE Trans. Circuits Syst.—I: Fundamental Theory and Applications.*

[9] D. B. Kuznetsov and J. E. Schutt-Ainé. "Modified direct rational interpolation method for the frequency-domain difference approximation," in preparation.

Difference Model Approach for the Transient Simulation of Transmission Lines

Dmitri Kuznetsov and José E. Schutt-Ainé

Electromagnetic Communication Laboratory
Department of Electrical and Computer Engineering
University of Illinois
1406 West Green Street
Urbana, Illinois 61801-2991 USA

Abstract—An optimal technique (in terms of computational efficiency, accuracy, and practical applicability) for the transient simulation of distributed multiconductor *RLGC* lines was developed by applying the indirect numerical integration method (the most efficient and accurate transient simulation method) to the device model for a distributed line (the most efficient and practically applicable model). The technique can be directly used in a circuit simulator. The computational complexity is linearly proportional to the number of time-steps. Nonuniform lines, lines with frequency-dependent parameters, and real lines, characterized with a few samples of time- or frequency-domain measurements or electromagnetic simulations, can be accurately and efficiently simulated.

I. INTRODUCTION

The transient simulation of distributed lines has gained special importance with the development of high-speed digital electronics. Previously developed techniques are quite diverse, but not always computationally efficient and applicable to real circuits in which distributed lines are surrounded by thousands of active devices. In [1] an attempt was made to develop a technique that would be optimal in computational efficiency, accuracy, and applicability to real problems. The results obtained in [1] are summarized in this paper.

II. SYSTEM MODEL FOR A DISTRIBUTED LINE

The system-diagram representation of a single line is shown in Fig. 1. W_{vf} and W_{vb} represent the forward and backward voltage propagation functions, respectively; T_1, T_2 and Γ_1, Γ_2 are the near- and far-end transmission and reflection coefficients, respectively.

The system-diagram representation of a multiconductor line is given in Fig. 2. W_{vmf} and W_{vmb} are the diagonal forward and backward modal voltage propagation function matrices; T_1, T_2 and Γ_1, Γ_2 represent the near- and far-end transmission and reflection coefficient matrices; and M_{vf}, M_{vb} are the forward and backward modal voltage transfor-
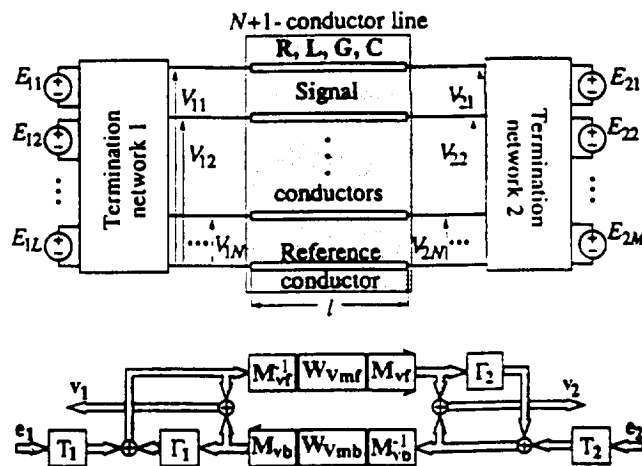

Fig. 2. System model for a multiconductor line.

mation matrices.

The models reproduce the general relationship between the physical processes of wave propagation, reflection, and coupling in a distributed system and can represent arbitrary distributed systems such as uniform and nonuniform transmission lines, waveguides, and plane-wave propagation. For distributed *RLGC* lines, the mathematical justification of the models was obtained [1]. The models can be used for system analysis of distributed networks. They also allow one to obtain the solution for a distributed system without complex mathematical derivations.

From Figs. 1 and 2, it can be observed that a distributed line along with the terminations forms a feedback system. This explains why a global-parameter characterization (such as Z-, Y-, H-, or S-parameter characterization) results in complex, non-monotonous functions for the parameters. A direct characterization in terms of open-loop transfer functions (the propagation functions) leads to simpler transfer functions and transient characteristics and should be used for the transient simulation.

III. DEVICE MODEL FOR A DISTRIBUTED LINE

Distributed line models can be divided into circuit and non-circuit models. Non-circuit models cannot be directly inserted into a circuit simulator, and, consequently, can not be applied with efficiency for the transient analysis of real circuits. The system models described in the preceding section may serve as an example of non-circuit models.

Circuit models can be directly placed into a circuit simulator, and, therefore, are of prime practical interest. They relate
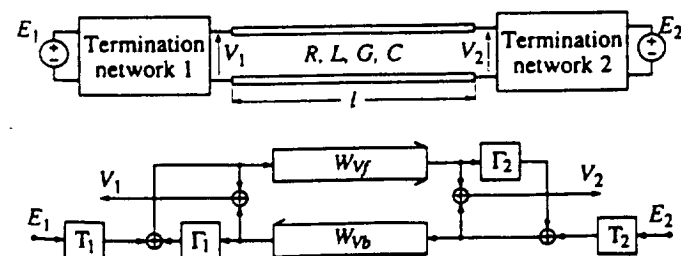

Fig. 1. System model for a single line.

tion. The resulting difference equation is called the difference model of the continuous system [4]. Depending on the discretization technique, one recognizes the direct and indirect numerical integration methods.

For the direct methods, the differential equation is discretized using approximations for integrals or derivatives. Indirect numerical integration methods are based on the analytical relationship between discrete samples of the system excitation and response (analytical relationship between the continuous and discrete time domains). The relationship is obtained using the time-response invariance method. For this method the excitation is assumed to be piecewise of a certain form, for instance, staircase, piecewise linear, piecewise quadratic, cubic, etc. Then, the general solution of the system differential equation can be found and expressed in terms of the discrete samples of the excitation and response (by using the samples as boundary conditions). The resulting difference model is then used to recursively compute the response in the time domain [4].

The indirect numerical integration provides the exact system response to an excitation which is piecewise of the same form as the difference model invariance. For instance, the ramp-invariant difference model provides the exact system response to a piecewise linear excitation such as a pulse with linear rise and fall. The indirect numerical integration has ideal stability and convergence properties, because, in the absence of an excitation, it always provides the exact system response, irrespective of the value of time step and form of invariance. It is also more accurate than the direct method.

From the foregoing discussion one can conclude that an optimal technique (in terms of computational efficiency, accuracy, and practical applicability) for transient analysis of distributed lines should be based on the device model and the indirect numerical integration. This combination was first proposed by A. J. Gruodis and C. S. Chang [5], but using the direct numerical integration method.

Due to the distributed nature, modules of a transmission line model can not be exactly described with finite-order ordinary differential equations. Consequently, an approximate ordinary differential equation representation has to be found before numerical integration can be applied. This can be achieved by approximating a frequency- or time-domain response with the corresponding response of a system described with ordinary differential equations. The following difference approximation procedure was developed that allows one to apply indirect numerical integration to an arbitrary system. In general, a system may contain an attenuation component A, a delay component τ, and a dynamic part. The difference approximation procedure consists of one step: represent the transfer function in the form

$$W(j\omega) = \left(A + \sum_{i=1}^{L} \frac{a_i}{1 + j\omega / \omega_{ci}} \right) e^{-j\omega\tau} , \qquad (3)$$

or the transient characteristic in the form

$$h(t) = \left(B - \sum_{i=1}^{L} a_i \, e^{-\omega_{ci}(t-\tau)} \right) u(t-\tau) . \qquad (4)$$

Then, the step-invariant difference model is given by

$$y(t_n) = A\,x(t_n - \tau) + \sum_{i=1}^{L} y_i(t_n) , \qquad (5a)$$

where

$$y_i(t_n) = a_i \left(1 - e^{-\omega_{ci}T_n} \right) x(t_{n-1} - \tau) + e^{-\omega_{ci}T_n} y_i(t_{n-1}) , \qquad (5b)$$

and the ramp-invariant difference model is

$$y(t_n) = B\,x(t_n - \tau) - \sum_{i=1}^{L} y_i(t_n) , \qquad (6a)$$

where

$$y_i(t_n) = \frac{a_i \left(1 - e^{-\omega_{ci}T_n} \right)}{\omega_{ci}T_n} \left[x(t_n - \tau) - x(t_{n-1} - \tau) \right]$$
$$+ e^{-\omega_{ci}T_n} y_i(t_{n-1}) . \qquad (6b)$$

A and B are the final and initial values of the transfer function, $x(t)$ and $y(t)$ are the excitation and response, $T_n = t_n - t_{n-1}$ is the value of the time-step at n-th iteration, and $u(t)$ is the unit-step function. Further increase in the order of the time-response invariance results in a difference model of higher order than the system differential equation without a significant increase in the difference model accuracy. Eqs. (3)–(6) correspond to the parallel canonic form of the difference model. Other forms (including direct and cascade canonic ones) can be found in [1].

In general, second-order terms representing complex-conjugate poles of the transfer function have to be added to the sum in (3) and the corresponding harmonic terms to the sum in (4). These terms were omitted here, because the elements of the device model for a distributed line represent aperiodic systems, and, therefore, have to be approximated using only real poles.

The frequency-domain difference approximation procedure is more general, because it can directly handle lines with arbitrary frequency-dependent parameters or lines characterized with frequency-domain measured data. The time-domain difference approximation procedure should be employed only if transient characteristics are available. For a single RLGC line, the analytical expressions were obtained for the transient characteristics and limiting values (A and B) for all the modules of the system and device models [1].

The difference approximation procedure is applied to the characteristic admittances and propagation functions. In the case of a multiconductor line, all entries of the characteristic admittance and propagation function matrices need to be approximated. The resulting time-domain device models have the same form as the frequency-domain models shown in Figs. 3 and 4. At each time iteration the instantaneous values of the conductances and current sources are recursively computed from the old values using the corresponding difference models. If the step-invariant difference model (5) is employed, the conductances are constant throughout the simulation (because the first-order difference models (5b) do not contain the current value of the excitation), and only the cur-

ementation of Surface
ary Conditions for the
Time-Domain Method

EE and Jose E. Schutt-Aine, *Member, IEEE*

the SIBC, it is represented by a convolution integral in the time domain. Tesche [6] has formulated a time-domain integral equation based on this convolution integral and pointed out that the direct computation of this convolution integral is impractical due to the large computation time and storage requirements. On the other hand, Maloney and Smith [7] have applied the SIBC to the finite-difference time-domain method. To overcome the computational difficulties associated with the convolution integral, they use an approximate recursive formula. Their implementation, however, requires the exponential approximation to be performed prior to the FDTD simulation. Beggs *et al.* [8] have eliminated this preprocessing time by performing the exponential approximation based on the high conductivity surface impedance approximation. It should be noted that when the SIBC is applied to the finite-difference time-domain (FDTD) method, in addition to the reduction of discretization space, further computational saving is achieved due to the larger discretization step compared to that for the nonreduced original problem. A detailed discussion of this computational saving is given in [7] and [8].

In this paper, the implementation of the SIBC in the FDTD method is considered for a lossy dielectric half-space and a thin lossy dielectric medium. For a lossy dielectric half-space, the normalized impedance function for a lossy medium is approximated in the frequency domain using a series of first-order rational functions. Since the normalized impedance function used in this paper is independent of medium properties, the rational approximation has to be performed only once. The results of this approximation are tabulated for rational functions of various orders. Then, using the approximate normalized impedance function and assuming the waves to be piecewise linear in time, a closed-form expression is derived to evaluate the time-domain convolution integral recursively. Thus, the presented formulation is numerically more efficient than that in [7] because the preprocessing time for the exponential approximation is eliminated and more accurate than that in [8] since the high conductivity approximation is not utilized.

Although several methods have been proposed to model a thin lossless dielectric shell for the FDTD method [9]–[12], little work has been performed for a perfect electric conductor-(PEC-)backed P lossy dielectric shell in spite of its frequent occurrence in practical problems. A full time-domain implementation of the SIBC, which accounts for the frequency
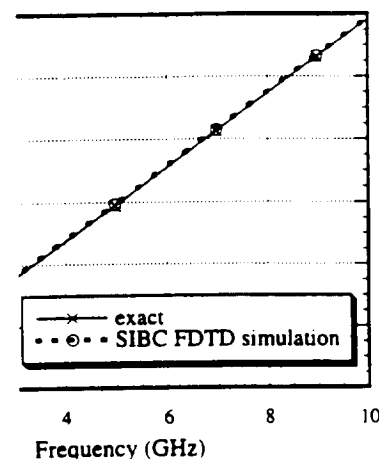
the FDTD simulation.
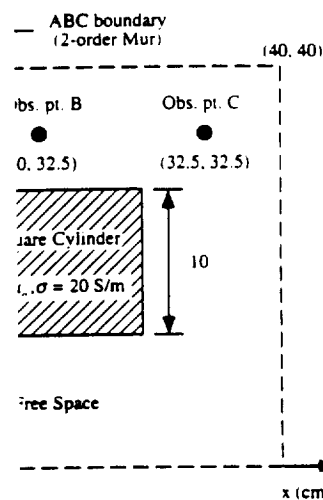
>-dimensional TM FDTD example.

ler (see Fig. 6). The simulation is ormal FDTD and the SIBC FDTD iers

μm

;

$(t-0.646 \times 10^{-10})/0.1874 \times 10^{-11})^2$.

ilation results of the normal FDTD vell at the observation point B, and for the points A and C. The same using the SIBC FDTD with five : steps than for the previous ones. imensional plot of the simulation ormal FDTD simulation, whereas . from the SIBC FDTD with the igh the same excitation is used for excitation[4] and difference in the

rce excitation is added to the FDTD field iereas, in the hard excitation, the source at the excitation point.

REFERENCES

[1] M. A. Leontovich. "On the approximate boundary conditions for electro-magnetic fields on the surface of well conducting bodies," in *Investigations of Propagation of Radio Waves*. B. A. Vvedensky, Ed. Moscow: Academy of Sciences USSR. 1948, pp. 5–20.

[2] T. B. A. Senior. "Impedance boundary conditions for imperfectly conducting surfaces," *Appl. Sci. Res.*, vol. 8. Sec. B. pp. 418–436. 1960.

[3] ———. "Approximate boundary conditions," *IEEE Trans. Antennas Propagat.*, vol. AP-29, pp. 826–829, Sep. 1981.

[4] K. M. Mitzner. "An integral equation approach to scattering from a body of finite conductivity," *Radio Sci.*, vol. 2, pp. 1159–1470, Dec. 1967.

[5] ———. "Effective boundary conditions for reflection and transmission by an absorbing shell of arbitrary shape," *IEEE Trans. Antennas Propagat.*, vol. AP-16, pp. 706–712. Nov. 1968.

[6] F. M. Tesche, "On the inclusion of loss in time-domain solutions of electromagnetic interaction problems," *IEEE Trans. Electromagn. Compat.*, vol. 32, pp. 1–4, Feb. 1990.

[7] J. G. Maloney and G. S. Smith. "The use of surface impedance concepts in the finite-difference time-domain method," *IEEE Trans. Antennas Propagat.*, vol. 40, pp. 38–48, Jan. 1992.

[8] J. H. Beggs. R. J. Luebbers, K. S. Yee, and K. S. Kunz. "Finite-difference time-domain implementation of surface impedance boundary conditions," *IEEE Trans. Antennas Propagat.*, vol. 40, pp. 49–56, Jan. 1992.

[9] J. G. Maloney and G. S. Smith. "The efficient modeling of thin material shells in the finite-difference time-domain (FDTD) method." *IEEE Trans. Antennas Propagat.*, vol. 40, pp. 323–330, Mar. 1992.

[10] R. J. Luebbers and K. Kunz. "FDTD modeling of thin impedance shells," *IEEE Trans. Antennas Propagat.*, vol. 40, pp. 349–351, Mar. 1992.

[11] L.-K. Wu and L.-T. Han. "Implementation and application of resistive sheet boundary condition in the finite-difference time-domain method," *IEEE Trans. Antennas Propagat.*, vol. 40, pp. 628–633, June 1992.

[12] P. A. Tirkas and K. R. Demarest, "Modeling of thin dielectric structures using the finite-difference time-domain technique," *IEEE Trans. Antennas Propagat.*, vol. 39, pp. 1338–1344, Sept. 1991.

[13] S. Wolfram. *Mathematica*. Reading, MA: Addison-Wesley, 1991.

Kyung Suk Oh (SM'91) was born in Pusan, South Korea, in 1965. He received the B.S. and M.S. degrees in electrical engineering from the University of Illinois, Champaign, in 1990 and 1992, respectively.

Since 1990, he has been involved in research work on modeling and simulation of high speed digital circuits in the electromagnetic communication laboratory at the University of Illinois, where he is pursuing the Ph.D. degree.

Jose E. Schutt-Aine (S'87–M'88) received the B.S. degree from Massachusetts Institute of Technology, Cambridge, MA, and the M.S. and Ph.D. degrees from the University of Illinois, Urbana, in 1984 and 1988, respectively.

Following graduation from MIT, he spent two years with Hewlett-Packard Microwave Technology Center in Santa Rosa, CA, where he worked as a Device Application Engineer. While pursuing graduate studies at the University of Illinois, he held summer positions at GTE Network Systems in Northlake, IL. He is presently serving as an Assistant Professor in the Department of Electrical and Computer Engineering at the University of Illinois. His current research interests are microwave theory and measurements, electromagnetics, high-speed digital circuits, solid-state electronics, circuit design, and electronic packaging.

Computation of Excess Capacitances of Various Strip Discontinuities Using Closed-Form Green's Functions

Kyung S. Oh, Jose E. Schutt-Aine, and Raj Mittra

Abstract— An efficient quasi-static method to compute excess (equivalent) capacitances of various strip discontinuities in a multilayered dielectric medium is presented. The excess charge distribution on the surface of a conductor is obtained by solving an integral equation in conjunction with closed-form Green's functions. A complete list of expressions of the closed-form Green's functions for a point charge, a line charge, and a semi-infinite line charge is presented. An open end, a bend, a step junction and a T junction are considered as numerical examples.

I. INTRODUCTION

Quasi-static analysis is often performed to characterize strip discontinuities when the dimensions of the discontinuities are much smaller than the wavelength. Under the quasi-static analysis, the dominant effect of strip discontinuities is fringing fields due to the physical irregularities of discontinuity geometries. The modeling of these fringing fields in terms of an excess capacitance is discussed in this paper.

Numerous papers have been published to compute excess capacitances of various microstrip discontinuities, and a summary of popular methods can be found in [1]. The most successful approach is one based on the formulation of an integral equation in terms of the excess charge distribution, which was first proposed by Silvester and Benedek [2] and has been applied to analyze various microstrip discontinuities [2]-[5]. The Green's function for a layered medium is employed in this approach. For N dielectric layers, the expression for this Green's function would consist of an N-1 nested infinite series [6]; hence, in practice, this form of the Green's function may not be applied to a multilayered medium. Recently, Sarkar et al. [7] solved discontinuity problems for a multilayered medium using the free-space Green's function, but additional unknown charges (over unknown charges on the surface of a conductor) had to be placed on the dielectric interfaces and the top ground plane to model the polarization charge and the free charge. Although such inclusion of unknowns may be tolerable for 2-D problems, it is computationally too burdensome for 3-D problems.

In this paper, the closed-form Green's function discussed in [8] is employed to formulate an integral equation in terms of the excess charge distribution. A complete list of expressions of the closed-form Green's functions for a point charge, a line charge, and a semi-infinite line charge

with or without a top ground plane is presented in this paper. The presented method requires neither additional unknowns to model dielectric interfaces and the top ground plane nor evaluations of any infinite series except for cases where the top ground plane is present. When the top ground plane is present, using the closed-form Green's function is still numerically advantageous since the nested infinite series in the expression of the usual Green's function becomes a simple infinite series without nesting.

II. CLOSED-FORM GREEN'S FUNCTIONS

Closed-form expressions of the electrostatic Green's functions for a point charge, a line charge, and a semi-infinite line charge are derived in this section based on the approach used in [8]. Consider N dielectric layers which are backed by a ground plane as depicted in Fig. 1. The Nth layer is either a half-space or terminated by an optional top ground plane. All dielectric layers and ground planes are assumed to be planar and infinite in the xz-plane. The electrostatic Green's function in the spectral domain is described by the following closed-form formula [8]:

$$\tilde{G}(\gamma, y|r_o) = \frac{1}{2\varepsilon_m \gamma}\Big(K_1^+(\gamma, m, n)e^{\gamma(y+y_o-2d_n)} + K_2^+(\gamma, m, n)e^{\gamma(y-y_o+2(d_{m-1}-d_n))}$$
$$+ K_3^+(\gamma, m, n)e^{\gamma(-y+y_o)} + K_4^+(\gamma, m, n)e^{\gamma(-y-y_o+2d_{m-1})}\Big) \qquad y \geq y_o \qquad (1a)$$

$$\tilde{G}(\gamma, y|r_o) = \frac{1}{2\varepsilon_m \gamma}\Big(K_1^-(\gamma, m, n)e^{\gamma(y+y_o-2d_m)} + K_2^-(\gamma, m, n)e^{\gamma(y-y_o)}$$
$$+ K_3^-(\gamma, m, n)e^{\gamma(-y+y_o+2(d_{n-1}-d_m))} + K_4^-(\gamma, m, n)e^{\gamma(-y-y_o+2d_{n-1})}\Big) \qquad y \leq y_o \qquad (1b)$$

where $\tilde{G}$ is the spectral-domain Green's function, and r and r_o are the observation and source points located in the nth and mth layers, respectively. The superscripts + and - are used to denote the cases for $y \geq y_o$ and $y \leq y_o$. The expressions for the four coefficient functions $K_i^\pm$ can be found in [8]. A closed-form expression of the Green's function in the space domain is obtained by approximating these four coefficient functions $K_i^\pm$ using exponential functions. It is important to mention that although $K_i^\pm$ is dependent on m and n, it is not a function of y and y_o; hence, the approximation can be performed without any prior knowledge of the junction geometry. The following two subsections detail the derivation of the closed-form Green's functions due to a point charge, a line charge, and a semi-infinite line charge with or without the top ground plane.

A. Closed-Form Green's Functions for Geometries Without the Top Ground Plane

When there is no top ground plane, the four coefficient functions $K_i^{\pm}$ in (1a) or (1b) are nonoscillatory and smooth functions of γ; hence, each coefficient function can be sufficiently approximated with real-valued exponential functions as follows [8]:

$$K_i^{\pm}(m,n,\gamma) = \sum_{j=1}^{N_{m,n,i}^{\pm}} C_{m,n,i}^{\pm,j} e^{a_{m,n,i}^{\pm,j}\gamma}, \qquad i = 1,2,3,4 \quad (2)$$

where $N_{m,n,i}^{\pm}$ denotes the number of exponential functions used in the approximation of $K_i^{\pm}$, which typically ranges from 5 to 10. The exponential functions used in the spectral-domain approximation can be physically interpreted as weighted images in the space domain [8]. Compared to the exact Green's function in the space domain, which consists of an infinite number of images, the expression for the closed-form Green's function consists of only a finite number of weighted images.

Once the exponential approximation is performed in the spectral domain, the closed-form Green's functions for 2-D and 3-D can be obtained in the space domain by using the inverse Fourier transformation formulas (14a) and (14b) in [8], and the resulting expressions are given by

$$G^{2D}(\rho|\rho_o) = -\frac{1}{2\pi\varepsilon_m}\sum_{i=1}^{4} f_i^{2D,\pm}(\rho|\rho_o) \qquad (3a)$$

$$G^{3D}(r|r_o) = \frac{1}{4\pi\varepsilon_m}\sum_{i=1}^{4} f_i^{3D,\pm}(r|r_o) \qquad (3b)$$

For $i=1$ and $y \geq y_o$, the expressions of $f_i^{2D,\pm}$ and $f_i^{3D,\pm}$ are given by

$$f_1^{2D,+}(\rho|\rho_o) = \sum_{j=1}^{N_{m,n,1}^{+}} C_{m,n,1}^{+,j} \cdot \ln\left(\sqrt{(x-x_o)^2 + (y+y_o-2d_n+a_{m,n,1}^{+,j})^2}\right) \qquad (4a)$$

$$f_1^{3D,+}(r|r_o) = \sum_{j=1}^{N_{m,n,1}^{+}} \frac{C_{m,n,1}^{+,j}}{\sqrt{(x-x_o)^2 + (y+y_o-2d_n+a_{m,n,1}^{+,j})^2 + (z-z_o)^2}} \qquad (4b)$$

Similar expressions can be obtained for $f_i^{2D,\pm}$ and $f_i^{3D,\pm}$ for other values of i.

To derive the Green's function for a semi-infinite uniform line charge, the auxiliary Green's function for a line charge with polarity reversal is employed [2]. Consider a uniform line charge,

which starts from $z = \xi$ and is infinitely extended in the positive z-direction; then the Green's function for a semi-infinite line charge G^{semi} can be expressed as

$$G^{semi}(r|r_o,\xi) = \frac{1}{2}\left[G^{2D}(\rho|\rho_o) + G^P(r|r_o,\xi)\right] \qquad (5)$$

where G^{semi} is the Green's function for a line charge with an abrupt polarity reversed from minus to plus at $z = \xi$. The expression for G^P is obtained by integrating the potential due to a point charge [2]:

$$G^P(r|r_o,\xi) = -\int_{-\infty}^{\xi} G^{3D}(r|r_o) + \int_{\xi}^{\infty} G^{3D}(r|r_o) = \frac{1}{4\pi\varepsilon_m}\sum_{i=1}^{4} f_i^{p,\pm}(r|r_o,\xi) \qquad (6)$$

Again, for $i=1$ and $y \geq y_o$, $f_i^{p,\pm}$ is given by

$$f_1^{p,+}(r|r_o,\xi) = \sum_{j=1}^{N_{m,n,1}^+} C_{m,n,1}^{+,j} \cdot \ln\left(\frac{\sqrt{(x-x_o)^2 + (y+y_o-2d_n+a_{m,n,1}^{+,j})^2 + (z-\xi)^2} + (z-\xi)}{\sqrt{(x-x_o)^2 + (y+y_o-2d_n+a_{m,n,1}^{+,j})^2 + (z-\xi)^2} - (z-\xi)}\right) \qquad (7)$$

B. Closed-Form Green's Functions for Geometries with the Top Ground Plane

When the top ground plane is present, all of the four coefficient functions $K_i^{\pm}$ are still nonoscillatory but contain a pole at $\gamma = 0$; as a consequence, $K_i^{\pm}$ can no longer be accurately approximated with exponential functions [8]. To overcome this difficulty, let us rewrite $\tilde{G}$ in the following manner:

$$\tilde{G}(\gamma,y|r_o) = R_{m,n}\tilde{G}^h(\gamma,y|r_o) + \tilde{G}'(\gamma,y|r_o) \qquad (8)$$

where $\tilde{G}^h$ is the spectral-domain Green's function for a homogeneous medium, i.e., all dielectric layers are replaced by the source layer. $R_{m,n}$ is a constant which is determined such that $\tilde{G}^h$ contains a pole at $\gamma = 0$ and $\tilde{G}'$ is a well-behaved function without any poles. $R_{m,n}$ can be obtained either numerically or analytically by taking limits of $\tilde{G}$ and $\tilde{G}^h$ as $\gamma \to 0$. Now the technique used in the previous section can be applied to obtain the closed-form expression for $\tilde{G}'$ in the space domain, and the space-domain expressions of $\tilde{G}$ are obtained once the corresponding expressions of $\tilde{G}^h$ are determined.

Expressions of $\tilde{G}^h$ in the space domain can be easily obtained using the image theory approach and are given by

$$G^{2D,h}(\rho|\rho_o) = -\frac{1}{2\pi} \sum_{k=-\infty}^{\infty} \ln\left(\frac{\sqrt{(x-x_o)^2 + (y-y_o-2kh)^2}}{\sqrt{(x-x_o)^2 + (y+y_o-2kh)^2}} \right) \tag{9a}$$

$$G^{3D,h}(r|r_o) = \frac{1}{4\pi} \sum_{k=-\infty}^{\infty} \left(\frac{1}{\sqrt{(x-x_o)^2 + (y-y_o-2kh)^2 + (z-z_o)^2}} \right.$$

$$\left. - \frac{1}{\sqrt{(x-x_o)^2 + (y+y_o-2kh)^2 + (z-z_o)^2}} \right) \tag{9b}$$

$$G^{p,h}(r|r_o,\xi) = \frac{1}{4\pi} \sum_{k=-\infty}^{\infty} \ln\left(\frac{\sqrt{(x-x_o)^2 + (y-y_o-2kh)^2 + (z-\xi)^2} + (z-\xi)}{\sqrt{(x-x_o)^2 + (y-y_o-2kh)^2 + (z-\xi)^2} - (z-\xi)} \right.$$

$$\left. \cdot \frac{\sqrt{(x-x_o)^2 + (y+y_o-2kh)^2 + (z-\xi)^2} - (z-\xi)}{\sqrt{(x-x_o)^2 + (y+y_o-2kh)^2 + (z-\xi)^2} + (z-\xi)} \right) \tag{9c}$$

Unfortunately, all expressions are written in terms of infinite series. Although $G^{2D,h}$ can be alternatively expressed using a closed-form formula [8], such closed-form formulas cannot be been found for $G^{3D,h}$ and $G^{p,h}$. Since the closed-form formula for $G^{2D,h}$ requires numerical integration when the moment matrix is computed, we will simply use (10a) to evaluate $G^{2D,h}$. Therefore, an infinite-series expression, in general, cannot be avoided for G^{2D}, G^{3D}, and G^p when the top ground plane is present. However, the expressions for G^{2D}, G^{3D}, and G^p given in this paper are still numerically more efficient than the ones obtained from the conventional image method since a nested infinite series of the conventional method is reduced to a simple infinite series without nesting as shown in the above equations.[1] For this reason we shall still refer to G^{2D}, G^{3D}, and G^p given by (9), (10a), (10b), and (10c) as closed-form Green's functions.

IV. FORMULATION OF AN INTEGRAL EQUATION

In this section, an integral equation is formulated in terms of the excess charge distribution using the closed-form Green's functions derived in the previous section. Figure 2 shows the planar view of the general geometry of a discontinuity, which consists of traces and a junction region. This general geometry represents most of the common strip discontinuities, e.g., an open-end, a nonothogonal bend, and various junctions. Although the present approach can handle conductors with finite thicknesses, the conductor thicknesses are assumed to be infinitely thin in this paper. The discontinuity structure is embedded in a layered dielectric medium, which is shown in Fig. 1.

---

[1] Alternatively, infinite series can be avoided by modeling the top ground plane as an additional conductor and using the Green's functions in the previous section.

The integral equation relating the electrostatic potential ϕ and the charge density q on the surface of a conductor is given by

$$\phi(r) = \int_{\Omega} G^{3D}(r|r')q(r')dr' = \left\langle G^{3D}, q \right\rangle \tag{10}$$

where Ω are the surfaces of a conductor: traces and a junction region. To simplify the notation the integration is symbolically written as $\langle \cdot, \cdot \rangle$. Now let us rewrite the charge density q in the following manner:

$$q(r) = \begin{cases} q_J(r), & \text{if } r \text{ is on the junction region} \\ q_T^i(r), & \text{if } r \text{ is on the } i\text{th trace} \end{cases} \tag{11}$$

Then, (10) becomes

$$\phi(r) = \left\langle G^{3D}, q \right\rangle = \left\langle G^{3D}, q_J \right\rangle + \sum_{i=1}^{N_t} \left\langle G^{3D}, q_T^i \right\rangle \tag{12}$$

Decomposing the charge densities q_T^i into the uniform charge density $q_T^{unif,i}$ and the excess charge density $q_T^{excess,i}$ for each trace:

$$q_T^i(r) = q_T^{unif,i}(r) + q_T^{excess,i}(r) \tag{13}$$

Here, the uniform charge density $q_T^{unif,i}$ is obtained by solving a 2-D problem, in which it is assumed that only the ith trace is present in the medium and that the ith trace is infinitely long in both directions. A detailed discussion for solving 2-D problems is given in [8]. The uniform charge density $q_T^{unif,i}$ exists only on the ith trace, which is a semi-infinite line; hence, G^{semi} should be used to compute the potential due to $q_T^{unif,i}$. Using (13), (12) can be written as follows:

$$\phi(r) - \sum_{i=1}^{N_t} \left\langle G^{semi}, q_T^{unif,i} \right\rangle = \left\langle G^{3D}, q_J \right\rangle + \sum_{i=1}^{N_t} \left\langle G^{3D}, q_T^{excess,i} \right\rangle \tag{14}$$

The integral equation (14) can now be solved by using the method of moments. The collocation method is used in this paper. The closed-form formula for the integration involving G^{3D} is given discussed in [8], whereas the integration involving G^{semi} can be analytically integrated using the following formula:

$$\int\limits_{l_1}^{l_2} \ln\left[\frac{\sqrt{a^2+b^2+l^2}+a}{\sqrt{a^2+b^2+l^2}-a}\right]dl = 2|b|\left[\tan^{-1}\left(\frac{al_1}{|b|\sqrt{a^2+b^2+l_1^2}}\right)-\tan^{-1}\left(\frac{al_2}{|b|\sqrt{a^2+b^2+l_2^2}}\right)\right]$$
$$+2a\ln\left(\frac{l_2+\sqrt{a^2+b^2+l_2^2}}{l_1+\sqrt{a^2+b^2+l_1^2}}\right)+l_2\ln\left(\frac{\sqrt{a^2+b^2+l_2^2}+a}{\sqrt{a^2+b^2+l_2^2}-a}\right)-l_1\ln\left(\frac{\sqrt{a^2+b^2+l_1^2}+a}{\sqrt{a^2+b^2+l_1^2}-a}\right) \quad (15)$$

Now once (15) is solved, the excess (equivalent) capacitance c^e can be obtained by

$$c^e = \left[Q_J + \sum_{i=1}^{N_T} Q_T^{excess,i}\right]\Big/\phi_o \quad (16)$$

where Q_J is the total charge on the junction region, and $Q_T^{excess,i}$ is the total excess charge on the ith trace. Throughout the formulation, we have assumed that the junction region exists between traces. The formulation for cases without the junction region, such as an open end and step junctions, can be easily obtained simply by removing terms corresponding to q_J.

IV. NUMERICAL EXAMPLES

A computer program is written based on the technique discussed in the previous sections. The program assumes that the shape of the junction region, (see Fig. 2), if it exists, is polygonal, and it can handle an arbitrary number of dielectric layers as well as traces.

Excess capacitances for four common strip discontinuities, an open end, a step junction, a bend, and a T junction, are computed using the program. The geometries of discontinuities with their corresponding equivalent circuits are shown in Fig. 3. The following parameters are used: 1) an open end: $w = 0.5$ mm, 2) a step junction: $w_1 = 0.1$ mm and $w_2 = 0.2$ mm, 3) a right-angle bend: $w_1 = w_2 = 0.15$ mm, and 4) a T junction: $w_1 = w_2 = w_3 = 0.15$ mm. Three different types of media are considered for each discontinuity with the following parameters (see Fig. 5): 1) an open end: $\varepsilon_1 = 4.2$, $\varepsilon_2 = 2.5$, $y_1 = 1.0$ mm, $y_2 = 1.5$ mm, and $y_3 = 2.0$ mm, 2) a step junction: $\varepsilon_1 = 6.0$, $\varepsilon_2 = 4.2$, $y_1 = 0.1$ mm, $y_2 = 0.2$ mm, and $y_3 = 0.3$ mm, 3) a bend: $\varepsilon_1 = 2.5$, $\varepsilon_2 = 4.2$, $y_1 = 0.15$ mm, $y_2 = 0.3$ mm, and $y_3 = 0.5$ mm, 4) a T junction: $\varepsilon_1 = 2.5$, $\varepsilon_2 = 4.2$, $y_1 = 0.15$ mm, $y_2 = 0.3$ mm, and $y_3 = 0.5$ mm. All discontinuities are assumed to be embedded at $y = y_1$. To place 3-D unknowns for the excess charge distribution, the length of each trace is truncated at $l = 8w$. The total numbers of unknowns per each trace were 50 for a 2-D problem and 160 for a 3-D problem, whereas 100 unknowns were used for the junction region. The maximum number of exponentials used to approximate each coefficient function $K_i^{\pm}$ was 5.

The computed results are shown in Table I with the comparison data for a microstrip case (Fig. 4(a)). A good agreement was found overall as shown in the table. It is interesting to note that for some cases the value of an excess capacitance turns out to be negative. Although a physical capacitance must be positive, an excess (equivalent) capacitance is hypothetical and can be negative.

V. CONCLUSIONS AND FUTURE WORK

An efficient method to compute excess capacitances of strip discontinuities was discussed in this paper. Complete expressions of closed-form Green's functions for a point charge, a line charge, and a semi-infinite line charge have been derived. Unlike other approaches, only one integral equation is employed in this paper to handle various strip discontinuities instead of formulating an integral equation for each discontinuity type. The numerical results for a microstrip case agreed well with other published results.

REFERENCES

[1] K. C. Gupta, R. Garg, and I. J. Bahl, *Microstrip Lines and Slotlines*. Norwood, MA: Artech House, 1979.

[2] P. Silvester and P. B. Benedek, "Equivalent capacitances of microstrip open circuits," *IEEE Trans. Microwave Theory Tech.*, vol. 20, pp. 511-516, Aug. 1972.

[3] P. B. Benedek and P. Silvester, "Equivalent capacitances for microstrip gaps and steps," *IEEE Trans. Microwave Theory Tech.*, vol. 20, pp. 729-733, Nov. 1972.

[4] P. Silvester and P. B. Benedek, "Microstrip discontinuity capacitances for right-angle bends, T junctions, and crossings," *IEEE Trans. Microwave Theory Tech.*, vol. 21, pp. 341-346, May 1973.

[5] P. Silvester and P. B. Benedek, "Correction to 'Microstrip discontinuity capacitances for right-angle bends, T junctions, and crossings'," *IEEE Trans. Microwave Theory Tech.* (letter), vol. 23, p. 456, May. 1975.

[6] C. Wei, R. F. Harrington, J. R. Mautz, and T. K. Sarkar, "Multiconductor transmission lines in multilayered dielectric media," *IEEE Trans. Microwave Theory Tech.*, vol. 32, pp. 439-450, April 1984.

[7] T. K. Sarkar, Z. A. Maricevic, J. B. Zhang, and A. R. Djordjevic, "Evaluation of excess inductance and capacitance of microstrip junctions," *IEEE Trans. Microwave Theory Tech.*, vol. 42, pp. 1095-1097, June 1994.

[8] K. S. Oh, D. B. Kuznetsov, and J. E. Schutt-Aine, "Capacitance computations in a multilayered dielectric medium using closed-form spatial Green's functions," *IEEE Trans. Microwave Theory Tech.*, vol. 42, pp. 1443-1453, Aug. 1994.

Optional Top Ground Plane

$y=d_{Nd}$

ε_{Nd}, μ_o N_d

$y=d_{Nd-1}$

$y=d_2$

ε_2, μ_o 2

$y=d_1$

ε_1, μ_o 1

$y=0$

y

x

Bottom Ground Plane
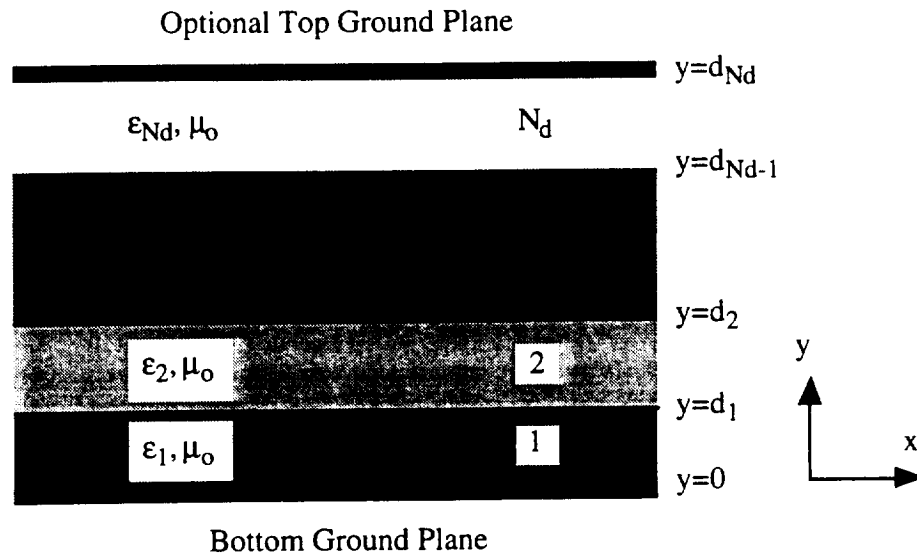
Fig. 1. Cross-sectional view of a multilayered dielectric medium.

Trace N_t

Trace 1

Junction Region
(Arbitrary Shape)

Trace 2   Trace 3

z

x
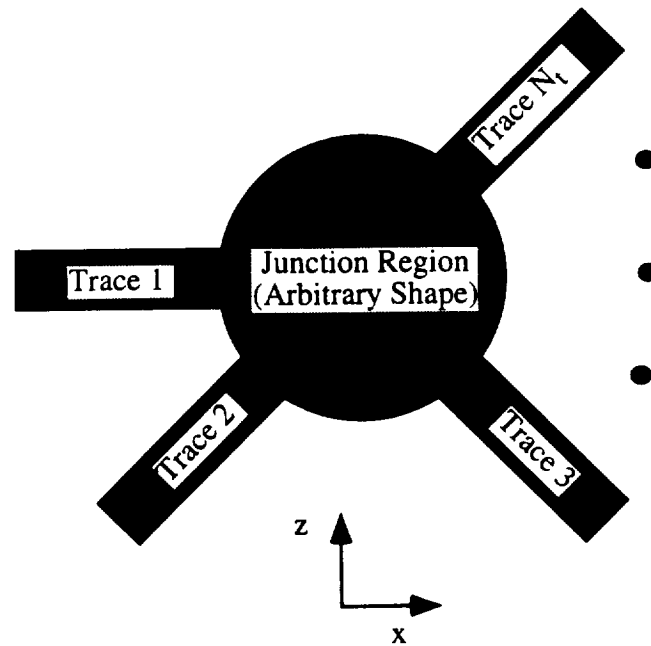
Fig. 2. General geometry of a strip discontinuity.

(a) An open end

(b) A step junction

(c) A bend

(d) A T junction
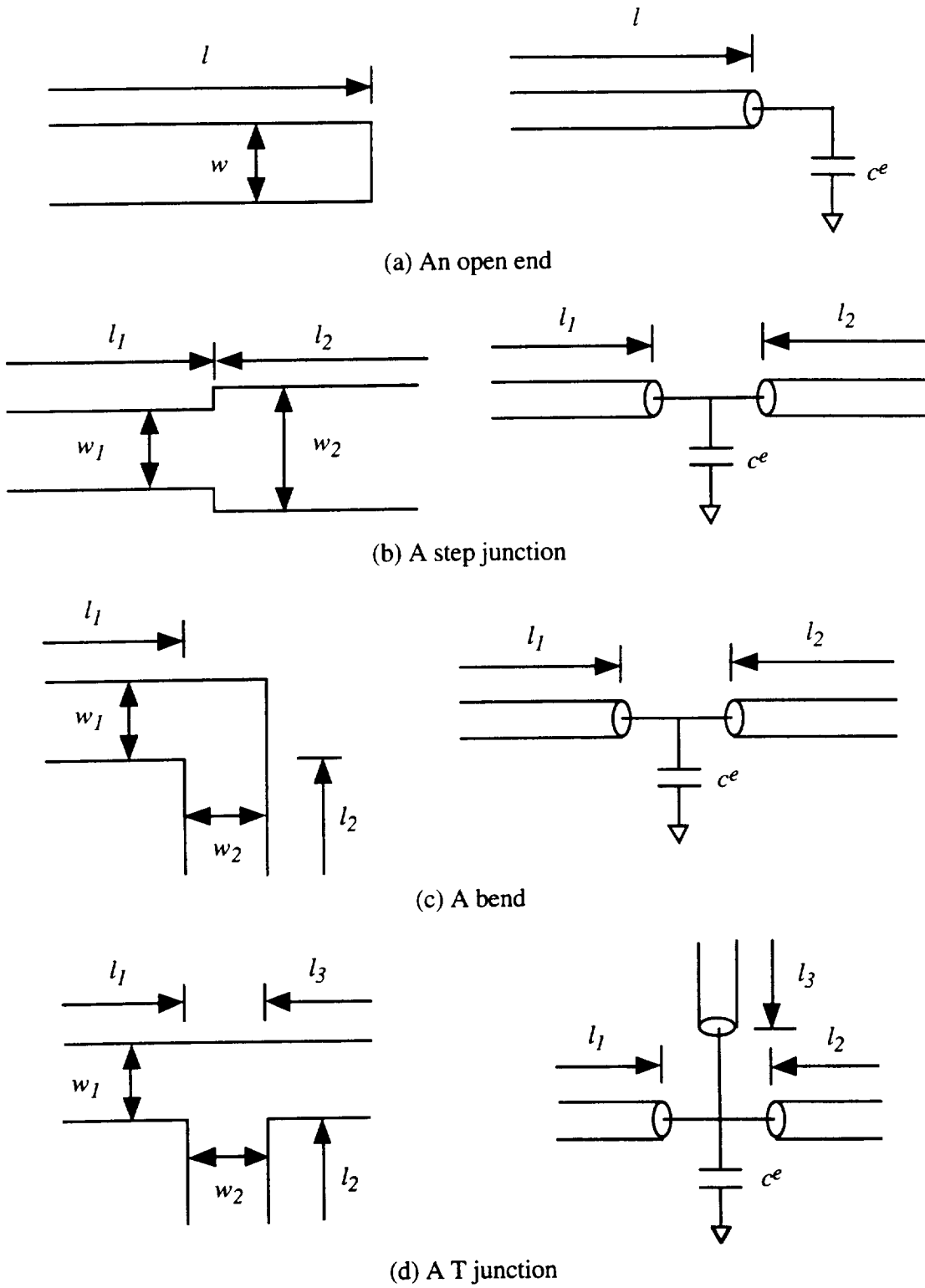
Fig. 3. Discontinuities and their equivalent circuit representations.

ε_o, μ_o

ε_1, μ_o

— y_1

— y=0 mm

Bottom Ground Plane

(a) Medium 1

ε_o, μ_o

ε_2, μ_o

— y_2

— y_1

ε_1, μ_o

— y=0 mm

Bottom Ground Plane

(b) Medium 2

Top Ground Plane

ε_1, μ_o

— y_3

— y_2

ε_2, μ_o

— y_1

ε_1, μ_o

— y=0 mm

Bottom Ground Plane
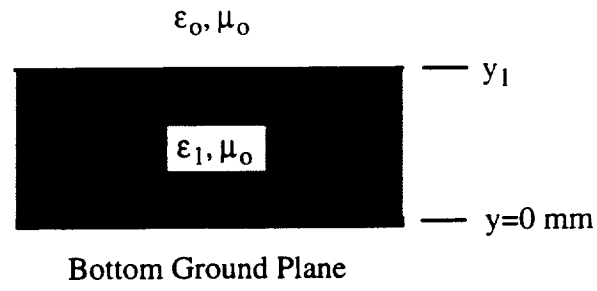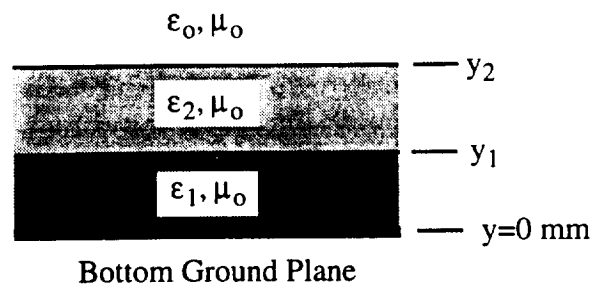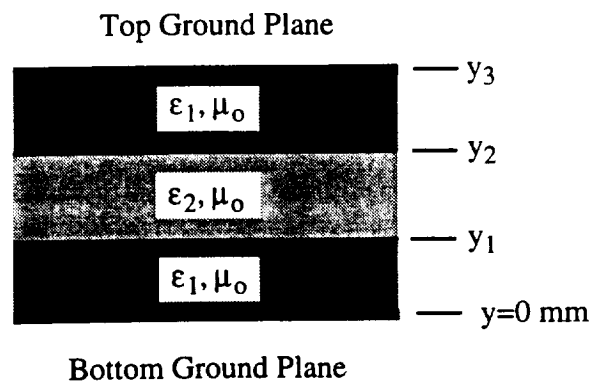
(c) Medium 3

Fig. 4. Three media considered for numerical examples.

Table I. The numerical results (Units are in femtofarad).

	Medium 1		Medium 2	Medium 3
	Computation	Others	Computation	Computation
Open End	17.33	17.0 [1]	23.52	19.62
Step Junction	1.120	1.05 [1], 0.74 [7]	1.352	0.609
Bend	6.210	6.75 [1], 5.8 [7]	7.006	9.184
T Junction	1.385	1.9 [7]	-4.917	-0.818

Efficient Circuit Simulation of Lossy Coupled Transmission Lines with Frequency-Dependent Parameters

Dmitri Kuznetsov, C. Kumar and José E. Schutt-Ainé

D. B. Kuznetsov, J. E. Schutt-Aine
Dept. of ECE, M/C 702
University of Illinois
1406 W. Green St.
Urbana, IL 61801-2991, USA
Fax: (217)333-8986
e-mail: vdm@decwa.ece.uiuc.edu

C. Kumar
Cadence Design Systems
270 Billerica Rd.
Chelsmford, MA 01824
Fax: (508)262-6600
e-mail: cpk@cadence.com

A b s t r a c t—This paper presents a method for the circuit simulation of uniform multiconductor lossy frequency-dependent lines characterized by sampled frequency-domain responses. The implementation includes ac, dc and transient analyses. The method combines element characteristics which do not require introduction of current variables, open-loop characterization which results in the simplest transfer functions, novel frequency-domain matrix rational approximation method, novel matrix delay separation technique, and matrix indirect numerical integration formulas. The method is reliable, accurate and as efficient as the simple replacement of interconnects by lumped resistors.

I. INTRODUCTION

THE PROBLEM of the transmission line simulation gained special importance with the development of high-speed digital electronics. As transient times become faster, the transmission line behavior of electronic interconnects starts to significantly affect transient waveforms, and accurate modeling of on-board and even on-chip interconnects becomes an essential part of the design process. The complexity of contemporary digital circuits calls for

accurate transmission line models efficient enough to perform the simultaneous circuit simulation of thousands of lossy coupled frequency-dependent lines surrounded by thousands of nonlinear active devices. Lines to be simulated may be characterized by measured or electromagneticly simulated samples of their responses.

A substantial amount of study has been devoted to the transient simulation of transmission lines in recent years [1]-[19]. This paper presents a method for circuit simulation of uniform multiconductor lossy frequency-dependent transmission lines characterized by sampled frequency-domain responses. The method is based on the approach described in [20]. The method supports variable time stepping and has linear computational complexity. The method has been adopted in several industrial and commercial circuit simulators, and, in numerous real-life simulation exercises, proved to be reliable, accurate and as efficient as the simple replacement of interconnects with lumped resistors.

The method employs element characteristics which do not require the introduction of current variables. As a result, the method increases neither the number of nodes nor the number of circuit variables, and the lines are incorporated into the circuit simulation without any increase in the circuit solution time. Element characteristics for the ac and dc analyses are based on the Y parameters.

For the transient analysis, the method uses open-loop transfer function characterization (direct characterization in terms of the propagation functions and characteristic admittances), which opens the feedback loop formed by the reflections from the terminations, and results in the simplest characteristic responses. It is shown that the open-loop characterization is equivalent to the generalized method characteristic .

The transient analysis is carried out by matrix indirect numerical integration. It has linear computational complexity, and ideal convergence, accuracy and stability properties.

To apply numerical integration to the propagation functions and characteristic admittances given as a set of frequency-domain samples, the method employs difference approximations. It fits the samples with a rational polynomial function and expresses the numerical integration

formulas in terms of the approximation parameters. Because of the simplicity and aperiodicity of the open-loop transfer functions, excellent approximation accuracy is attained with low-order real-pole approximation and a few original samples.

The approximation is performed by novel matrix direct constrained method. The method fits arbitrary number of arbitrary-spaced complex samples of a matrix transfer function with the matrix rational polynomial functions with poles constrained to the left half of the complex plane to insure stability. The method employs no iterative or relaxation techniques, only direct linear solutions and a polynomial factoring, and is computationally efficient and free from convergence problems.

Before the approximation, the delay is separated from the matrix propagation functions by a novel matrix delay separation technique. The technique eliminates the problems associated with the delay separation based on the diagonalization with the frequency-dependent modal transformation matrices, which are nonminimum-phase functions of frequency with unstable time-domain responses.

Throughout the paper, capital boldface, small boldface and normal italic symbols will be used to denote matrices, vectors and scalars, respectively. Since only multiconductor lines will be considered, the modifier "matrix" for the transfer functions will be omitted in the future for brevity.

II. FREQUENCY-DOMAIN LINE MODEL FOR TRANSIENT ANALYSIS

The frequency-domain element characteristic (for the transient analysis) which does not require the introduction of current variables and is suitable for the line modeling is given by

$$\begin{cases} i_1(\omega) = Y_1(\omega) \, v_1(\omega) - j_1(\omega) \\ i_2(\omega) = Y_2(\omega) \, v_2(\omega) - j_2(\omega). \end{cases} \tag{1}$$

The conventions for the terminal voltages and currents are shown in Fig. 1. The expressions relating the matrix admittances Y_1 and Y_2 and vector current sources j_1 and j_2 to the transmission line characteristics are derived directly from the continuity conditions for the voltages

and currents at the line terminals. To separate forward and backward waves and open the feedback loop, the current source j_1 must depend only on the backward wave, and j_2 only on the forward wave. This condition uniquely defines Y_1, Y_2 and j_1, j_2 as follows:

$$Y_1(\omega) = Y_2(\omega) = Y_c(\omega) \tag{2}$$

and

$$\begin{cases} j_1(\omega) = 2i_{b1}(\omega) \\ j_2(\omega) = 2i_{f2}(\omega), \end{cases} \tag{3}$$

where Y_c stands for the characteristic admittance, and the forward and backward current waves, i_{f1}, i_{f2} and i_{b1}, i_{b2} are related as:

$$\begin{cases} i_{b1}(\omega) = W_{1b}(\omega)\left[i_{b2}(\omega) = i_2(\omega) + i_{f2}(\omega)\right] \\ i_{f2}(\omega) = W_{1f}(\omega)\left[i_{f1}(\omega) = i_1(\omega) + i_{b1}(\omega)\right]. \end{cases} \tag{4}$$

The propagation functions for the forward and backward current waves are equal, $W_{1f} = W_{1b} = W_1$. The open-loop device model (1)-(4) is equivalent to the generalized method of characteristics [14], [11], [12].

The propagation function and characteristic admittance can be computed from the insertion loss data [14], scattering parameters [19], or distributed RLGC parameters:

$$W_1(\omega) = e^{-K_1(\omega)l},$$

$$Y_c(\omega) = K_1(\omega) Z^{-1}(\omega),$$

where l is the length of the line,

$$K_1(\omega) = \left(Y(\omega) Z(\omega)\right)^{\frac{1}{2}}$$

is the propagation constant for current waves,

$$Y(\omega) = G(\omega) + j\omega C(\omega),$$

$$Z(\omega) = R(\omega) + j\omega L(\omega)$$

are the admittance and impedance per unit length, and R, L, G and C are the resistance, inductance, conductance and capacitance per unit length. Boldface $(.)^{\frac{1}{2}}$ and $e^{(.)}$ denote matrix

square root and matrix exponential, respectively.

III. DIFFERENCE APPROXIMATION

To perform the transient analysis, indirect numerical integration is applied to the propagation functions and characteristic admittances in the frequency-domain line model (1)-(4) by using the difference approximation method.

For the difference approximation in the parallel canonic form, samples of the frequency-domain transfer function are approximated with the rational polynomial function

$$\tilde{H}(j\omega) = \tilde{H}_\infty + \sum_{m=0}^{M} \frac{1}{1 + j\omega/\omega_{cm}} A_m, \tag{5}$$

or samples of the time-domain unit-step response are approximated with the exponential series

$$\tilde{h}(t) = \tilde{H}_0 - \sum_{m=1}^{M} e^{-\omega_{cm} t} A_m,$$

where $\tilde{H}_0$ and $\tilde{H}_\infty$ denote the initial and final values of the approximating transfer function $\tilde{H}(j\omega)$.

Once the approximation has been performed, indirect numerical integration formulas (discrete-time difference equations) are readily given in terms of the approximation parameters. For the step invariance the formulas are

$$\begin{cases} y(t_n) = \tilde{H}_\infty x(t_n) + \sum_{m=1}^{M} z_m(t_n) \\ z_m(t_n) = \left(1 - e^{-\omega_{cm} T_n}\right) A_m x(t_{n-1}) + e^{-\omega_{cm} T_n} z_m(t_{n-1}), \end{cases} \tag{6}$$

where x, y and z_m stand for the excitation, response and state variables, respectively, and $T_n = t_n - t_{n-1}$ is the time step at the nth transient iteration.

For the ramp invariance

$$\begin{cases} y(t_n) = \tilde{H}_0 x(t_n) - \sum_{m=1}^{M} z_m(t_n) \\ z_m(t_n) = D_m(T_n)\left(x(t_n) - x(t_{n-1})\right) + e^{-\omega_{cm} T_n} z_m(t_{n-1}), \end{cases} \tag{7}$$

where

$$\mathbf{D}_m(T_n) = \frac{1 - e^{-\omega_{cm} T_n}}{\omega_{cm} T_n} \mathbf{A}_m.$$

An alternative form of the ramp-invariant indirect numerical integration formula has the coefficients of the present-time sample of the excitation lumped together

$$\begin{cases} \mathbf{y}(t_n) = \left(\tilde{\mathbf{H}}_0 - \sum_{m=1}^{M} \mathbf{D}_m(T_n) \right) \mathbf{x}(t_n) - \sum_{m=1}^{M} \mathbf{z}_m(t_n) \\ \mathbf{z}_m(t_n) = \left(\mathbf{D}_m(T_{n-1}) e^{-\omega_{cm} T_n} - \mathbf{D}_m(T_n) \right) \mathbf{x}(t_{n-1}) + e^{-\omega_{cm} T_n} \mathbf{z}_m(t_{n-1}). \end{cases} \tag{8}$$

This form is especially suitable for discretization of characteristic admittance, because, for admittances, the present- and past-time terms of the numerical integration formulas have different physical meaning.

Before the approximation, the delay is separated from the matrix propagation function using the matrix delay separation technique. It represents the matrix propagation function in the following form:

$$\mathbf{W}_1(\omega) = \hat{\mathbf{W}}_1(\omega) \, \hat{\mathbf{M}}_1 \, e^{-j\omega T_{1m}} \, \hat{\mathbf{M}}_1^{-1},$$

where T_{1m} and $\hat{\mathbf{M}}_1$ are the constant eigenvalue and eigenvector matrices of the propagation delay matrix

$$T_1 = (\mathbf{C}(\infty) \, \mathbf{L}(\infty))^{\frac{1}{2}} \, l = \mathbf{K}_1(\infty) \, l.$$

Difference approximation is applied to the delayless propagation function

$$\hat{\mathbf{W}}_1(\omega) = \mathbf{W}_1(\omega) \, e^{j\omega T_1}.$$

The delays in the diagonal modal-delay matrix T_{1m} are modeled using a low-order spline of the simulated time points.

The difference approximation is applied to the delayless propagation function and characteristic admittance. For the characteristic admittances in (1), the excitations are the terminal voltages and the responses are the terminal currents. For the propagation functions in (4), the excitations and responses are the current waves.

Since the open-loop functions are aperiodic, they have to be approximated with only real poles, $-\omega_{cm}$. In addition, the poles have to be negative to assure stability.

To represent the original functions accurately with the minimum number of samples, the variation of the original function from sample to sample should be about the same. The following empirical formula for the sampling frequencies was found to provide good results

$$\omega_k = \omega_K \left(1 - \cos\frac{\pi k}{2K}\right), \quad k = 0, 1, \ldots, K .$$

The end of the approximation interval, ω_K, should be chosen so that the original function would closely approach its final value. This assures that the resulting indirect numerical integration formulas will be accurate in the full frequency and time ranges from zero to infinity.

IV. MATRIX COMPLEX RATIONAL APPROXIMATION METHOD FOR FREQUENCY-DOMAIN DIFFERENCE APPROXIMATION

The method fits samples of an $N \times N$ complex matrix transfer function $\mathbf{H}(\omega)$ with the rational polynomial function (5) at the set of arbitrary spaced frequencies $\{0, \omega_1, \omega_2, \ldots, \omega_K\}$. The method proceeds in three steps.

First, the real part of the sum of the elements of the original matrix function,

$$H_\Sigma(\omega) = \sum_{i=1}^{N} \sum_{j=1}^{N} [\mathbf{H}(\omega)]_{ij} ,$$

is fit with the real part of the complex rational polynomial function, which is a real rational polynomial function of squared frequency

$$Re\left(\bar{H}_\Sigma(j\omega)\right) = \frac{c_0 + c_1 \omega^2 + c_2 (\omega^2)^2 + \ldots + c_M (\omega^2)^M}{1 + \beta_1 \omega^2 + \beta_2 (\omega^2)^2 + \ldots + \beta_M (\omega^2)^M} . \tag{9}$$

The following linear system of equations results from matching the real part of the original function with (9) at the set of frequencies and premultiplying both sides of each equation with the denominator

$$\begin{bmatrix} 1 & 0 & \cdots & 0 & \vline & 0 & \cdots & 0 \\ 1 & \omega_1^2 & \cdots & \omega_1^{2M} & \vline & -\omega_1^2\,Re(H_\Sigma(\omega_1)) & \cdots & -\omega_1^{2M}\,Re(H_\Sigma(\omega_1)) \\ & & \vdots & & \vline & & \vdots & \\ 1 & \omega_K^2 & \cdots & \omega_K^{2M} & \vline & -\omega_K^2\,Re(H_\Sigma(\omega_K)) & \cdots & -\omega_K^{2M}\,Re(H_\Sigma(\omega_K)) \end{bmatrix} \begin{bmatrix} c_0 \\ \vdots \\ c_M \\ \hline \beta_1 \\ \vdots \\ \beta_M \end{bmatrix} = \begin{bmatrix} Re(H_\Sigma(0)) \\ Re(H_\Sigma(\omega_1)) \\ \vdots \\ Re(H_\Sigma(\omega_K)) \end{bmatrix}. \tag{10}$$

For interpolation, $K = 2M$ and solving (10) produces a rational polynomial function which coincides with the real part of the original function at all of the sampling points. For a set of samples larger than $2M + 1$, the least square solution of the system (10) can be obtained. However, it minimizes the approximation error premultiplied with the denominator, which can lead to inaccurate approximation. Better results are achieved with the method of averages [21], which partitions the larger number of equations into $2M + 1$ subsets in order of the increasing of ω. The equations within each subset are added up, which makes the system consistent. The method is effective in averaging out the noise in measured data.

After the real part has been approximated, the denominator of (9) is factored yielding the squared poles, $-\omega_{cm}^2$. Consequently, no unstable right-half-plane poles can be produced. However, there still can be spurious complex conjugate and purely imaginary poles, which are removed. The remaining real negative poles are used to formulate the equations for the partial expansion coefficients, A_m, of (5). As a result, the order M of (5) is less or equal to that of (9).

Matching the real and imaginary parts of each element of the original matrix transfer function $H(\omega)$ with the corresponding parts of elements of (5) at the set of frequencies $\{0, \omega_1, \omega_2, \ldots, \omega_K\}$ leads to the following linear systems of equations

$$\left(\begin{bmatrix} 1 & 1 & \cdots & 1 \\ 1 & \dfrac{1}{1+\omega_1^2/\omega_{c1}^2} & \cdots & \dfrac{1}{1+\omega_1^2/\omega_{cM}^2} \\ & & \vdots & \\ 1 & \dfrac{1}{1+\omega_K^2/\omega_{c1}^2} & \cdots & \dfrac{1}{1+\omega_K^2/\omega_{cM}^2} \\ 0 & \dfrac{-\omega_1/\omega_{c1}}{1+\omega_1^2/\omega_{c1}^2} & \cdots & \dfrac{-\omega_1/\omega_{cM}}{1+\omega_1^2/\omega_{cM}^2} \\ & & \vdots & \\ 0 & \dfrac{-\omega_K/\omega_{c1}}{1+\omega_K^2/\omega_{c1}^2} & \cdots & \dfrac{-\omega_K/\omega_{cM}}{1+\omega_K^2/\omega_{c1}^2} \end{bmatrix}\right) \mathbf{A} = \quad \mathbf{x} = \begin{pmatrix} [\mathbf{H}_\infty]_{ij} \\ [\mathbf{A}_1]_{ij} \\ [\mathbf{A}_2]_{ij} \\ \vdots \\ [\mathbf{A}_M]_{ij} \end{pmatrix} = \mathbf{b} = \begin{bmatrix} [\mathbf{H}(0)]_{ij} \\ Re\left([\mathbf{H}(\omega_1)]_{ij}\right) \\ \vdots \\ Re\left([\mathbf{H}(\omega_K)]_{ij}\right) \\ Im\left([\mathbf{H}(\omega_1)]_{ij}\right) \\ \vdots \\ Im\left([\mathbf{H}(\omega_K)]_{ij}\right) \end{bmatrix}. \qquad (11)$$

For interpolation $M = 2K$, and both real and imaginary parts of the original transfer function are matched exactly at all of the K frequency points and dc. For an arbitrary larger number of points, the least square solution of (11) is obtained from

$$\mathbf{A}^T\mathbf{A}\mathbf{x} = \mathbf{A}^T\mathbf{b}.$$

The total computational complexity of the approximation method is that of $N^2 + 1$ real linear solutions and one polynomial factoring. The orders of the polynomial and linear systems depend only on the order of the approximation and not on the number of the original function samples. Since no iterative or relaxation techniques are involved, the method is free from convergence problems.

Fig. 2 shows an example of the fourth-order approximation of an open-loop transmission-line transfer function. As can be observed, although only nine samples of the original function were used, the approximation exhibits an excellent match in the full frequency range. In general, due to their simplicity, the open-loop functions can be accurately fit with the 3rd-9th-order approximation.

V. COMPANION MODEL

By applying the difference approximation to the propagation function and characteristic admittance, the frequency-domain element characteristic (1) is transformed into the following discrete-time element characteristic, or companion model

$$\begin{cases} i_1(t_n) = \hat{Y}_1(t_n)\, v_1(t_n) - \hat{j}_1(t_n) \\ i_2(t_n) = \hat{Y}_2(t_n)\, v_2(t_n) - \hat{j}_2(t_n). \end{cases} \tag{12}$$

The circuit-diagram interpretation of the companion model is shown in Fig. 3.

The admittances $\hat{Y}_1$ and $\hat{Y}_2$ represent present-time coefficients in the indirect numerical integration formulas for the admittances Y_1 and Y_2. The current sources $\hat{j}_1$ and $\hat{j}_2$ combine the currents j_{Y_1} and j_{Y_2} corresponding to the remaining parts of the numerical integration formulas for the admittances, and j_1 and j_2 which are given by the discretized Eqs. (3) and (4)

$$\begin{cases} \hat{j}_1(t_n) = -j_{Y_1}(t_n) + j_1(t_n) \\ \hat{j}_2(t_n) = -j_{Y_2}(t_n) + j_2(t_n). \end{cases} \tag{13}$$

Eqs. (3) and (4) do not contribute to the admittance part of the companion model because the propagation functions contain a delay.

The Modified Nodal Approach (MNA) stamp corresponding to the companion model (12) is:

$$\tag{14}$$

In the circuit simulator during the transient analysis, the lines are represented by the tables of numbers (14) which are recursively updated at each time iteration using numerical integration. The left-hand side of the stamp (14) has to be updated only when the value of the time step changes. If

the step-invariant indirect numerical integration formulas (6) are used, the left-hand side of the stamp becomes independent of the time step, and only the right-hand side vector has to be updated.

Since the terminal currents are not introduced as variables, the values of i_1 and i_2 in (4) are computed from (12).

VI. LINE MODEL FOR AC AND DC ANALYSES

For ac and dc analyses, the complexity of the transfer functions is not important, and the element characteristic which does not require the introduction of current variables and is suitable for the ac/dc modeling of transmission lines is the Y-parameter characteristic

$$\begin{cases} i_1(\omega) = Y_{11}(\omega)\, v_1(\omega) + Y_{12}(\omega)\, v_2(\omega) \\ i_2(\omega) = Y_{21}(\omega)\, v_1(\omega) + Y_{22}(\omega)\, v_2(\omega). \end{cases} \tag{15}$$

The Y-parameters are related to the open-loop functions as follows

$$\begin{aligned} Y_{11}(\omega) = Y_{22}(\omega) &= Y_c(\omega) + 2\big[I - W_1^2(\omega)\big]^{-1} W_1^2(\omega) Y_c(\omega), \\ Y_{12}(\omega) = Y_{21}(\omega) &= -2\big[I - W_1^2(\omega)\big]^{-1} W_1(\omega) Y_c(\omega), \end{aligned} \tag{16}$$

where I is the identity matrix. The expressions were derived by eliminating j_1 and j_2 from Eqs. (1)-(4), and transforming them to the form of (15).

The dc model is merely the ac model at zero frequency. For the limiting case of lines with zero distributed conductance, $G = 0$, the dc values of the Y-parameters are

$$Y_{11}(0) = Y_{22}(0) = -Y_{12}(0) = -Y_{21}(0) = \frac{1}{l} R^{-1}.$$

The MNA stamp corresponding to (15) is

The matrix equation (16) with KCL at nodes:

$$
\begin{bmatrix}
\mathbf{Y}_{11} & -\sum_{j=1}^{N}[\mathbf{Y}_{11}]_{ij} & \mathbf{Y}_{12} & -\sum_{j=1}^{N}[\mathbf{Y}_{12}]_{ij} \\
-\sum_{i=1}^{N}[\mathbf{Y}_{11}]_{i1}\cdots-\sum_{i=1}^{N}[\mathbf{Y}_{11}]_{iN} & \sum_{i=1}^{N}\sum_{j=1}^{N}[\mathbf{Y}_{11}]_{ij} & -\sum_{i=1}^{N}[\mathbf{Y}_{12}]_{i1}\cdots-\sum_{i=1}^{N}[\mathbf{Y}_{12}]_{iN} & \sum_{i=1}^{N}\sum_{j=1}^{N}[\mathbf{Y}_{12}]_{ij} \\
\mathbf{Y}_{21} & -\sum_{j=1}^{N}[\mathbf{Y}_{21}]_{ij} & \mathbf{Y}_{22} & -\sum_{j=1}^{N}[\mathbf{Y}_{22}]_{ij} \\
-\sum_{i=1}^{N}[\mathbf{Y}_{21}]_{i1}\cdots-\sum_{i=1}^{N}[\mathbf{Y}_{21}]_{iN} & \sum_{i=1}^{N}\sum_{j=1}^{N}[\mathbf{Y}_{21}]_{ij} & -\sum_{i=1}^{N}[\mathbf{Y}_{22}]_{i1}\cdots-\sum_{i=1}^{N}[\mathbf{Y}_{22}]_{iN} & \sum_{i=1}^{N}\sum_{j=1}^{N}[\mathbf{Y}_{22}]_{ij}
\end{bmatrix}
\begin{bmatrix} V_{1,1}\\ \vdots\\ V_{1,N}\\ V_r\\ V_{2,1}\\ \vdots\\ V_{2,N}\\ V_r \end{bmatrix}
=
\begin{bmatrix} 0\\ \vdots\\ 0\\ 0\\ 0\\ \vdots\\ 0\\ 0 \end{bmatrix}
\tag{16}
$$

VII. Initial Conditions for Transient Analysis

The dc model is used to perform the operating-point (op) analysis before the transient simulation. The op solution is then used as initial conditions for the transient analysis. The initial conditions for the indirect numerical integration are the dc values of the state variables, which are related to the dc value of the excitation, x_0, as follows: $z_m(t_0) = a_m x_0$ for the step-invariant case (6), $z_m(t_0) = 0$ for the ramp-invariant case (7), and $z_m(t_0) = -d_m(T_1)x_0$ for the ramp-invariant case (8). The dc values of $\mathbf{i}_{r1}$ and $\mathbf{i}_{b2}$, which serve as excitations for the propagation functions in (4), have to be expressed in terms of the terminal voltages obtained from the op analysis. Resolving Eqs. (1)-(4) leads to

$$
\begin{cases}
\mathbf{i}_{r1}(0) = \left[\mathbf{I} - \mathbf{W}_1^2(0)\right]^{-1}\left[\mathbf{Y}_c(0)\mathbf{v}_1(0) - \mathbf{W}_1(0)\mathbf{Y}_c(0)\mathbf{v}_2(0)\right]\\
\mathbf{i}_{b2}(0) = \left[\mathbf{I} - \mathbf{W}_1^2(0)\right]^{-1}\left[\mathbf{Y}_c(0)\mathbf{v}_2(0) - \mathbf{W}_1(0)\mathbf{Y}_c(0)\mathbf{v}_1(0)\right].
\end{cases}
$$

For the limiting case of $\mathbf{G} = 0$, the expressions become

$$
\mathbf{i}_{r1}(0) = -\mathbf{i}_{b2}(0) = \frac{1}{2l}\mathbf{R}^{-1}\left[\mathbf{v}_1(0) - \mathbf{v}_2(0)\right].
$$

VIII. SIMULATION ALGORITHM

For an MNA-based simulator, the line simulation algorithm is as follows.

1. Before the transient analysis:

    a) Perform op analysis of the circuit to find the initial conditions for the transient analysis. Use the ac/dc model (15)-(16).

    b) For each line in the circuit, perform the difference approximation of each element of the propagation function and characteristic admittance matrices.

2. At each time iteration:

    Recursively update the line stamps using the indirect numerical integration formulas obtained at step 1(b) and companion model (12)-(14).

Since the method introduces neither additional nodes nor current variables, the line modeling does not increase at all the circuit solution time. The only additional time is required to perform a low-order interpolation once in the beginning of the simulation, and for a low-order numerical integration. As shown in the next section, this time is negligibly small compared to the circuit solution time.

IX. NUMERICAL RESULTS

The method has been adopted in several industrial and commercial circuit simulators, and, in numerous real-life simulation exercises, proved to be reliable, accurate and efficient. Table II presents relative runtime data for circuits of various types and sizes. As can be observed, even for the worst case of a small circuit consisting of lines only, the model is virtually as efficient as the simple replacement of interconnects with lumped resistors. The resistive model was chosen for the comparison because it represents the limiting case in the simplicity and computational efficiency of the interconnect modeling.

Fig. 4 verifies the method's accuracy with Spice3e2 lossy multiconductor line model [8]. A simple network was chosen as an example to reduce the influence of factors other than the line

model on the simulation accuracy. A variable, third- to fifth-order frequency-domain difference approximation was applied. As can be observed, the compared waveforms are indistinguishable. The runtime for the presented method was three orders of magnitude shorter than that for the Spice model, which is, in turn, an order of magnitude faster than segmentation models.

The presented line model has been implemented in a commercial CAD product DFSignoise from Cadence. The following examples show results for real circuits analyzed with *tlsim*, the simulator deployed by Cadence's DFSignoise. The examples compare the suggested line model with segmentation models. The suggested model included frequency-dependent loss, whereas the segmentation models included no frequency dependence.

The first example is a long cable driven by an ECL buffer at a high, 400 MHz, speed. The nonlinear characteristics of the driver and receiver were described in the I/O Buffer Information Standard (IBIS) data format [22]. Fig. 5 shows the circuit schematic and the IBIS data. and compares the simulation results obtained with the lumped *RLGC* and pseudo-lumped (distributed-*LC*/lumped-*RG*) segmentation models and the suggested line model. The number of segments for the segmentation models was over 400. The automatic algorithms used to determine the number of segments took into account the rise and fall times and the expected attenuation.

The waveform simulated with the suggested line model shows considerable attenuation due to the frequency-dependent dielectric loss and conductor loss with the skin effect. As can be observed, the segmentation models without the frequency-dependent loss consistently underpredict the attenuation and resulting loss of the noise margin, accurate prediction of which is important at these speeds. The lumped segmentation model also shows spurious peaks which are artifacts of that method.

Fig. 6 shows a similar comparison between the pseudo-lumped segmentation model and suggested line model for a circuit driven by IBIS CMOS buffers at 200 MHz. This network is complicated and contains 45 two-conductor, 8 three-conductor and 5 four-conductor lines. The longest transmission line in this case was a two-conductor line of 0.5 m. The longest multiconductor line was a four-conductor line of 0.26 m. The largest delay was 7.8 ns. In this

case, the two models produced comparable results, since the rise time of the driver was 0.9 ns as opposed to the 0.3 ns of the ECL driver. The figure also shows the crosstalk waveform V_1. The crosstalk waveforms for the suggested and segmentation models were very close.

X. CONCLUSIONS

This paper presented a method for circuit simulation of uniform multiconductor lossy frequency-dependent lines characterized by sampled frequency-domain responses. The method uses element characteristics which do not require the introduction of current variables, simple open-loop transmission line characterization, matrix indirect numerical integration formulas, novel direct matrix rational approximation method, and novel matrix delay separation technique. The complete step-by-step implementation of the method was presented, including ac, dc and transient analyses, extraction of initial conditions from the op analysis, and MNA stamps.

The method is compatible with recursive time-domain solvers employed by circuit simulators and supports variable time-stepping. The method has been adopted in several industrial and commercial circuit simulators, and, in numerous real-life simulation exercises, proved to be reliable and accurate. It was shown on an extensive set of runtime data that the method is as efficient as simple replacement of interconnects with lumped resistors.

ACKNOWLEDGMENT

REFERENCES

[1] T. Dhaene, L. Martens and D. De Zutter, "Transient simulation of arbitrary nonuniform interconnection structures characterized by scattering parameters," *IEEE Trans. Circuits Syst.*, vol. 39, pp. 928-937, Nov. 1992.

Syst., vol. 39, pp. 928-937, Nov. 1992.

[2] J. E. Bracken, V. Raghavan and R. A. Rohrer, "Interconnect simulation with asymptotic waveform evaluation (AWE)," *IEEE Trans. Circuits Syst.*, vol. 39, pp. 869-878, Nov. 1992.

[3] T. Dhaene and D. De Zutter, "Selection of lumped element models for coupled lossy transmission lines," *IEEE Trans. Computer-Aided Design*, vol. 11, pp. 805-815, Jul. 1992.

[4] K. S. Oh and J. E. Schutt-Ainé, "Transient analysis of coupled, tapered transmission lines with arbitrary nonlinear terminations," *IEEE Trans. Microwave Theory Tech.*, vol. 41, pp. 268-273, Feb. 1993.

[5] J. E. Schutt-Ainé and R. Mittra, "Nonlinear transient analysis of coupled transmission lines," *IEEE Trans. Circuits Syst.*, vol. 36, pp. 959-967, Jul. 1989.

[6] I. Maio, S. Pignari and F. Canavero, "Influence of the line characterization on the transient analysis of nonlinearly loaded lossy transmission lines," *IEEE Trans. Circuits Syst.*, vol. 41, pp. 197-209, Mar. 1994.

[7] F. Romeo and M. Santomauro, "Time-domain simulation of n coupled transmission lines," *IEEE Trans. Microwave Theory Tech.*, vol. MTT-35, pp. 131-137, Feb. 1987.

[8] J. S. Roychowdhury and D. O. Pederson, "Efficient transient simulation of lossy interconnect," in *Proc. 28th ACM/IEEE Design Automation Conf.*, 1991, pp. 740-745.

[9] F.-Y. Chang, "Transient analysis of lossy transmission lines with arbitrary initial potential and current distributions," *IEEE Trans. Circuits Syst.*, vol. 39, pp. 180-198, Mar. 1992.

[10] F. H. Branin, Jr., "Transient analysis of lossless transmission lines," *Proc. IEEE*, vol. 55, pp. 2012-2013, Nov. 1967.

[11] F.-Y. Chang, "Transient simulation of nonuniform coupled lossy transmission lines characterized with frequency-dependent parameters, Part I: Waveform relaxation analysis," *IEEE Trans. Circuits Syst.*, vol. 39, pp. 585-603, Aug. 1992.

[12] F.-Y. Chang, "Transient simulation of frequency-dependent nonuniform coupled lossy transmission lines," *IEEE Trans. Components Packaging Manufacturing Technology*, vol. 17, pp. 3-14, Feb. 1994.

[13] J. E. Bracken, V. Raghavan and R. A. Rohrer, "Extension of the asymptotic waveform evaluation technique with the method of characteristics," *Tech. Dig. IEEE Int. Conf. Computer-Aided Design*, 1992, pp. 71-75.

[14] A. J. Gruodis and C. S. Chang, "Coupled lossy transmission line characterization and simulation," *IBM J. Res. Develop.*, vol. 25, pp. 25-41, Jan. 1981.

[15] A. Semlyen and A. Dabuleanu, "Fast and accurate switching transient calculations on transmission lines with ground return using recursive convolutions," *IEEE Trans. Power Appar. Syst.*, vol. PAS-94, pp. 561-569, Mar./Apr. 1975.

[16] T. K. Tang, M. S. Nakhla and R. Griffith, "Analysis of lossy multiconductor transmission lines using the Asymptotic Waveform Evaluation technique," *IEEE Trans. Microwave Theory Tech.*, vol. 39, pp. 2107-2116, Dec. 1991.

[17] C. R. Paul, "On uniform multimode transmission lines," *IEEE Trans. Microwave Theory Tech.*, pp. 556-558, Aug. 1973.

[18] L. T. Pillage and R. A. Rohrer, "Asymptotic waveform evaluation for timing analysis," *IEEE Trans. Computer-Aided Design*, vol. 9, pp. 352-366, Apr. 1990.

[19] J. E. Schutt-Ainé, "Modeling and simulation of high-speed digital circuit interconnections," Ph.D. dissertation, University of Illinois at Urbana, 1988.

[20] D. B. Kuznetsov and J. E. Schutt-Ainé, "Optimal transient simulation transmission lines," accepted for publication in *IEEE Trans. Circuits Syst.*.

[21] I. N. Bronshteyn and K. A. Semendyaev, *Spravochnik po matematike*. Moscow: Nauka, 1967, p. 578. In Russian.

[22] D. Duehren, W. Hobbs, A. Muranyi and R. Rosenbaum, "I/O-buffer modeling spec simplifies simulation for high-speed systems," *Electronic Design News (EDN)*, p. 65, Mar. 1995.

FIGURE CAPTIONS

Fig. 1. Conventions for the voltages and currents at the line terminals.

Fig. 2. An example of the 4th-order complex rational approximation. The original function is shown by the thin continuous curves and the approximating function by the thick dashed curves.

Fig. 3. Companion model for a transmission line.

Fig. 4. (a) the network configuration and (b) comparison of the transient waveforms generated using the line model installed in an MNA-based circuit simulator (thick broken curves) and Spice3e2 (thin continuous curves). $R_1=R_5=50$ Ω, $R_2=R_6=1$ kΩ, $R_3=R_4=10$ MΩ; self-inductance $L_s=418$ nH/m, self-capacitance $C_s=94$ pF/m, mutual inductance $L_m=125$ nH/m, mutual capacitance $C_m=22$ pF/m, $R=15$ Ω/m, $G=0$, $l=0.677$ m (all signal conductors are the same).

Fig. 5. (a) the circuit schematic, (b) IBIS model for the ECL buffers, and (c) the transient waveforms simulated with the segmentation and suggested line models. The line parameters are: $L=502$ nH/m, $C=67.9$ pF/m, $R=\{3.25$ Ω/m at dc, 87.7 Ω/m at 10 GHz$\}$, $G=\{430$ fS/m at dc, 4.3 mS/m at 10 GHz$\}$, $l=0.88$ m.

Fig. 6. (a) the circuit block schematic, (b) IBIS model for the CMOS buffers, and (c) the transient waveforms simulated with the segmentation and suggested line models.

TABLE CAPTIONS

Table I. Relative runtimes.

FOOTNOTES

Illinois, Urbana, IL 61801, USA.
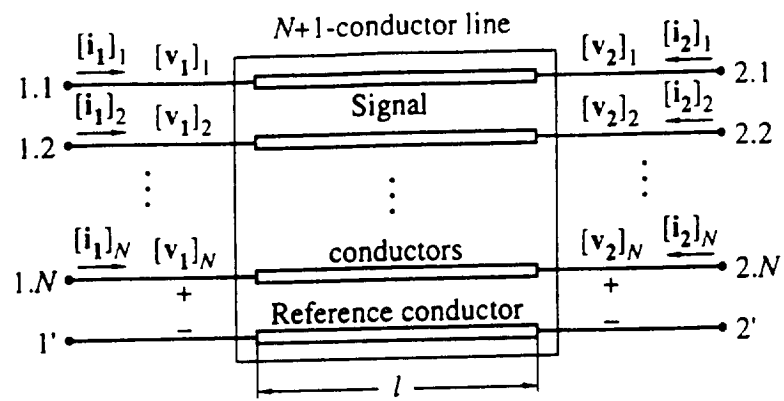
Fig. 1
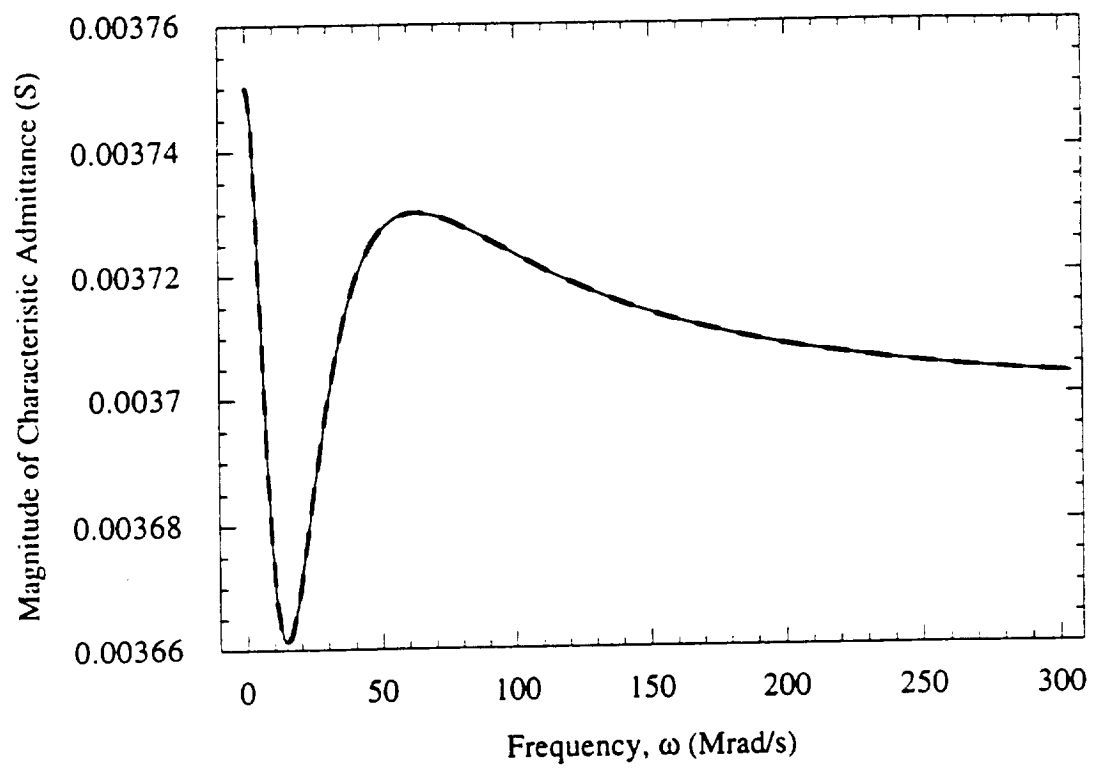
Fig. 2 (a)
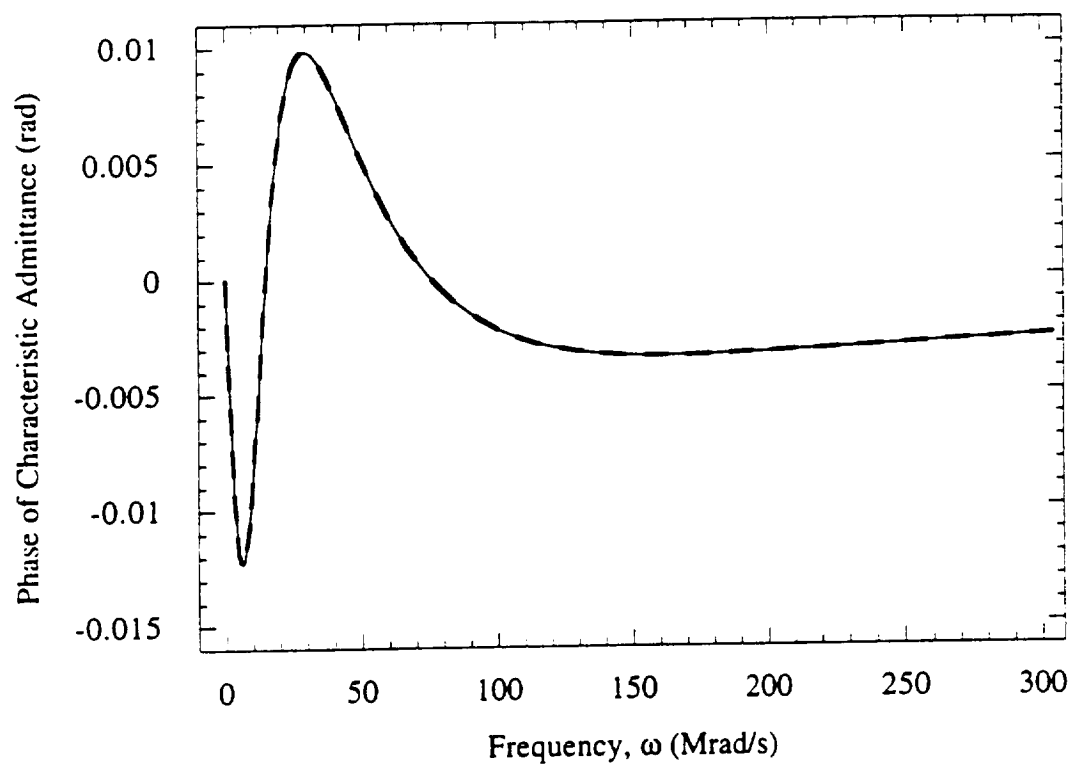
Fig. 2(b)

Fig. 3

Fig. 4(a)

Fig. 4(b)

R, L, G, C

V
+
− 50 Ω
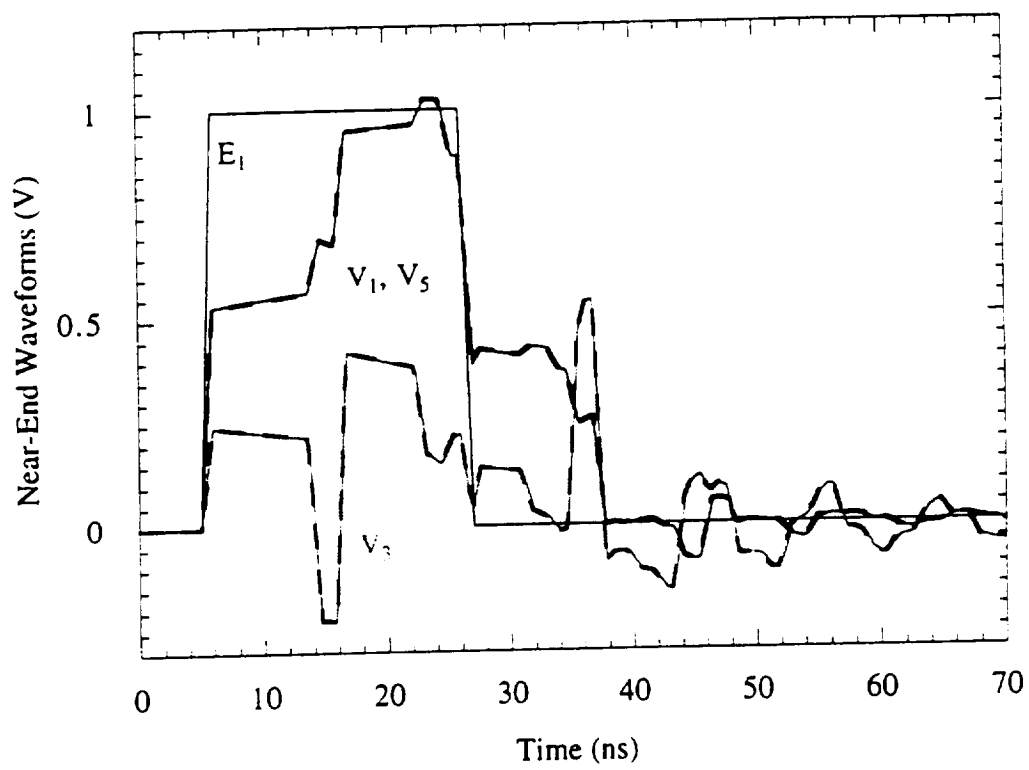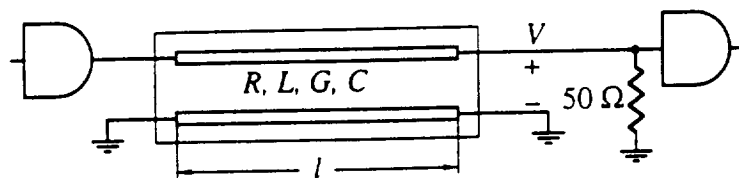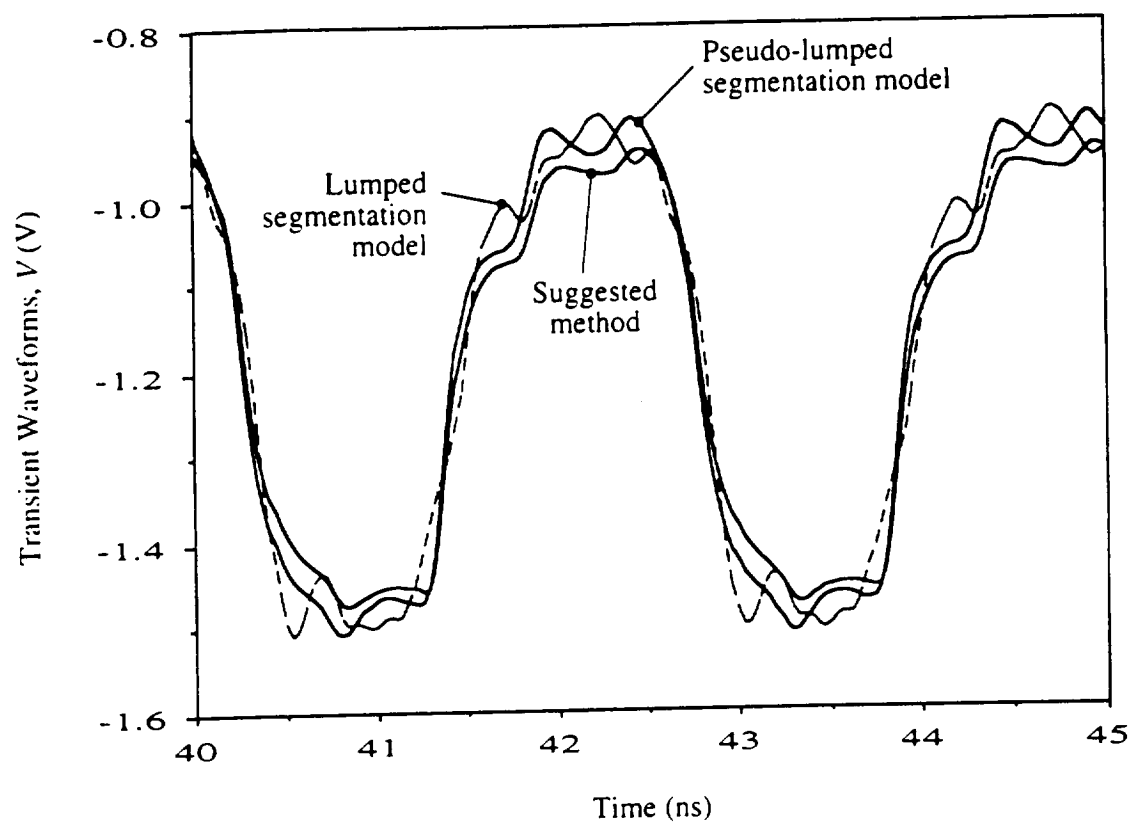
l
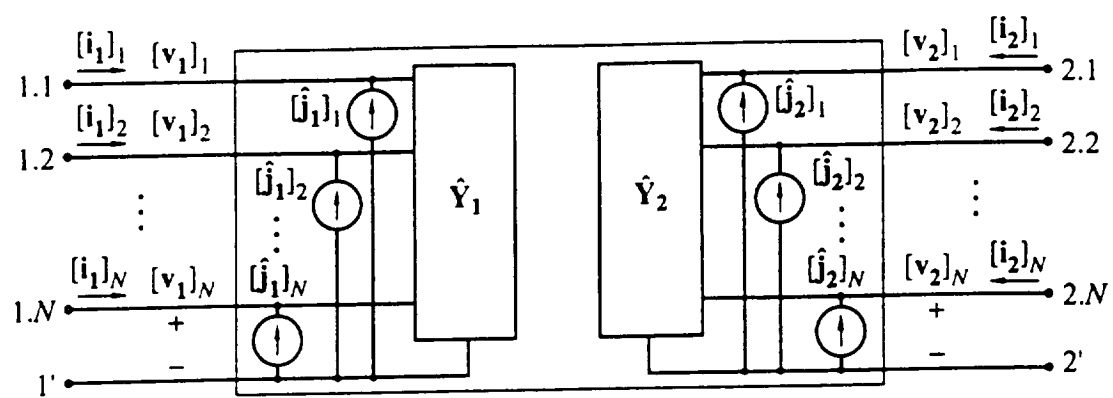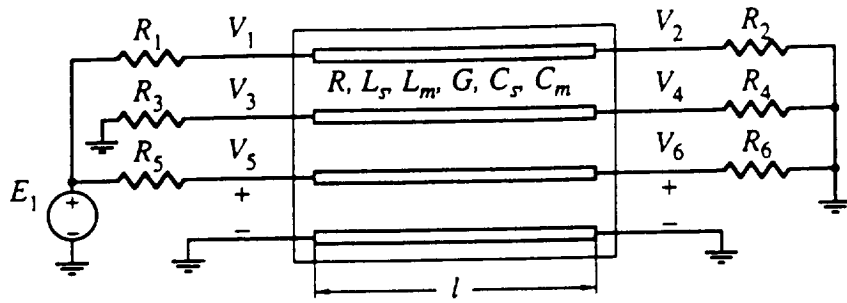
Fig. 5(a)

Fig. 5(c)
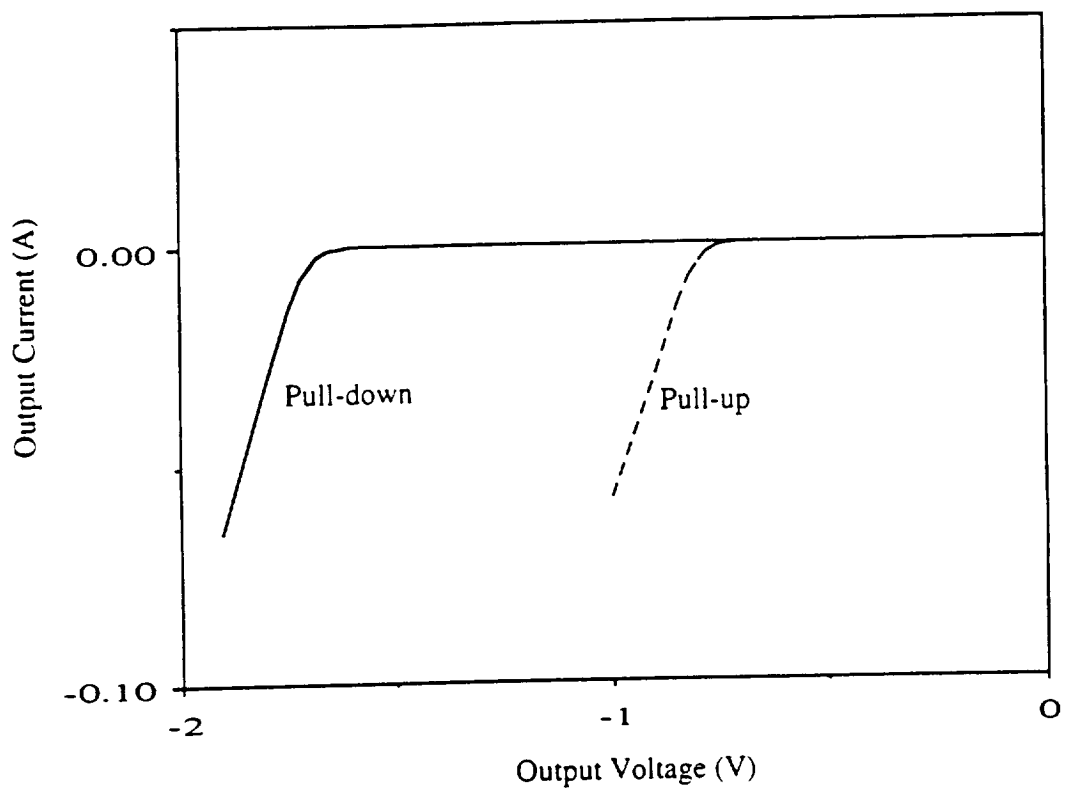
Fig. 5(b)
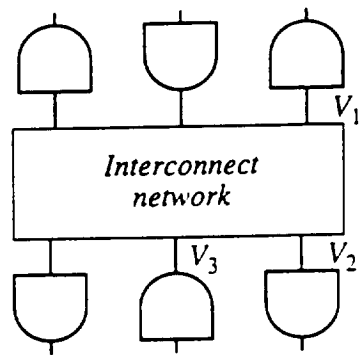
Fig. 6(a)

Fig. 6(b)

Fig. 6(c)

| Number of Nodes | Circuit Description | Lines Modeled with Lumped Resistors[b] | Relative Runtime[a] | | |
| | | | Lines Modeled with Suggested Method | | |
			Total Circuit Simulation[c]	Indirect Numerical Integration[d]	Difference Approximation[d]
10	2 two-conductor lines, 1 four-conductor line (lines and excitation sources only)	0.937	1.00	0.0927	0.0793
10	2 two-conductor lines, 12 MOSFETs	1.00	1.00	$9.66 \cdot 10^{-3}$	$9.47 \cdot 10^{-3}$
100	20 two-conductor lines, 10 four-conductor lines (lines and excitation sources only)	0.999	1.00	$2.06 \cdot 10^{-3}$	$1.75 \cdot 10^{-3}$
1000	200 two-conductor lines, 100 four-conductor lines (lines and excitation sources only)	1.00	1.00	$1.64 \cdot 10^{-5}$	$1.39 \cdot 10^{-5}$

a For 1000 time points.
b One resistor per signal conductor.
c Does not include the difference approximation time.
d Seventh-order.

Table I